

Davy-Faraday Research Laboratory,
The Royal Institution of Great Britain

Department of Geological Sciences, University College London,
University of London

Computer Modelling of Halocarbon Sorption in Zeolite Y

Thesis submitted for the degree of Doctor of Philosophy

by

Naseem Ahmed Ramsahye

2003

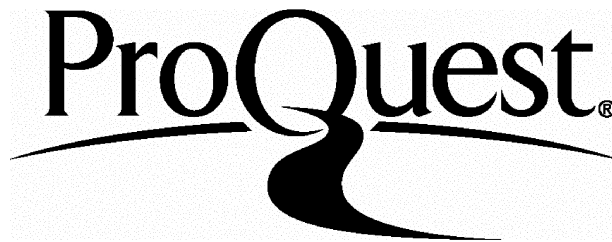
ProQuest Number: U642422

All rights reserved

INFORMATION TO ALL USERS

The quality of this reproduction is dependent upon the quality of the copy submitted.

In the unlikely event that the author did not send a complete manuscript and there are missing pages, these will be noted. Also, if material had to be removed, a note will indicate the deletion.



ProQuest U642422

Published by ProQuest LLC(2015). Copyright of the Dissertation is held by the Author.

All rights reserved.

This work is protected against unauthorized copying under Title 17, United States Code.
Microform Edition © ProQuest LLC.

ProQuest LLC
789 East Eisenhower Parkway
P.O. Box 1346
Ann Arbor, MI 48106-1346

Abstract

The question of cation mobility upon the adsorption of polar molecules is crucial in terms of understanding the fundamental chemistry of basic zeolites, containing exchangeable alkali cations and electron-rich framework oxygen atoms. Experimental techniques have not as yet provided unambiguous answers.

Computational methods, such as molecular dynamics (MD), can help to find answers to some of these questions. The MD study conducted in this thesis (chapters 3 and 4) has shown that sodium cations in NaY are mobile upon sorption of various halocarbon molecules and that cations located in different sites exhibit different types of mobility. The main migration activity takes place when an SII cation migrates from its site on a six-ring by interacting with the Cl atoms on the chloroform molecule. SI' cations are then able to traverse a six-ring window to take a position in a vacant SII site.

The defect energy minimization technique has been used to study the energetic barriers to the cation motion through zeolite six-rings, and the effect of the aluminium content on these energetic barriers. It has been found that the greater the Al content, the lower the energy barriers for sodium cations traversing the six-ring from the SII' to the SII site. The six-ring has been found to exhibit a 'breathing' motion as the cation traverses through it. The full results are described in chapter 5.

Electronic structure methods using Density Functional Theory and semi-empirical methods have been used to study the effect of the cation motion on the zeolite six-ring where a polar molecule is adsorbed. These calculations were performed using large clusters, embedded clusters, and using a periodic zeolite primitive cell. The results have shown the importance of including the long range electrostatic effects when calculating adsorption energies. The full results of this study are reported in chapter 6.

Acknowledgements

First and foremost, I would like to thank my supervisor, Dr. Rob Bell, for all his help, guidance, patience and encouragement throughout my PhD research. Thanks also to Prof Richard Catlow for taking an interest and giving me opportunities to travel to interesting places abroad (MSI trip to San Diego, USA and a NATO ASI on Computational Materials Science in Lucca, Italy). Prof David Price is my UCL supervisor, and I thank him for his assistance on various matters. I also thank the EPSRC for funding my PhD research.

Dr Alex Simperler, Dr Scott Woodley, Dr Sam French, Dr Alexei Sokol, Dr Ben Slater, Dr Dave Coombes, Dr Spencer Braithwaite and Dr Carolyn Barker have been great sources of help on the various computational chemistry theories I've used over the three years of my PhD research (as well as being good friends), and so I express my appreciation to them now. Thanks also to Dr Guillaume Maurin, Dr Sylvain Cristol, and Dr Manuel Sanchez-Sanchez. Dr Ben Slater has been very patient with me during the preparation of this thesis, and so extra thanks go out to him.

I must also thank Dr Stefan Bromley, firstly for his help and guidance through the quantum mechanical calculations, secondly for allowing me the chance to work at TUDelft in Holland for a few months (twice), and finally, for being a good friend throughout my PhD. On that note, I also thank Martijn, Mike, Sylvia, Luca, Angel, Bruno, Luuk, Heidi, Paolo, Leon and all the people at TUDelft who made me feel very welcome during my stays in Holland, and Prof Thomas Maschmeyer and TUDelft for allowing and funding my visits.

I'd like to thank Martin (Foster & Attfield), Tom, Donna, Matt, Andy, Howard, Marta, Manisha, Kate, Will, Mark (Green & Calmiano), Jo S, Toni C, Kylie M and Rachel H, and also the members of the Dynamo Faraday Football Team and everyone else who have all made the RI a great place to work. Thanks to Ashley George and the SmithKline Beecham group (now GSK) for starting me in this field, and for their early encouragement. Also, special thanks to Sophia for some last minute encouragement. Finally, I would like to thank my parents for all their support throughout my education.

Table of Contents

Abstract.....	2
Acknowledgements.....	3
List of Figures.....	8
List of Tables.....	12
Chapter 1: An Introduction to the Structure, Chemistry and Uses of Zeolites. 16	
Introduction	17
Structure and Composition	17
Cation Placement in Faujasite-structured Zeolites	22
Uses of Zeolites	25
Acidity and Basicity in Zeolites.....	27
Sorption in Zeolites.....	29
Adsorption of Halocarbons	32
Aims of the Thesis	36
References	38
Chapter 2: General Overview of Some Computational Chemistry Methods..... 41	
Introduction	42
Molecular Mechanics and Atomistic Methods.....	45
<i>Bond Stretch and Angle Terms</i>	45
<i>Non-Bonded Interactions</i>	47
<i>Other Terms</i>	50
Energy Minimisation	50
<i>Steepest Descents</i>	51
<i>Conjugate Gradients</i>	52
<i>Second Derivative Methods</i>	53
Periodic Boundary Conditions.....	54
Long Range Forces: Ewald Summation.....	55
Molecular Dynamics.....	58
<i>Equilibration and Production Phases of the Calculation</i>	61
<i>Some analyses applied to MD simulations</i>	62

Monte Carlo Methods	64
Statistical Ensembles	67
Electronic Structure (or Quantum Mechanical) Methods.....	68
<i>Brief Background to Electronic Structure Methods and Hartree Fock Theory</i>	69
<i>Basis Sets</i>	71
<i>Density Functional Theory</i>	73
<i>Semi Empirical Methods</i>	77
<i>Population Analysis: Mulliken Population Analysis</i>	80
References	81
Chapter 3: Molecular Dynamics of Cation Motion Upon CHCl₃ Adsorption.....	83
Introduction	84
The Forcefield.....	88
Monte Carlo Simulations	91
Molecular Dynamics Simulations.....	92
Results	93
<i>Canonical Monte Carlo Simulations</i>	93
<i>Simulation of the Adsorption Isotherm for CHCl₃ in NaY</i>	97
<i>Molecular Dynamics: Bare Zeolite</i>	99
<i>Cation Motion in Chloroform Loaded NaY Zeolite</i>	103
<i>Loading of 10 Molecules per Unit Cell</i>	121
<i>Movement of Chloroform Molecules</i>	121
<i>Effect of a Rigid Framework on Cation Motion in Sorbate Loaded NaY</i>	126
<i>Evacuation of the Sorbates</i>	127
Prediction of Vibrational Frequencies	128
<i>Predictions for NaY in the Loaded and Unloaded Zeolite</i>	129
Conclusions	136
References	138

Chapter 4: CCl₂F₂ and CHF₃ Molecules Adsorbed in NaY Zeolite: A Monte Carlo and Molecular Dynamics Study 141

Introduction142
Methodology.....143
Results and
Discussion.....146
Docking of the Molecules.....146
Cation motions.....149
Molecular Motions.....154
Conclusions.....158
References160

Chapter 5: Calculation of the Energetic Barriers to Na Cation Motion through Zeolite Y Six Rings (SI' to SII)..... 161

Introduction162
Methodology.164
The Shell Model, Defect Energy Minimisation and The Mott-Littleton Method. .164
Creating the Model.....167
Potential Parameters.....170
Results and Discussion171
Energetic barriers – general features.....173
Effect of Differing Aluminium Content in the Six Ring.....178
Conclusion.....183
References185

Chapter 6: Cluster and Periodic DFT Studies of CHCl₃ Sorption on Aluminosilicates 186

Introduction.....187
The Cluster Model.....187
Embedded Cluster Models and Periodic Systems.....189
Adsorption of Halocarbon Molecules in Zeolite Y – Lessons From Classical Simulations.....193

Methodology.....	194
<i>The ONIOM Method.....</i>	<i>194</i>
<i>Building and Testing the Clusters.....</i>	<i>195</i>
<i>Embedded Cluster Calculations.....</i>	<i>199</i>
<i>Periodic DFT Calculations.....</i>	<i>200</i>
Results and Discussion.....	201
<i>ONIOM and DMol Cluster Calculations – Adsorption Geometries</i>	<i>201</i>
<i>Adsorption Energies: DMol and ONIOM.....</i>	<i>206</i>
<i>Cluster Calculation of Original Monte Carlo Generated Geometry.....</i>	<i>207</i>
<i>Differences Between DMol and ONIOM.....</i>	<i>208</i>
<i>Relaxation of the Cation Position.....</i>	<i>209</i>
<i>Periodic DFT Calculations – Adsorption Energies and Geometries.....</i>	<i>211</i>
<i>Periodic Single Point Calculation of ONIOM Derived Adsorption Site.....</i>	<i>212</i>
<i>Effect of the Sodium Relaxation on Six Ring Electronic Charge.....</i>	<i>215</i>
<i>Contribution of the Hydrogen–Oxygen Interaction to the Adsorption Energy...222</i>	<i>222</i>
Conclusions	226
References	227

List of Figures

1.1: (a) A 6 ring in a zeolite. (b) An alternative representation of a six ring.	19
1.2: The mineral sodalite, made up of sodalite cages (units), also known as β -cages.	20
1.3: The structure of zeolite A (LTA)	21
1.4: The structure of faujasite, showing the cavity with the 12 membered ring.	22
1.5: Cation positions and the names of the sites in FAU type zeolite structures.	24
1.6: Possible configurations of halocarbon interactions with cation containing basic zeolites.	34
1.7: The adsorption isotherm for chloroform sorption on NaY zeolite measured by Kawai <i>et al.</i>	36
2.1: The Buckingham potential function for non-bonded interactions	48
2.2: The Lennard-Jones Potential energy-separation plot, showing the repulsive and attractive components.	49
3.1: The final configuration of the Monte Carlo run of 500000 iterations.	95
3.2: The configuration showing the dual interaction whereby the molecule is bound to the zeolite via a hydrogen bond to a framework oxygen atom, and via an electrostatic interaction between a chlorine atom (green spheres) and a sodium cation.	96
3.3: A Monte Carlo generated configuration showing the hydrogen atom (white sphere) on a CHCl_3 molecule interacting with an oxygen atom on the zeolite framework.	97
3.4: The calculated isotherm plot for chloroform sorption in NaY zeolite.	99
3.5: MSD plots for the sodium cations at 390K in unloaded NaY.	101
3.6: MSD plot for SII, SI' and SI cations for a simulation of unloaded NaY at 390K. The framework atoms were held fixed for the duration of this simulation.	102
3.7: MSD plot for the SII cations between 0 and 100 ps of MD simulation	105
3.8: MSD plot for SII cations from 100 to 200 ps of MD simulation	105
3.9: Radial Distribution Function plot for SII cations and Cl atoms between 0 and 100 ps of MD simulation.	106
3.10: Radial Distribution Function plot for SII cations and Cl atoms between	107

100 and 200 ps of MD simulation.	
3.11: Movement of sodium cations from SII sites towards the middle of the supercage over the initial 100 ps of MD simulation.	108
3.12: MSD plot for SI' cations between 0 and 100 ps of MD simulation.	111
3.13: MSD plot for Site I' cations between 100 and 200 ps of MD simulation.	111
3.14: Radial Distribution Function plot for SI' cations and Cl atoms between 0 and 100 ps of MD simulation	112
3.15: Radial Distribution Function plot for SI' cations and CL atoms between 0 and 100 ps of MD simulation	113
3.16: Migration path of sodium cation (yellow balls) from a Si' site to a SII site.	115
3.17: MSD plot for SI cations between 0 and 100 ps of MD simulation at 270K, 330K and 390K.	118
3.18: MSD plot for SI cations between 100 and 200 ps of MD simulation at 270K, 330K and 390K.	118
3.19: MSD plot for all cations between 0 and 100 ps of MD simulation at 330K.	119
3.20: MSD plot for all cations between 100 and 200 ps of MD simulation at 330K	119
3.21: Graphic showing the various cation motions described.	120
3.22: Orientation of a chloroform molecule adsorped in NaY.	124
3.23: MSD plot for carbon atoms for the MD simulations at 390K, 330K and 270K with a loading of 10 molecules per unit cell.	125
3.24: MSD plot for carbon atoms for the MD simulations at 390K, 330K and 270K with a loading of 40 molecules per unit cell.	125
3.25: MSD plot for SII cations at 700K and 390K after sorbate evacuation.	128
3.26: Power spectrum of SI cations in unloaded NaY	133
3.27: Power spectrum of SI cations in chloroform loaded NaY	133
3.28: Power spectrum of SI' cations in unloaded NaY	134
3.29: Power spectrum of SI' cations in chloroform loaded NaY	134
3.30: Power spectrum of SII cations in unloaded NaY	135
3.31: Power spectrum of SII cations in chloroform loaded NaY	135
4.1: A low energy docking configuration of a fluoroform molecule	147

4.2: A low energy docking configuration of a CFC-12 molecule.	148
4.3: MSD plot for the SII' cations between 0 and 100 ps of simulation of NaY zeolite loaded with 40 molecules of CHF ₃	150
4.4: MSD plot for the SII cations between 0 and 50 ps of simulation of NaY zeolite loaded with 40 molecules of CHF ₃	151
4.5: MSD (in Å ²) plot for the SII cations between 50 and 100 ps of simulation of NaY zeolite loaded with 40 molecules of CHF ₃	151
4.6: RDF plot for the F – Na interaction during the MD simulation of CCl ₂ F ₂ adsorbed in zeolite NaY.	153
4.7: RDF plot for the Cl – Na interaction during the MD simulation of CCl ₂ F ₂ adsorbed in zeolite NaY.	153
4.8: Plot of number of sorbate molecules with halogen atoms that are within 3.2 Å of a cation for each molecule simulated over 500 picoseconds	156
4.9: Plot of number of sorbate molecules with hydrogen atoms that are within 2.6 Å of a framework oxygen atom for each molecule simulated over 500 picoseconds	156
5.1: An illustration of the shell model	165
5.2: The partitions of the Mott-Littleton method.	166
5.3 Three of the migration paths used as points in the Mott-Littleton calculations.	168
5.4: The diagram of the six ring through which the migration occurs, showing the Al atoms (represented by the pink spheres) in the para positions (left) and the meta position (right)	169
5.5: A plot of defect energy vs Region 1 radius	172
5.6: energetic barriers for cation motion between SII' and SII sites in NaY for 1 aluminium atom in a six ring.	174
5.7: energetic barriers for cation motion between SII' and SII sites in NaY for 2 aluminium atoms in a six ring, arranged in a meta position.	175
5.8: energetic barriers for cation motion between SII' and SII sites in NaY for 2 aluminium atoms in a six ring, arranged in a para position.	175
5.9: energetic barriers for cation motion between SII' and SII sites in NaY for 3 aluminium atoms in a six ring	176

5.10: Labelling scheme of the oxygen atoms for the O – O distances reported in tables 5.5-5.8.	181
6.1: Sodalite cage cluster showing the site II cation.	196
6.2: Sodalite cage cluster showing the site I' cation site.	197
6.3: 'Extended SII cluster' showing the site II cation site.	198
6.4: Sodalite cage cluster showing the binding site copied from Monte Carlo docking	202
6.5: Sodalite cage cluster showing the new binding site.	203
6.6: DMol Optimised 'Extended SII cluster' showing the site II cation site and the sorbate molecule in the newly found docking site.	205
6.7: Optimised 'Extended SII cluster' showing the site II cation site and the sorbate molecule docked in the original Monte Carlo generated configuration.	208
6.8: The cation—oxygen distances are shown in this figure.	210
6.9: The geometry optimised primitive cell of NaY.	214
6.10: Adsorption geometry of the periodic DFT calculation using the PW91 functional.	215
6.11: Partial charges on the six ring as calculated by the Mulliken scheme for the DMol calculations on the extended cluster.	218
6.12: Partial charges on the chloroform molecule as calculated by the Mulliken scheme for the DMol calculations on the extended cluster.	219
6.13: Partial charges on the zeolite SII six-ring as calculated by the Mulliken scheme for the ONIOM calculations on the extended cluster.	220
6.14: The close-up docking configuration from the periodic DMol calculation (PW91 with the DNP basis set) showing the charges on various atoms, as well as interaction distances	221
6.15: The T—O bond lengths before and after adsorption for the extended cluster optimised with the DMol program.	222
6.16: The cluster used to calculate the energy due to the H-O _{zeolite} interaction.	224
6.17: The optimised geometry of the calculation to determine the strength of the hydrogen—oxygen interaction when chloroform is adsorbed on an aluminosilicate cluster.	225

List of Tables

3.1: Partial charges on the atoms in MD simulation	90
3.2: Buckingham terms for the framework-framework and framework-cation interactions	90
3.3: Lennard-Jones parameters for the sorbate-sorbate, zeolite-sorbate and cation-sorbate interactions	90
3.4: Harmonic bond terms from cvff forcefield for bonding within the chloroform molecules	90
3.5: Three body terms for the T atoms in the zeolites framework	91
3.6: Harmonic three body terms for chloroform	91
3.7: Simulated and experimental values of the NaY zeolite lattice parameters and volume after optimisation with the new Bell potentials.	93
3.8: Table of results of the isotherm simulation for chloroform sorption on NaY zeolite	98
3.9: Masses used to covert molecules/unit cell to mmol/g	99
3.10: Areas of region A from figures 3.9,3.10 and 3.14, 3.15	114
3.11: Areas of region B from figures 3.9,3.10 and 3.14, 3.15	114
3.12: Diffusion coefficients for 10 molecules diffusing through NaY zeolite	123
3.12: Diffusion coefficients for 40 molecules diffusing through NaY zeolite	123
4.1: Partial charges for the atoms in the CCl ₂ F ₂ molecule	144
4.2: Partial charges for the atoms in the CHF ₃ molecule	144
4.3: Lennard-Jones parameters for the non bonded interactions between the sorbate molecule's consitituent atoms and the cation / framework oxygen atom, and also the sorbate – sorbate interactions	145
4.4: Harmonic bonding parameters for the CCl ₂ F ₂ molecule	145
4.5: Harmonic bonding parameters for the CHF ₃ molecule	145
4.6: Harmonic bonding parameters for the CCl ₂ F ₂ molecule	146
4.7: Harmonic bonding parameters for the CHF ₃ molecule	146

4.8: Diffusion coefficients for CHF ₃ diffusing in NaY zeolite	158
4.9: Diffusion coefficients for CCl ₂ F ₂ diffusing in NaY zeolite	158
5.1: The species and their charges used in the Mott-Littleton calculations	170
5.2: The Buckingham potential parameters used in the Mott-Littleton calculations	170
5.3: The three body potential parameters used in the Mott-Littleton calculations	170
5.4: Number of ions corresponding to the various Region 1 radii tested	172
5.5: Oxygen – oxygen distances (in Å) during the traverse of a Na cation from SII' site to SII site for the case where there is 1 aluminium in the six ring	181
5.6: Oxygen – oxygen distances (in Å) during the traverse of a Na cation from SII' site to SII site for the case where there are 2 aluminiums in the six ring (meta position)	182
5.6: Oxygen – oxygen distances (in Å) during the traverse of a Na cation from SII' site to SII site for the case where there are 2 aluminiums in the six ring (para position)	182
5.6: Oxygen – oxygen distances (in Å) during the traverse of a Na cation from SII' site to SII site for the case where there are 3 aluminiums in the six ring	182
6.5: The calculated adsorption energies for chloroform adsorbing on a silica cluster substituted with one aluminium atom and containing one cation.	207









Copyright

The copyright of this thesis rests with the author and no quotation from it or information derived from it may be published without the prior written consent of the author.

Copyright © 2003 N. A. Ramsahye

Conventions

Unless otherwise stated, the following colour scheme is used to represent the various atoms in the diagram present in this thesis from chapters 3 to 6.

	Silicon
	Aluminium
	Oxygen
	Sodium
	Carbon
	Hydrogen
	Chlorine
	Fluorine

Chapter 1: An Introduction to the Structure, Chemistry and Uses of Zeolites

Introduction

Catalysts essentially increase the rate of reaction, and can be defined as “Any substance that increases the rate of attainment of chemical equilibrium without itself undergoing chemical change...”.¹ Catalysts may be in the same phase as the reactants, in which case they are called a homogeneous catalyst, or the catalyst may be in a different phase, known as a heterogeneous catalyst, a prime example being zeolite and zeotype catalysts.

In the industrial world, zeolite catalysts are used on the megaton scale, especially in the petrochemical industry.² The catalyst industry is said to be worth many millions of US dollars per annum due to the fact that this is the magnitude of monetary profit gained from using catalyst driven processes over alternative, non-catalyst driven processes.² This is especially true in the case of zeolites. For instance, it is estimated that the use of zeolite materials has reduced the cost of petroleum refining by ten billion US dollars per annum. The use of zeolites for catalytic purposes has also been driven by environmental concerns and legislation. The use of these solid materials means that there is less toxic waste because, for instance, one can easily separate the required product from the catalyst and by products. Furthermore, zeolites offer an environmentally friendly alternative to toxic and corrosive catalysts.

Structure and Composition

Zeolites are crystalline aluminosilicates. They are found naturally in the Earth’s crust, and represent one of the largest classes of minerals. Zeolites can also be synthetically

made, and examples include ZSM-5, zeolites A, X and Y, all of which are commercially important materials.³

These minerals are made up of $[\text{SiO}_4]^{4-}$ and $[\text{AlO}_4]^{5-}$ tetrahedra, which are corner shared via oxygen bridges.³ Although the aluminium atoms are distributed randomly throughout the structure, their relative placings are subject to two rules. The first, Löwenstein's rule, dictates that AlO_4 tetrahedra cannot be neighbours with each other, although SiO_4 tetrahedra can be neighbours with either AlO_4 or other SiO_4 tetrahedra. This rule comes about as a result of highly electrostatic repulsion between the negatively charged AlO_4 tetrahedra. The second is Dempsey's Rule, which essentially states that the aluminium atoms will be distributed as far apart as possible, thereby minimising the number of Al-O-Si-O-Al bridges.

Silicon-oxygen tetrahedra are electrically neutral when connected together as a three dimensional network having an overall composition of SiO_2 , whereas aluminium-oxygen tetrahedra connected in the same way each carry a charge of -1. The electrical imbalance is created due to the fact that Si(IV) is substituted by Al(III). Therefore, to make the framework electrically neutral, exchangeable cations are present in the zeolite. These cations are held electrostatically in the framework on various sites by way of coordination with one or more framework oxygen atoms, with examples including alkali metals such as Li^+ , Na^+ , K^+ , and alkaline earth metals such as Mg^{2+} and Ca^{2+} . In the natural state, such cations are also often solvated by water molecules present within the zeolite. Extra-framework cations are also able to form clusters. Examples of these include Na and K in the A, Y and X zeolites. These systems have been studied by Anderson *et al.*⁴⁻⁶ and Woodall *et al.*⁷ by ESR spectroscopy. An alternative method of

charge compensation is via the “bridging” hydrogen, bonded to a framework oxygen which usually possesses high Brønsted acidity.

The general formula for the composition of a zeolite is $M_{x/n}[(AlO_2)_x(SiO_2)_y] \cdot mH_2O$, where cations M of valence n neutralise the negative charges on aluminosilicate framework.³ The Si and Al atoms are sometimes referred to as T (tetrahedral) atoms.

The tetrahedra are linked at the corners via oxygen atoms, and these links are often represented by straight lines in the literature, with an oxygen in the middle of the line, and T atoms at the corners. It should be noted that in reality T—O—T bonds are rarely linear. This nomenclature is illustrated in figures 1.1a and b, where a 6-ring is shown. It is also possible to form 4-rings and 5-rings. These rings can join together to form cages that can also join together, and hence the framework of the zeolite is built.

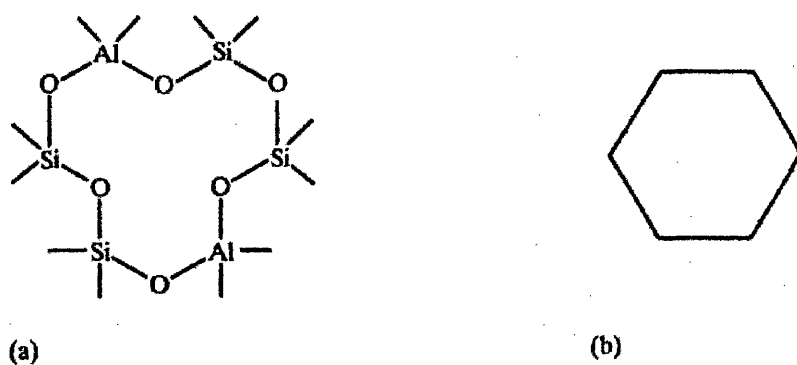


Figure 1.1 (a) A six-ring in a zeolite. (b) An alternative representation of a six-ring.
(Figure taken from reference 3)

A basic building unit for many zeolites is the sodalite cage (or β -cage), as illustrated in figure 1.2. This cage is made up of 4-rings and 6-rings linked together. The mineral

sodalite is made from β -cages connected together via the four rings and packed in a cubic array (i.e. each 4-ring is shared by 2 β -cages).

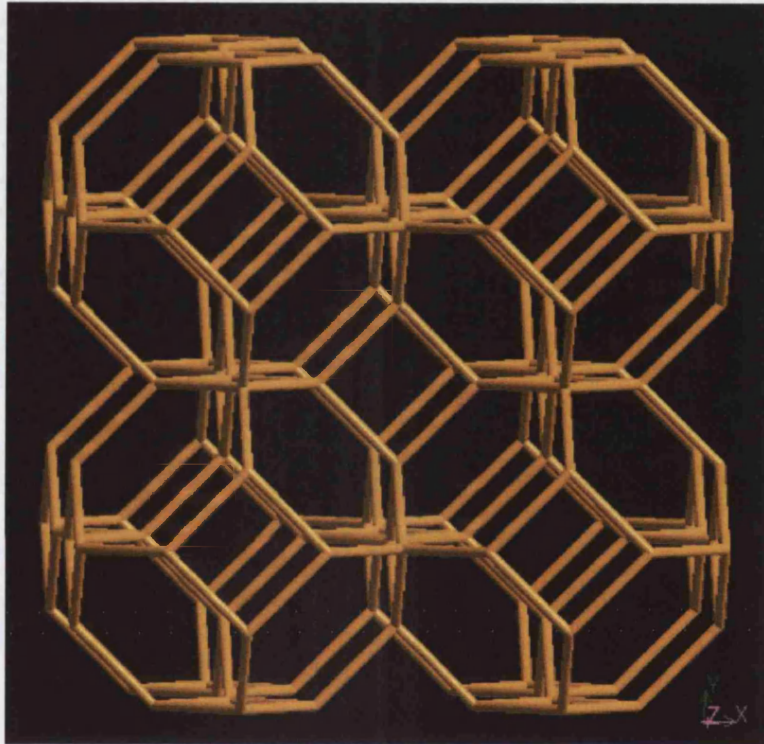


Figure 1.2: The mineral sodalite, made up of sodalite cages (units), also known as β -cages.

If the 4-rings in β -cages were connected via oxygen bridges, then zeolite A would be formed. Zeolite A is a synthetic zeolite, and contains a large cavity of molecular dimensions. The cavity in zeolite A has an 8-ring window and has an aperture of about 4 Ångstroms. The structure of zeolite-A is shown in figure 1.3. The sodalite cages can be seen at each corner of the cubic array, with the 8-ring window, and the supercage.³

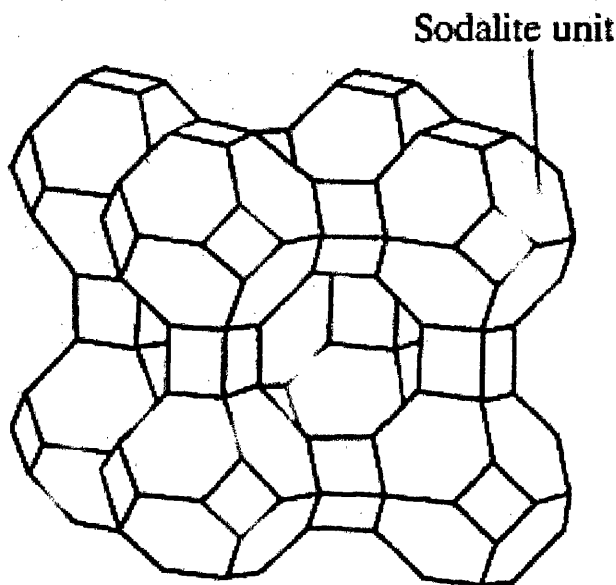


Figure 1.3: The structure of zeolite A (LTA)³

Faujasite is a naturally occurring, but rare mineral, and is built up of sodalite units linked by oxygen bridges between the 6-rings in a tetrahedral array. There is a large supercage enclosed by this array, and this cage has 12-ring windows, with an aperture diameter of about 7.4 Ångstroms.³ Zeolites X and Y (which are synthetic) both have the faujasite structure (see figure 1.4). Zeolite X structures have a Si:Al ratio between 1 and 1.5, and zeolite Y has a Si:Al ratio of between 1.5 and 3.0.³ The work described in this thesis uses the faujasite structure, and so further details regarding cation positions in this structure are given below.

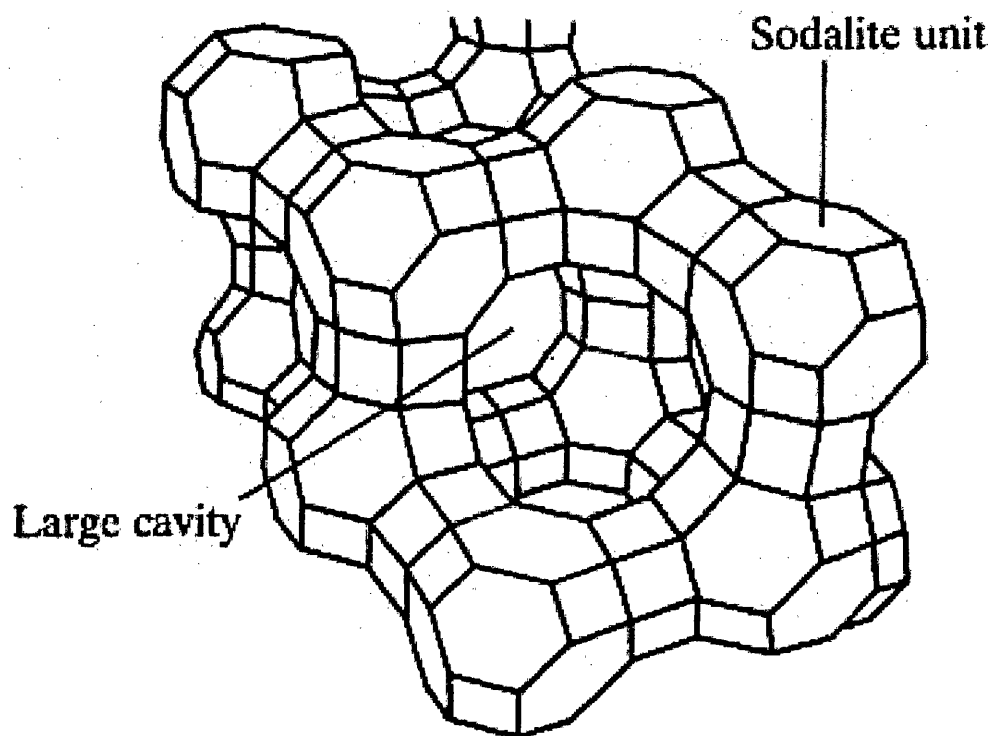


Figure 1.4: The structure of faujasite, showing the cavity with the 12 membered ring.³

Cation Placement in Faujasite-structured Zeolites

The positions of the various cation sites in faujasite-structured zeolites are illustrated in figure 1.5. Site II cations are located in the zeolite supercage. They are coordinated to six oxygen atoms that are part of a six ring of the sodalite cages. The SI site is situated inside the double six ring prism that interconnects the sodalite cages. These cation locations are usually considered to be at the centre of these prisms, although calculations by Jaramillo and Auerbach⁸ have indicated that they may be found slightly displaced from the centre of the prism (about 0.6 Angstroms from the centre in the case of Na^+ , although distances may vary for other cations). SI' sites are to be found coordinated to six oxygen atoms on one side of a double six ring prism, inside the

sodalite cage. These are the three sites normally found to be occupied in dehydrated zeolite Y. Three other cation sites exist in faujasite structures, SII', SIII and SIII'. SII' sites are located inside the sodalite cages, directly opposite the SII sites. SIII sites are to be found inside the supercage, sitting above a four ring, making up part of the sodalite cages. They are coordinated to four oxygen atoms, and sit closer to the centre of the supercage than SII cations. SIII' cations are in a similar location to the SIII counterparts, except that they are coordinated to one oxygen atom, as opposed to four. These extra sites can be found occupied in zeolite X. The sites described above are "ideal" crystallographic sites which are useful as reference points. In reality the cations may be displaced from these sites depending on the cation and Al distribution. The distribution of the cations amongst the sites in the faujasite structure is also dependent on the exact Si:Al ratio. There is further a general assumption that the distribution is also dependent upon the repulsive Coulombic cation-cation interactions.

Various distributions of cations amongst the sites described above have been proposed for NaY zeolite with a number of Si:Al ratios, determined from both experiment and simulation. Some authors have proposed that sites other than SI, SI' and SII are occupied in NaY, for example SIII'. Full occupation of SII sites equates to 32 SII cations in a unit cell. Monte Carlo simulations by Buttefey *et al.*⁹ investigating cation distributions in NaY and NaX have indicated that SI and SII sites are usually filled first, and any extra cations are distributed among SI' sites, and SIII or SIII' thereafter.

The model of NaY used in the simulations had the composition $\text{Na}_{56}\text{Si}_{136}\text{Al}_{56}\text{O}_{394}$, built from the structure refined from powder neutron diffraction data by Fitch, Jovic and Renouprez¹⁰ for benzene adsorbed on NaY. The 56 sodium atoms per unit cell were

distributed among the various possible sites as follows: 6 on SI sites, 18 on SI' and 32 on SII. Neighbouring SI and SI' sites were not allowed to be populated, due to the aforementioned electrostatic repulsive interactions that would prevent such a configuration of cations. Aluminium atoms were also randomly distributed among the framework T sites, subject to Löwenstein's rule.

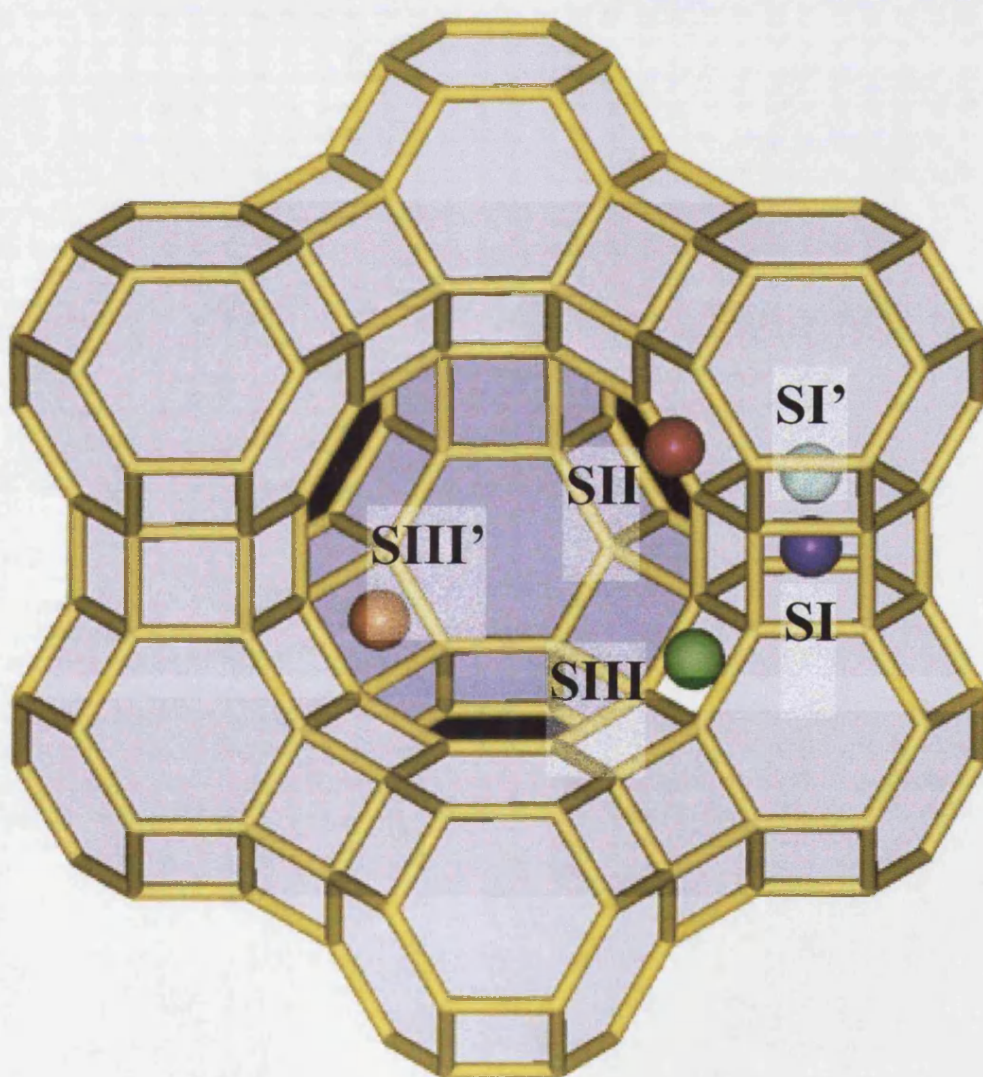


Figure 1.5: Cation positions and the names of the sites in FAU type zeolite structures.

Uses of Zeolites

Zeolites are widely used in industry for various purposes. Their ability to act as solid acids and bases makes them suitable for applications such as catalysis and as sorbent materials. Although only about a dozen of the 126 existing zeolite structures are used for industrial applications, there is a number of different feasible hypothetical structures that are yet to be synthesised, but may have potential uses in the field of catalysis¹¹. Each structure, either existing or hypothetical, has different shapes and sizes of pores and channels, which is an important factor for the use of a specific zeolite for a specific purpose in the field of catalysis. In this application, the molecular sieve properties of a zeolite can control which reactant molecules have access to, and which product molecules can depart from the active site. The selection can be on the basis of the reactant shape, and this is known as shape selective catalysis. For example, a zeolite pore may only be big enough to accommodate an alkane of a certain chain length or shape, and so the branched alkane may not be able to enter the zeolite, whereas a straight alkane could enter the zeolite.³

An example of this type of catalysis is in the dehydration of butanols over zeolite-A with Ca as the extraframework cation. Butan-1-ol can enter the zeolite and react to produce the corresponding alkene, whereas the branched butan-2-ol cannot enter the zeolite.³

Zeolites can also act as product selective catalysts, that is, the reaction is allowed to take place, but for reactions where there is a mixture of products, one product can pass out of the pore, whereas the other cannot do so. An example is in the preparation of xylene

using the zeolite ZSM-5 (Zeolite Socony Mobil-5), where methanol and toluene are the reactants, and three possible products are formed, 1,2-xylene, 1,3-xylene and 1,4-xylene. Only the 1,4-xylene is allowed out of the pore, as here the methyl groups are in a para position to each other, and this molecular shape means that it can exit the pore.³

Another selection ability of a zeolite is the ability to select on the basis of transition state. The transalkylation of dialkylbenzene serves as an example of this. A diphenylbenzene is formed as a transition state, splitting to give either the 1,2,4-isomer or the 1,3,5-isomer. However, when this reaction is performed with mordenite, the 1,2,4-isomer is obtained in almost 100% yield, due to the fact that the transition state for the 1,3,5-isomer is too large to fit in the zeolite pore.

Zeolites can act as ion exchangers. For example, zeolite-A can readily exchange Na^+ ions for Ca^{2+} ions, making it useful for water softening. It is present in detergents such as washing powder for this particular purpose. Clinoptilolite, a naturally occurring mineral, can exchange Na^+ ions for Cs^+ ions, thereby making it useful for the separation and storage of radioactive waste. Zeolite-A can also be used for this purpose due to its ability to recover radioactive strontium.³ Other applications include the use of the zeolite clinoptilolite in cat litter.

Another use for zeolites lies in the area of gas and solvent separation, making use of the zeolite as a molecular sieve. Chabazite has been used commercially to absorb polluting SO_2 emissions, illustrating the adsorbent property of zeolites. Work has also been conducted by others in studying the sorption of various gases such as CO_2 , O_2 , N_2 and other gases such as CFCs, HFCs and other halocarbons using various basic zeolites.

The sorption properties of zeolites can also be applied to removing chlorinated solvents from contaminated groundwater and soils. Separation and storage of halocarbons have important environmental implications.¹²

Acidity and Basicity in Zeolites

The fact that zeolites are important in the heterogeneous catalysis industry is due to their ability to act as solid acids and bases.^{13,14}

Acid zeolites have been widely studied in the past due to the huge number of applications they have in the field of catalysis, especially in the petrochemical industry. Acid sites can be Lewis acids sites, and these sites arise from the presence of extraframework cations in the framework, or the presence of Al atoms. The acid sites in a zeolite may also be of the Bronsted type, and this is so when protons are present in the zeolite, bonded to the framework oxygen atoms.¹³

Basic zeolites, containing exchangeable alkali cations and electron-rich framework oxygen atoms, also have potential applications in catalysis as well as the separation and storage of halocarbon molecules, an area of increasing environmental importance. In recent times, there has been an increase in the study of basic zeolites, both experimental and computational, their properties and their potential applications in heterogeneous base catalysis. The fact that zeolite catalysts are potential replacements for toxic or corrosive catalysts and that important processes such as the side chain alkylation of toluene to form styrene uses a basic medium¹⁴ provides some explanation for this increase in research on base catalysis using zeolites.

Basic zeolites are so due to the fact that aluminium is substituted for silicon in the framework, a consequence of which is that alkali metal cations, such as sodium or lithium, are present in the zeolite to compensate the net negative charge left by this substitution.¹⁵ There is an increasing realisation that the distribution of the extraframework cations may be substantially perturbed upon adsorption of different molecules, leading to changes in the framework electron density and in the mode of physical binding of the guest species. The distribution and siting of the extraframework cations therefore play a major role in the action of zeolites as adsorbents and catalysts, as this may affect the strength of the basic sites.

As with acid sites, the basic sites can be either Brønsted or Lewis base sites. The Lewis base sites are attributed to the negatively charged framework oxygen atoms, with the magnitude of the charge being an indicator of the basic strength of that particular site. The charges are partly related to the framework geometry, in particular, Si-O-Al and Si-O-Si angle and the bond length between the atoms¹⁵. This in turn will be influenced by the type, number and siting of the extraframework cations and their possible redistribution during adsorption and catalytic processes. For instance, movement of cations has been deemed to be a key aspect of the activation process for the trimerisation of acetylene when using a zeolite catalyst^{16,17}. The question of cation mobility is thus crucial in terms of understanding the fundamental chemistry of these materials, and one to which experimental techniques have not as yet provided unambiguous answers. Due to their direct nature in the sense that interactions at the atomic level can be explicitly modelled, computational techniques can help to find answers to these questions. If the compensating cations present are from lower down in

Group 1 of the periodic table, the basicity of the zeolite will increase. Therefore, if considering zeolites such as A, Y or X substituted with monovalent cations, then in decreasing order of basicity the cations might be $Cs > Rb > K > Na > Li$. Thus it can be seen that as the extraframework cation radius increase, the basicity of the zeolite increases. It should also be remembered that the number of cations present will correspond directly to the number of aluminium atoms present, and so the basicity is also determined by the number of aluminium atoms present in the framework.

Sorption in Zeolites

“...Catalysis must always be preceded by adsorption...”¹. The term *adsorption* is applied to describing the accumulation of material (the adsorbate) at a surface. In contrast, the term *absorption* refers to a bulk phenomenon. The term *sorption* has been coined to cover both adsorption and absorption.¹⁸ In any case, before any catalytic activity can take place, some sort of sorptive phenomena must occur, and hence the importance placed on the study of sorption in zeolite materials.

The sorptive properties of a given zeolite are partly determined by steric factors.¹⁹ The size and shape of the pores and channels of the zeolite structure will have a say in which type of molecule will be able to enter the cage and be adsorbed on the internal surface of the cage, and which type will not. Therefore, a zeolite has the ability to select sorbates on the basis of shape and size (known as shape selectivity).

The sorptive and diffusive properties are not only governed by steric factors, but also by the composition and the presence of extraframework cations, which will render the

zeolite either acidic or basic. Such factors will also control whether the sorption is physisorption (van der Waals, dipole, induced-dipole or quadrupole interactions) or chemisorption (where chemical bonds might be formed with the framework). The composition will also have an effect on the energetics of the adsorption. The presence of the cations and the aluminium atoms will generate an electric field.¹⁹ This will have a contribution to the adsorption energy of any sorbates in the supercage. Other contributions come from the dispersion-repulsion energy (which can be calculated using a Lennard-Jones potential function, as described in chapter 2) and the polarisation energy of the zeolite. Further terms in the energy calculation depend on permanent dipole and quadrupole moments in the sorbate molecules, and also on sorbate-sorbate interactions.¹⁹

One can measure adsorption isotherms by measuring the amount of adsorbate taken up by the zeolite at a fixed temperature. This can be done at different pressures, and so one can gain an idea of the maximum amount of adsorbate that can be adsorbed before the zeolite pores are saturated.^{18,19}

The sorption of various molecules on basic zeolites has been studied by use of experimental and computational methods. Information on the sorption and diffusion of small organic molecules and various gases is important to obtain in order to aid the selection of zeolites with suitable structures and compositions for specific purposes and to accommodate specific molecules. As such, a vast amount of work has been performed on determining the sorptive and catalytic properties of different zeolite structures. Past work has successfully used computational methods to study the sorption of CO₂, N₂ and O₂ on zeolites containing sodium and calcium cations. For

example, the work of Bell has successfully calculated sorption isotherms and sorption heats for CO₂ and N₂ adsorbing on NaA zeolite and CaA zeolite using the Grand Canonical Monte Carlo technique.

The sorption of krypton on silicalite has also been studied by Calmiano¹⁸ using Monte Carlo methods, and again, the results compared well with experimental values of adsorption heats and isotherms. Molecular dynamics was also used to study the diffusion of small molecules in zeolites, and this allowed the calculation of diffusion coefficients.

Computational methods have also been used to study organic molecules, for example Monte Carlo studies of methane adsorbing on Na zeolite-Y by Yashonath *et al.*²⁰ have yielded adsorption heats that compare favourably with experimental values. One can also study the diffusion of sorbates through the zeolite, as such a process must take place for sorbate to reach their sorption sites. The molecular dynamics technique (outlined in chapter 2) can be used to this end; Catlow, Freeman *et al.*²¹ studied the behaviour of methane and ethene in zeolite ZSM-5 using molecular dynamics. Their model included a flexible framework, and the results of the diffusion coefficient calculations were in good agreement with experimentally determined values. The results therefore indicated that the simulation was a realistic representation of the diffusion process, adding further weight to the case for the use of these techniques for studying zeolites. Sastre, Catlow and Corma²² have also used molecular dynamics to study the diffusion of ortho- and para-xylene in siliceous zeolite CIT-1. The authors found that the ortho isomer could not diffuse through the ten-membered ring channels, although they observed some penetration near the channel intersection with the twelve-membered rings, where the molecules can overcome the activation energy to enter the ten-

membered rings. The ortho-xylene molecules can diffuse through the twelve-membered rings, as this diffusion path is energetically favourable. The authors found that the para-xylene molecules showed larger mobility and could diffuse along a longer path through the 10 membered rings and the molecule also diffuses through the 12 membered rings. The authors concluded that the interactions between the molecules also play an important role in determining the nature of the diffusion of organic molecules in the zeolite, as well as the effects of the pore size.

A number of studies have employed *ab initio* and first principles methods to study sorption and its effects on zeolite models. Some of these works are further discussed in Chapter 6 of this thesis where they serve as examples of the usefulness of this technique in the study of sorption.

Adsorption of Halocarbons

In terms of chloroform and CFC sorption, previous work using computational modelling and vibrational spectroscopies²³⁻²⁵ has shed light on the mode of binding of CHCl_3 and CFC molecules in siliceous FAU, NaY and NaX. From MAS NMR spectra however there are still substantive questions regarding the role of the extra-framework alkali cations, although the interpretation of the spectra has led to the suspicion that certain cations migrate upon adsorption of polar molecules. Additional deployment of x-ray diffraction by Grey *et al.* has suggested that migration occurred in the case of adsorption of HFC-134²⁶.

The MAS NMR work on basic zeolites by Bosch *et al.*²⁷ and Sanchez-Sanchez *et al.*²⁸ indicates possible motion of the sodium cations upon adsorption. Sanchez-Sanchez *et*

al. concluded that the framework basicity plays a part in the chloroform adsorption. The low field shift of H resonance with increasing framework basicity observed by the authors indicates a hydrogen-bonding interaction, as the nucleophilic framework oxygen polarises the C—H bond of the chloroform molecule. The authors also performed ^{23}Na MAS NMR experiments and calculated the quadrupole coupling constants for the atoms in sites I' and II. The decrease in these constants upon chloroform sorption was attributed to the migration of sodium cations from site I' to the site II. Bosch *et al.* suggest that upon chloroform adsorption, there is a modification of the electron density of the entire zeolite lattice. They concluded from their NMR data that there is a decrease in site I population, and an interaction of the chloroform with site II cations. The authors also report that there is "an influence on the cations at site SI' " although direct sorbate-cation interaction was ruled out in this case due to the inability of the chloroform molecules to enter the sodalite cage. Hence the suggestion that instead, the electron distribution on the zeolite lattice is modified.

The adsorption of chloroform on faujasite type zeolites has been studied by various authors, including Cheetham and Mellot, who have performed Monte Carlo studies on halocarbon sorption in NaY and derived a forcefield for the sorbate-zeolite interactions²⁴. The results of these simulations were found to be in good agreement with the experimental (calorimetric) work performed by the same authors²⁹. The heats of sorption quoted by Cheetham and Mellot were in the order of about 50 kJ/mol. In the case of chloroform being adsorbed in Na-Y the results indicated that hydrogen bonding between the framework oxygen atom and the hydrogen atom on the chloroform could be an interaction responsible for the binding of the sorbate to the sorbent. Figure 1.5

shows the different cation sites in NaY zeolite. The III and III' sites are occupied in zeolite X and not Y⁸.

Additional NMR experiments and X-ray diffraction by Grey *et al.*^{12,30} have indicated that cations in the I' site migrate to site II positions upon adsorption of HFC-134, again possibly attributable due to interaction with the chlorine atom of the molecule.

Bosch *et al.*²⁷ have proposed possible configurations of the chloroform molecule inside the zeolite, and these are shown in figure 1.6. The proposed configurations also feature in the work by Kaszkur *et al.*³¹, who performed synchrotron based diffraction experiments on sorbed chloroform and dichlorobenzene in zeolite Y. The authors indicate that two configurations were possible, represented as Species II and III in figure 1.6. The Species III has the hydrogen atom pointing towards the centre of the supercage. The paper also notes that there is a decrease in site II occupancy upon chloroform sorption.

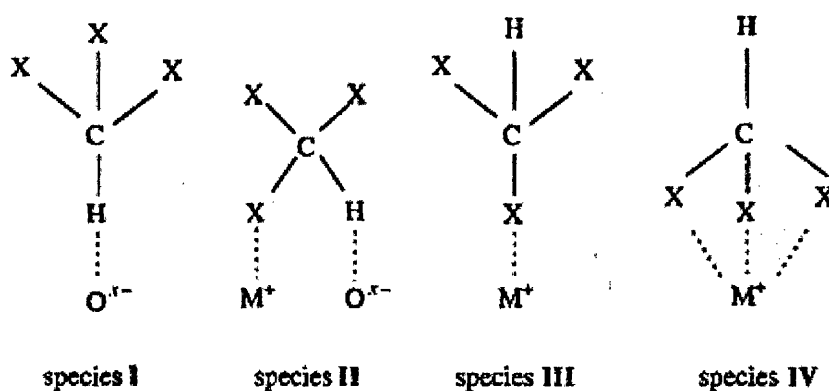


Figure 1.6: Possible configurations of halocarbon interactions with cation containing basic zeolites.

From their work in measuring the sorption isotherm for chloroform sorption on NaY zeolite, Kawai *et al.*³² have concluded that there is a possible dispersive interaction between the extra-framework cation and the chloroform molecule. Their experiments were performed using gravimetric methods. Kawai *et al.*³² found that gaseous chloroform adsorbing on Na-Y zeolite produced a Langmuir type isotherm, as shown below in figure 1.7. The conclusion drawn from the isotherm was that the absorption proceeds mainly by a dispersive interaction between the chlorine on the chloroform molecule and the Na⁺ cation. This was because there was only a slight increase in the maximum loading when the authors used zeolites with more aluminium atoms. Due to the fact that the increase in Al atoms means an increase in framework basicity, one would expect a larger increase in loading, hence the conclusion drawn by the authors.

Evidence for an electrostatic interaction playing a part in the sorption process was provided by the spectroscopy work of Davidson *et al.*²⁵. A downward shift in the C-Cl stretching mode indicates a weakening of the C-Cl bond, which was attributed to a Cl-Na electrostatic interaction.

One might also consider the possibility of the probe molecule reacting with the zeolite framework, as opposed to being simply physisorbed. Such a phenomenon has been reported by Sanchez-Sanchez *et al.*²⁸, where the authors found that a slow reaction between chloroform and the zeolite framework occurs to yield a dichloromethoxy species and CO, followed by the destruction of the zeolite framework. This has not been reported for other molecules such as CHF₃, studied by Bosch *et al.*²⁷, or any HFC type molecules studied by Grey *et al.*²⁶

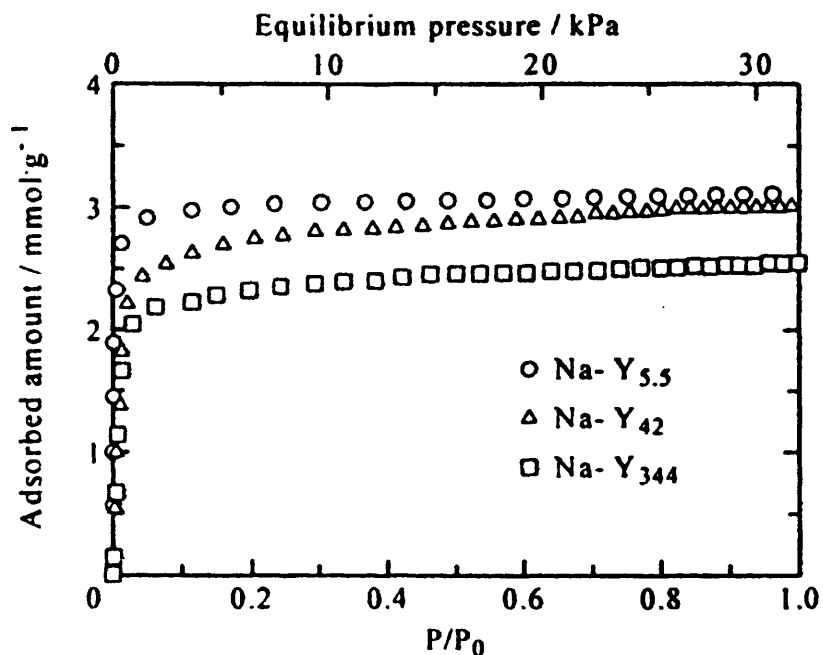


Figure 1.7: The adsorption isotherm for chloroform sorption on NaY zeolite measured by Kawai *et al.*³²

The interpretation of the NMR spectra is not unambiguous, and so we have turned to computational methods to look into the interactions between the probe molecules and the zeolite framework and cations.

Aims of the Thesis

The broad aim of the project is to study the sorption of various small organic molecules, such as chlorofluorocarbons and hydrofluorocarbons, in the basic zeolite, NaY, using computational methods. Chloroform is a good candidate as a probe molecule with which to study the properties of basic zeolites by computation for two reasons:

1. It is an acidic molecule, and can be used as a model compound for halocarbons.
2. There is experimental data available in the form of IR and NMR spectra, and x-ray and neutron diffraction studies with to compare computational results.

A portfolio of computational chemistry techniques is available to study the effect of the sorption of such molecules on the zeolite framework itself and on the cations. Experimental evidence suggests that the extraframework cations are mobile upon adsorption of halocarbon molecules. Such phenomena can be studied by the use of molecular dynamics simulations. Therefore the first aim of the thesis is to derive information on the cation migration via molecular dynamics simulations of halocarbon molecules in zeolite NaY and to elucidate the mechanism of such migrations. This has been performed using chloroform as the sorbate molecule in the first instance, and fluoroform and dichlorodifluoromethane in the second. One might expect some differences in the migration properties and their effect on the cations due to the fact the constituent atoms on the different molecules have different partial charges, and so the electrostatic interactions between the molecules and the cations would be different. Also, one must consider other non-bonded interactions, such as van der Waals interactions. Interactions between a certain type of atom in one molecule and a cation may be different to those of the same atom type in a different molecule and a cation. The experimental evidence further suggest that some of the migration occurs from SI' sites to SII sites. This would involve the crossing of a zeolite six ring, which would have an associated energy barrier. This barrier may also be affected by the aluminium content of the zeolite six-ring, as this would affect the flexibility of the ring. Therefore a second objective is to calculate the relative energy barriers to the cation migration, and

the effect of varying aluminium content on the six-ring. This work is described in chapter 5.

Electronic structure calculations can be used to extract information on the effect of the adsorption of these molecules on both the zeolite framework and the adsorbate molecule itself. These techniques can be used to study the changes in electron density on the zeolite framework's oxygen atoms upon adsorption, and also the polarisation of the adsorbate. One might ask the question of whether the factors controlling adsorption of molecules such as chloroform and fluoroform are local or whether the extended structure and the presence of cations have a role to play on the energetics of such a process. This would be an important piece of information, as it would help to determine the best model that can be used to represent the zeolite system when modelling such processes and situations. For example, how adequate is the use of a cluster quantum model? Do periodic quantum calculations offer a significant improvement over the cluster version? Details of such a study are reported in chapter 6.

Chapter 1 References

- (1) Thomas, J. M.; Thomas, W. J. *Principles and Practice of Heterogeneous Catalysis*; VCH, 1996.
- (2) Marcilly, C. *Studies in Surface Science and Catalysis* **2001**, 135, 37.
- (3) Smart, L.; Moore, E. *Solid State Chemistry: An Introduction*, 2nd ed.; Chapman and Hall, 1995.
- (4) Anderson, P. A.; Singer, R. J.; Edwards, P. P. *J. Chem. Soc., Chem. Commun.* **1991**, 915.
- (5) Anderson, P. A.; Edwards, P. P. *J. Chem. Soc., Chem. Commun.* **1991**, 914.

- (6) Anderson, P. A.; Armstrong, A. R.; Porch, A.; Edwards, P. P.; Woodall, L. J. *J. Phys. Chem. B* **1997**, *101*, 9892.
- (7) Woodall, L. J.; Anderson, P. A.; Armstrong, A. R.; Edwards, P. P. *J. Chem. Soc. Dalton Trans.* **1996**, 555.
- (8) Jaramillo, E.; Auerbach, S. M. *Journal of Physical Chemistry B* **1999**, *103*, 9589.
- (9) Buttefey, S.; Boutin, A.; Mellot-Draznieks, C.; Fuchs, A. H. *Journal of Physical Chemistry B* **2001**, *105*, 9569.
- (10) Fitch, A. N.; Jobic, H.; Renouprez, A. *Journal of Physical Chemistry* **1986**, *90*, 1311.
- (11) Foster, M. D. PhD Thesis, UCL, 2003.
- (12) Grey, C. P.; Ciruolo, M. F.; Lim, K. H. *Abstracts of Papers of the American Chemical Society* **1998**, *215*, 047.
- (13) Barthomeuf, D. *Studies in Surface Science and Catalysis* **1991**, *65*, 157.
- (14) Ono, Y.; Baba, T. *Catalysis Today* **1997**, *38*, 321.
- (15) Barthomeuf, D. *Catalysis Reviews-Science and Engineering* **1996**, *38*, 521.
- (16) George, A. R.; Sanderson, J. S.; Catlow, C. R. A. *Journal of Computer-Aided Materials Design* **1993**, *1*, 169.
- (17) George, A. R.; Catlow, C. R. A.; Thomas, J. M. *Journal of the Chemical Society-Faraday Transactions* **1995**, *91*, 3975.
- (18) Calmiano, M. D. Computer Simulation of Molecular Sorption in Zeolites, University College London, 2001.
- (19) Rees, L. V. C.; Shen, D. Adsorption of gases in zeolite molecular sieves. In *Introduction to Zeolite Science and Practice*; 2nd ed.; van Bekkum, H., Flanigen, E. M., Jacobs, P. A., Jansen, J. C., Eds.; Elsevier, 2001.
- (20) Yashonath, S.; Thomas, J. M.; Nowak, A. K.; Cheetham, A. K. *Nature* **1988**, *331*, 601.
- (21) Catlow, C. R. A.; Freeman, C. M.; Vessal, B.; Tomlinson, S. M.; Leslie, M. *Journal of the Chemical Society-Faraday Transactions* **1991**, *87*, 1947.
- (22) Sastre, G.; Corma, A.; Catlow, C. R. A. *Topics in Catalysis* **1999**, *9*, 215.
- (23) Mellot, C. F.; Davidson, A. M.; Eckert, J.; Cheetham, A. K. *Journal of Physical Chemistry B* **1998**, *102*, 2530.
- (24) Mellot, C. F.; Cheetham, A. K. *Journal of Physical Chemistry B* **1999**, *103*, 3864.

- (25) Davidson, A. M.; Mellot, C. F.; Eckert, J.; Cheetham, A. K. *Journal of Physical Chemistry B* **2000**, *104*, 432.
- (26) Grey, C. P.; Poshni, F. I.; Gualtieri, A. F.; Norby, P.; Hanson, J. C.; Corbin, D. R. *Journal of the American Chemical Society* **1997**, *119*, 1981.
- (27) Bosch, E.; Huber, S.; Weitkamp, J.; Knozinger, H. *Physical Chemistry Chemical Physics* **1999**, *1*, 579.
- (28) Sanchez-Sanchez, M.; Blasco, T.; Rey, F. *Physical Chemistry Chemical Physics* **1999**, *1*, 4529.
- (29) Mellot, C. F.; Cheetham, A. K.; Harms, S.; Savitz, S.; Gorte, R. J.; Myers, A. L. *Journal of the American Chemical Society* **1998**, *120*, 5788.
- (30) Lim, K. H.; Grey, C. P. *Journal of the American Chemical Society* **2000**, *122*, 9768.
- (31) Kaszkur, Z. A.; Jones, R. H.; Couves, J. W.; Waller, D.; Catlow, C. R. A.; Thomas, J. M. *J. Phys. Chem. Solids* **1991**, *52*, 1219.
- (32) Kawai, T.; Yanagihara, T.; Tsutsumi, K. *Colloid. Polym. Sci.* **1994**, *272*, 1620.

Chapter 2:

**General Overview of Some
Computational Chemistry
Methods**

Introduction

Chemistry is no longer considered to be a purely experimental subject¹, and in the areas of organic and inorganic chemistry computer modelling and simulation techniques play, an important role in applications such as the calculation of properties of compounds, elucidation of structure, designing new materials, prediction of protein conformations, drug design, the determination of active site, and numerous other complex problems. This is evident from the extensive use of computational chemistry methods in academia and industry. Over the past two decades the field has grown rapidly, concurrent with the increase in computer power.

Computational chemistry methods generally fall into two main categories: classical methods and electronic structure methods. The former allows treatment of systems containing up to the order of 10^5 atoms in a periodic model, and also treatment of individual molecules, whether small (e.g. small organic molecules) or large (e.g. proteins). This is achieved by the use of a set of interatomic potentials, or a 'forcefield', which describes the interactions between the constituent atoms (and/or ions) of the system, whether they be bonding or non-bonding interactions. These descriptions can then be used to calculate static and dynamic properties of the system under consideration.

Computational chemistry techniques based on classical interatomic potentials have been used to study a wide range of problems and systems, in both organic and inorganic chemistry. Our studies of cation placement in zeolites and docking of sorbate molecules have successfully used Monte Carlo methods. Low energy configurations can be found,

and the adsorption isotherms of the molecules can be predicted when performed within the Grand Canonical ‘ensemble’ (to be described later). Energy minimisation techniques can be used in conjunction with Monte Carlo methods to refine docking conformations. Molecular dynamics is used extensively to study diffusive properties of molecules in zeolites and calculate diffusion coefficients. Not limited to zeolites, this can be extended to studies in other materials such as ionic motion in perovskite oxides. One can use the techniques to calculate transport properties of liquids and transport across surfaces. The study of the structure of proteins, carbohydrates and other biomolecules are other applications. Data obtained from such simulations can be used to predict vibrational spectra via autocorrelation functions (velocity or dipole-dipole). As forcefield parameters have improved, comparison of properties derived from simulations (e.g. docking energies, diffusion coefficients, lattice constants, vibrational frequencies) with experimentally measured ones has become increasingly favourable.

Classical methods do not take into account the positions and motions of the electrons, relying only on nuclear positions and momenta (“alternative statement” of the Born-Oppenheimer approximation²). Effects due to electronic interactions are implicitly accounted for by the potential parameters, although polarisability of atoms is taken into account when the shell model of Dick and Overhauser³ is used. In this method, each ion is treated as a core with a massless shell connected together via a spring. The core represents the nucleus of the ion, while the shell represents the valence electrons and can be deformed in shape, thus representing polarisability due to interactions with other ions. This model is widely used in materials modelling and simulation, especially when performing calculations involving defects, for example in modelling superconducting oxides, the

photographic process, and in the modelling of solid oxide fuel cells, processes where movement of defects has proved to be a key aspect controlling the chemistry.

However, some studies, for example calculation of transition states and prediction of NMR shielding constants, and all problems involving the formation or breaking of bonds, and of polarisation, require an explicit treatment of the electrons in a system. For these studies methods such as Hartree-Fock and Density Functional Theory are used. The Hartree-Fock method attempts to solve the Schrödinger equation by finding the optimum coefficients for the set of wavefunctions that describe the system in question. Density Functional Theory relies on the proof by Hohenberg and Kohn⁴ that unique functionals of the electron density can be used to calculate the ground state energy of a system. Although exact solutions of the Schrödinger equation cannot be obtained for anything more complex than the hydrogen atom, current electronic structure methods can find solutions to an increasingly high degree of accuracy. As such these methods have been successfully applied to a number of systems, including complex oxide materials and zeolites. Applications have included studies of perovskite oxides, e.g. Li intercalation in V_2O_5 for battery systems⁵, determination of transition states and reaction mechanisms in zeolite catalysts and aluminophosphate materials⁶, such as in the study of the sidechain alkylation of toluene⁷, studies of reaction mechanisms on the surfaces of metals and metal oxides^{8,9}.

One more type of computational chemistry method exists and is known as the semi-empirical method. Semi-empirical methods can be used for electronic structure calculations, and use the same basic approximations as ab initio methods, although only the valence electrons are explicitly treated, and a minimal basis set is used to describe them.

Therefore the computational time required for these calculations is significantly lower than for ab initio methods.

Molecular Mechanics and Atomistic Methods

Atomistic methods are based on the theories of classical mechanics. They are useful in treating large systems as they calculate the energies of the system using nuclear positions only, and ignore the positions and motions of the electrons.

Atoms are treated using a 'ball and spring' model, and various equations based on classical physics are used to calculate the energy of the system. A fundamental aspect of these calculations is the forcefield, which describes the terms used in the energy calculations. The total energy of the system is calculated by summing the various contributions, and an example forcefield might contain terms shown below in equation 2.0.

$$E_{\text{total}} = E_{\text{bond}} + E_{\text{angle}} + E_{\text{torsion}} + E_{\text{nonbond}} \quad \text{Eq. 2.0}$$

Bond Stretch and Angle Terms

E_{bond} refers to the energy contribution from chemical bonds in the system. A function based on Hooke's Law can be used to describe this contribution, for example,

$$E_{\text{bond}} = \frac{1}{2} k (r - r_0)^2 \quad \text{Eq. 2.1}$$

where k is the spring constant and r_0 is the equilibrium bond length. The term is actually derived from a truncated Taylor expansion, and higher order terms can be neglected (as is the case here). This decreases the ‘computational cost’ of the calculation, and eradicates any artificial behaviour that would occur if the higher order terms were to be included. Such behaviour is illustrated if one was to include the cubic term in the series. This would cause the bond energy to tend towards negative infinity at long bond lengths. However, the use of only the quadratic term is also not ideal, as the function tends to positive infinity at long bond distances, and the function is thus useful only when the bonds are close to the equilibrium distance. A Morse function can be used instead to remedy the problems expressed by the harmonic function, as for long distances it converges towards the dissociation energy of the bond, as opposed to positive infinity, which is the behaviour that a harmonic term exhibits.

The form of a Morse function is:

$$E = D [1 - \exp(\alpha(r-r_0))]^2 \quad \text{Eq. 2.2}$$

D represents the dissociation energy, and α is a parameter related to the force constant.

E_{angle} refers to contributions from three body interactions, and can also be treated using a harmonic function, for example,

$$E_{\text{angle}} = \frac{1}{2} k (\theta - \theta_0)^2 \quad \text{Eq. 2.3}$$

θ_0 represents the equilibrium bond angle, and k represents a force constant. The same problems as for the bond stretching energy calculation exist for this term, and again, one

possible solution would be to include higher order terms. However, the confidence in such high order terms is currently at a low level, as insufficient experimental information is available for the parameterisation of the ‘higher order’ force constants.

Non-Bonded Interactions

Non-bonded terms are taken to be the sum of the van der Waals interactions and the Coulombic (electrostatic) interactions. The basic form of the potential for the interaction between two non-bonded particles could be defined as:

$$V(r_{ij}) = \frac{q_i \cdot q_j}{r_{ij}} + A \exp\left(\frac{-r_{ij}}{\rho_{ij}}\right) - \frac{C_{ij}}{r_{ij}^6} \quad \text{Eq. 2.4}$$

The first part of the function refers to the Coulombic interaction, with i and j being the interacting particles, q_i and q_j referring to the charges on each particle and r_{ij} being the distance between them. The contribution from this term is dealt with in many simulations of periodic systems by the Ewald summation method, which is outlined later on in this chapter.

The second part of the function accounts for the van der Waals interaction. In this particular case, a Buckingham potential is shown, with A, ρ and C being the potential parameters. The Buckingham term is made up of a repulsive part (the exponential term) and an attractive part (the r^{-6} term). The overlap of electronic wavefunctions causes the repulsions. Part of the justification of the choice of an exponential term to describe the

repulsive component arises from the fact that the decrease in electron density with increasing distance from the nucleus is approximately exponential.

A plot of energy vs distance for this function is shown in figure 2.1. The majority of computational chemistry studies of the solid state favour the use of the Buckingham form of describing non bonded interactions. The function is ideally suited to represent binding in ionic solids, due to the non-directionality of the bonds in such materials. Despite the fact that the bonding in zeolites is covalent, this approximation performs well for these materials also. Therefore, the Buckingham term has been used to describe the interactions in the zeolite model described later in this thesis.

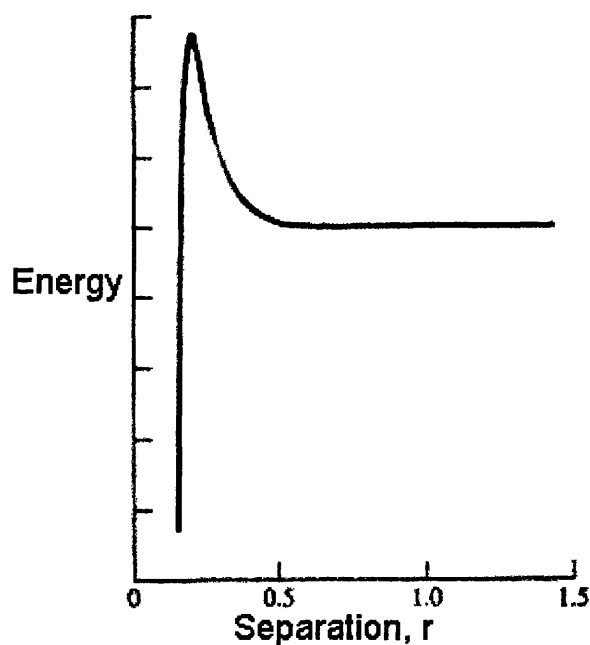


Figure 2.1: The Buckingham potential function for non-bonded interactions¹

Another way of treating van der Waals interactions is by the use of the Lennard-Jones function, which is shown below:

$$V(r_{ij}) = \left[\frac{A}{r^{12}} - \frac{B}{r^6} \right] \quad \text{Eq. 2.5}$$

Where A and B are adjustable parameters. The function also has another form i.e.

$$V(r_{ij}) = 4\epsilon \left[\left(\frac{\sigma}{r} \right)^{12} - \left(\frac{\sigma}{r} \right)^6 \right] \quad \text{Eq. 2.6}$$

where ϵ is the well depth, and σ is the separation at which the energy is zero. The r^{-12} part of the function is the repulsive component, and the r^{-6} part is the attractive component, this is illustrated in figure 2.2. The Lennard-Jones potential is traditionally used when dealing with liquid or gaseous systems.

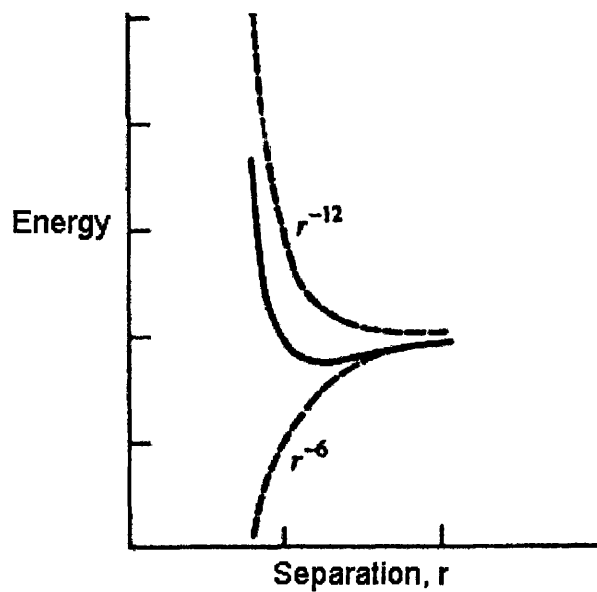


Figure 2.2: The Lennard-Jones Potential energy-separation plot, showing the repulsive and attractive components.¹

Other Terms

One final note on forcefield parameters is that ‘cross terms’ can be used to describe interactions such as simultaneous bond stretching and angle bending interactions. A description of such interactions can be important, depending on the purpose of the calculations, an example being the calculation of phonon frequencies. However, as before, inclusion of these extra terms would also mean an increase in computational effort for the calculation. Therefore one must balance the accuracy required for a calculation with the time and computational power available. However, the computer power currently available means that the balance is currently swinging in favour of accuracy when considering molecular mechanics calculations of systems containing about one thousand atoms or ions.

Energy Minimisation

In order to calculate properties of a system, a stable configuration of the atoms in the system must first be reached.¹⁰ This is done by using a technique called energy minimisation, which entails finding the minimum point on a potential energy surface generated by evaluating an energy function (such as that depicted in eq 2.0). The potential energy surface is analogous to a landscape with hills and valleys, with the minima being located in the valleys. The lowest energy minimum is the global minimum, while the others are referred to as local minima. There are various methods of minimisation, and the methods used in this work are derivative methods, i.e. they rely on finding the derivatives of the energy with respect to the system co-ordinates.

Steepest Descents

Steepest Descents is a method that moves an atom parallel to the net force on the said atom, and is analogous to walking straight downhill in our energy surface landscape. A direction is chosen, usually the one that has the steepest gradient from the starting point, and a line is followed from that point until the energy along that line is at a minimum. The direction of the search is then changed to one perpendicular to the current line, and the minimum along that direction is then found, and so forth. There are two ways of evaluating when a minimum is reached along a search direction:

1. A minimum is bracketed between two points of higher energy, and the distance between the two bracket points is reduced by an iterative procedure until a minimum is reached.
2. An arbitrary step approach can be employed where a step of arbitrary length is taken along the gradient vector (s_k), so that the new co-ordinates after a step k would be $x_{k+1} = x_k + g_k s_k$, where g_k is the step size. The step size is increased if the previous step results in a reduction of the energy. This continues until the energy increases again. At this stage the algorithm assumes that the search has jumped over the bottom of a minimum well, and so the step size is decreased again in order to reach the minimum.

The arbitrary step approach can require more steps to reach a minimum but often requires less function evaluations, and so therefore less computer time is used than the line search method.

The steepest descents method is a useful method when the starting configuration is far from the minimum, but converges slowly when approaching the minimum. A disadvantage of using the method is that the algorithm might explore areas of conformational space more

than once, hence its efficiency can be lower than other methods, such as conjugate gradients.

Conjugate Gradients

This method could also (and more properly) be called the conjugate directions method^{11, 12}. After each iteration the search is refined towards the minimum, as the algorithm gives a set of conjugate directions. This avoids the problem of searching conformational space that has already been covered, a problem that occurs when using the steepest descents method.

The direction vector h_{i+1} is calculated by adding the gradient, g , at the point $i+1$ to the previous direction h_i , which has been scaled by a constant γ_i .

$$h_{i+1} = g_{i+1} + \gamma_i h_i \quad \text{Eq. 2.7}$$

γ_i is defined in one of two ways:

1. The Polak-Ribiere method: $\gamma_i = \frac{g_{i+1} \cdot g_{i+1}}{g_i \cdot g_i}$ Eq. 2.8

2. The Fletcher-Reeves method: $\gamma_i = \frac{(g_{i+1} - g_i) \cdot g_{i+1}}{g_i \cdot g_i}$ Eq. 2.9

The next gradient is orthogonal to the previous one, and the direction is conjugate to the previous direction. The two methods have similar characteristics, although the Fletcher–Reeves method is more robust in certain cases.¹³

Second Derivative Methods

The Newton-Raphson method uses the second derivatives of the energy with respect to the co-ordinates, as well as the first derivatives. The second derivatives provide information about the curvature of the energy function. The method reaches a minimum in one step rather than the two needed for conjugate gradients, because the inverse of the second derivative matrix can be multiplied by the gradient to obtain a vector towards the nearest minimum. However, this method is computationally expensive as the second derivative matrix (called the Hessian matrix) and the inverse Hessian matrix are expensive to calculate.

Quasi-Newton methods attempt to circumvent this by gradually building up the inverse Hessian matrix at each iteration. Each new position at iteration k is obtained from the current position, x , the gradient, g , and the current inverse Hessian matrix, H .

$$x_{k+1} = x_k - H_k g_k \quad \text{Eq. 2.10}$$

Second-derivative methods are not useful if the system is far from the minimum, as the minimisation may become unstable, and it would take a long time to reach a minimum. An

appropriate strategy for minimisation might therefore be to use a method such as steepest descents or conjugate gradients when the system is far from the minimum, and then change to a second derivative method as the system nears a minimum, which will result in a faster convergence.

Periodic Boundary Conditions

Having set up a system of atoms, ions or molecules, one may wish to calculate various bulk properties, and look at the system's evolution over time. For solids, and for calculations involving other bulk systems, Periodic Boundary Conditions (PBC) can be applied to the system in order to eliminate surface effects and to allow the calculation of bulk properties.

In PBC, a unit cell of volume V , containing N particles is periodically repeated in three dimensions. Calculations are performed on the original cell, but the image cells and their contents are allowed to interact with each other and with the original cell. The number of particles in each cell is kept constant because all the image particles move in the same way as those in the original cell. For example, if a particle were to move from one cell to another, it would be replaced in the original cell by its image from the opposite cell. Here are two methods for treating image particles.¹³

1. **Minimum Image Model:** In this model, the particles in the original cell can only interact with a particle or image particle that is closest to it, whether the molecule is from the

original cell or not. The maximum cut-off distance for this model is half of the smallest unit cell dimension or half of the smallest length of the simulation box. Simplicity is the main advantage of this method, as only interactions with the closest particle are considered. The molecular dynamics algorithm used for the calculations presented in this thesis uses the minimum image convention.

2. Explicit Image Model: All image particles within a specified cut-off distance are considered and allowed to interact with the original particles. This means that image particles from all directions are considered to be interacting with the original at any one time.

Long Range Forces: Ewald Summation

The Ewald summation method^{11,14-16} is used to treat long range electrostatic forces between pairs of ions within the system. It is a technique that forces the fast convergence of summations which would otherwise converge slowly.

Interactions that decay no faster than r^{-n} , where n is the dimensionality of the system are problematic, especially since their range is usually greater than half the box length. For example, when calculating the Coulombic interactions on a periodic system, the Coulombic term is proportional to r^{-1} , and so this is the fastest that the function can decay.

One might consider the problem by imagining the system being built up as a series of simulation boxes in three dimensions, which can be imagined in the form of a sphere. When considering such a sphere, the surface area of the sphere, and therefore also the number of points over which the Coulomb summation must take place increases in proportion to r^2 . This is much greater than the rate at which the Coulombic term decays. Considering a spherical array of simulation boxes with the central box positioned at cubic lattice point n , the sum of the Coulombic interactions can be written as:

$$V = \frac{1}{2} \sum_{n=0}^{\infty} \left(\sum_{i=1}^N \sum_{j=1}^N \frac{q_i \cdot q_j}{4\pi\epsilon |r_{ij} + n|} \right) \quad \text{Eq. 2.11}$$

The prime in the first summation indicates that the scenario where $i = j$ for $n = 0$ is not included. However the summation detailed above converges very slowly and does not have a finite sum. The slow convergence is also due to the fact that the number of points is proportional to r^2 , whereas the energy decay is proportional to r^{-1} .

The Ewald method provides a solution to this problem. The summation is converted into two finite series, which both converge much more rapidly. Considering each point charge, a Gaussian charge cloud of equal value but opposite sign is placed over each charge, thus neutralising the point charges. This now gives a summation of the point charges plus the neutralising charges, and can be expressed as

$$V = \frac{1}{2} \sum_{n=0}^{\infty} \left(\sum_{i=1}^N \sum_{j=1}^N \frac{q_i \cdot q_j}{4\pi\epsilon} \frac{\text{erfc}(\alpha |r_{ij} + n|)}{|r_{ij} + n|} \right) \quad \text{Eq. 2.12}$$

where *erfc* is an error function, and α is a parameter in the Gaussian distribution. Another summation is also performed, but this time, it is a summation of the Gaussian charge cloud in reciprocal space, the form of which is:

$$V = \frac{1}{2} \sum_{\mathbf{k} \neq 0} \left(\sum_{i=1}^N \sum_{j=1}^N \frac{1}{\pi L^3} \frac{q_i \cdot q_j}{4\pi\epsilon} \frac{4\pi^2}{k^2} \right) \quad \text{Eq. 2.13}$$

The reciprocal sum also converges more rapidly than the original summation, and is added to the first Gaussian distribution, thereby cancelling the charge cloud. The real space and reciprocal space calculations must balance exactly, and to do this the value for α must be carefully chosen. Various other error functions also can be taken into account, for example a self-term must be subtracted due to the fact the sum of Gaussian functions in real space includes the interaction of each Gaussian with itself. Also a correction term must be added to the calculated energy, depending on the medium in which the simulation takes place.

The Ewald method is the most popular method for the calculation of long range forces, and it has been deemed to be the most accurate method available, despite the fact that it is fairly computationally expensive.¹¹

Molecular Dynamics

As will be illustrated in later chapters, the molecular dynamics technique can be useful in studying transport properties of molecules and ions in zeolites and other porous materials.

The technique allows the calculation of time dependent properties, such as diffusion coefficients, something that cannot be calculated using the time independent Monte Carlo methods (described later in this chapter). Use of the technique can help to enhance the interpretation of ambiguous experimental results, such as implications of diffusion of species and the diffusion mechanisms. One can extend the analysis of the trajectories calculated by a molecular dynamics algorithm to the calculation of vibrational spectra by the use of dipole-dipole autocorrelation functions and velocity autocorrelation functions.

The molecular dynamics method uses Newton's laws of motion and applies them to atoms and molecules within a system to calculate their movements and energies over time.

The particles in a system can be imagined to interact through a potential U_N , which is defined as:¹⁷

$$U_N = \frac{1}{2} \cdot \sum_i \sum_j \phi(r_{ij}) \quad \text{Eq. 2.14}$$

where Φ is the chemical potential, and r_{ij} is the distance between two particles. This means that the equation of Newton's Second Law can be expressed as:

$$m_i a_i = \sum_{i \neq j} \frac{1}{r_{ij}} \frac{d\phi}{dr_{ij}} r_{ij} \quad \text{Eq. 2.15}$$

m_i is the mass of particle i , a_i is the acceleration. This is comparable with the basic equation for calculating the forces on a molecule or atom in molecular dynamics (MD) i.e.

Newton's Second Law

$$F = m a \quad \text{Eq. 2.16}$$

F is the force on the atom or molecule, m is the mass of the molecule or atom, and a is the acceleration of the atom. Various algorithms exist for the integration of the equations of motion, the most popular being the Verlet algorithm¹⁸, developed in 1967.

The force can be obtained from the potential energy function $U_N(r)$. Therefore the force, F , would be

$$\frac{-dU_N}{dr} = m \cdot a \quad \text{Eq. 2.17}$$

Now, a is the second derivative of displacement with respect to time, therefore

$$\frac{-dU_N}{dr} = m \frac{d^2 r}{dt^2} \quad \text{Eq. 2.18}$$

Integrating twice with respect to time gives:

$$r = ut + \frac{1}{2}(at^2) + k \quad \text{Eq. 2.19} \quad (\text{equivalent to } r = ut + \frac{1}{2} (F/m)t^2 + k)$$

where k is a constant and u is the initial velocity. After displacement, the position of the atoms after a time, T , can be calculated using a Taylor Series type function:

$$r(t + T) = r(t) + \frac{dr}{dt} T + \frac{d^2r}{dt^2} \frac{T^2}{2} + \dots \quad \text{Eq. 2.20}$$

Verlet's algorithm also uses the information from previous step to calculate

$$r(t - T) = r(t) - \frac{dr}{dt} T + \frac{d^2r}{dt^2} \frac{T^2}{2} - \dots \quad \text{Eq. 2.21}$$

Adding the two equations gives Verlet expression for calculating the next position:

$$r(t + T) = 2r(t) - r(t - T) + \frac{d^2r}{dt^2} T^2 + \dots \quad \text{Eq. 2.22}$$

The initial velocities can be assigned at random from a Maxwell-Boltzmann function corresponding to the temperature that the system is at. Equation 2.18 can be used to calculate the acceleration and equation 2.22 to calculate the new co-ordinates, using the term $r(t + T)$. T is the timestep, and this is usually set to be 10^{-15} seconds, or 1 femtosecond. A timestep this small is used to overcome errors generated by the assumption that the acceleration is constant throughout the simulation. One should also ensure that the timestep used is smaller than the time period of any thermal vibrations of bonds in the

constituents of the system. Furthermore, errors arising from the truncation of the Taylor expansion can be minimised by the use of a small timestep.

The Leapfrog Verlet^{11,14} algorithm is useful for minimising such errors, and any errors that may occur due to the truncation of the Taylor series. In this algorithm, the velocity, v , is assumed to be almost equal to the velocity at time $(t+\frac{1}{2} T)$ is used to calculate the new position:

The new velocity is first calculated from the midpoint velocity in the previous interval, and the average acceleration. The acceleration is calculated using Newton's Second Law.

$$v(t + \frac{1}{2} T) = v(t - \frac{1}{2} T) + T \cdot a(t) \quad \text{Eq. 2.23}$$

From the newly calculated velocity, one can deduce the position $x(t + T)$ by:

$$x(t + T) = x(t) + T \cdot v(t + \frac{1}{2} T) \quad \text{Eq. 2.24}$$

Thus one can see the origin of the name of the algorithm. The velocities 'leapfrog' over the positions to give their values at $t + \frac{1}{2} T$. The positions then leapfrog over the velocities to give their values at $t + T$. Although the algorithm explicitly includes the velocities, a disadvantage is that the positions and velocities are not synchronised.

Equilibration and Production Phases of the Calculation

During a molecular dynamics simulation, the period of time when data is collected from which dynamical properties can be calculated is called the *production phase*. At the start of

this phase, the constituents of the system should have the necessary velocity and force vectors consistent for the temperature and pressure being simulated, so that when the production phase starts, all properties calculated can be considered valid for that temperature and pressure. The *equilibration phase* of a simulation precedes the *production phase* and its purpose is to allow the system to ‘equilibrate’ to the required temperature and pressure. The length of this phase should be sufficient that parameters such as temperature and energy are constant, and all memory of the initial configuration is lost. The initial velocities are distributed to the atoms from a Maxwell distribution. During the course of the equilibration, the velocities are scaled so as to maintain a constant temperature.

Some analyses applied to MD simulations

Having performed a molecular dynamics simulation and obtained information on the trajectories and velocities of the system’s constituents, one may wish to calculate various properties, such as transport coefficients, or vibrational spectra.

Assuming that an atom or molecule is diffusing through a homogeneous medium, its diffusion coefficient can be calculated via the mean square displacement:

$$\langle \Delta r^2(t) \rangle = \langle | \mathbf{r}(t) - \mathbf{r}(0) |^2 \rangle \quad \text{Eq. 2.25}$$

The Einstein relation links the three dimensional diffusion coefficient, D , to the MSD by:

$$6Dt = \langle \Delta r^2(t) \rangle \quad \text{Eq. 2.26}$$

The equation can be derived from Fick's law of diffusion, which for one dimensional diffusion, states that the mean square displacement of the atoms in one dimension is proportional to $2Dt$. The three dimensional analog is shown above (equation 2.26). Therefore the gradient of a plot of the MSD against simulation time can be used to calculate the diffusion coefficient of a migrating species in a simulated system.

Vibrational frequencies can be predicted from molecular dynamics simulations by the Fourier transform of the autocorrelation functions calculable from information derived from the molecular dynamics trajectory. The fact that spectroscopic methods are widely used in the study of zeolites makes comparison with experiment possible.

Velocity autocorrelation functions give an indication of the 'memory' of the velocity of certain particles in the system. In this case, the velocity at time t is correlated with a velocity at time 0. Equation 2.27 shows the calculation of a normalised VACF, averaged over N , the number of particles of interest. Its Fourier transform reveals the power spectrum which gives vibrational frequencies for the species being studied. Information gleaned from such a power spectrum can be compared to inelastic neutron scattering data. If one wished to simulate the infrared spectrum, then the Fourier transform of the dipole-dipole correlation function is used.

$$VACF(t) = \frac{1}{N} \sum_{i=1}^N \frac{\langle v_i(t) \cdot v_i(0) \rangle}{\langle v_i(0) \cdot v_i(0) \rangle} \quad \text{Eq. 2.27}$$

One final piece of analysis that is commonly performed is the calculation of the radial distribution function. This function gives the probability of finding a particle at certain distances from another defined particle, and can give an idea of the structure within a system.

Monte Carlo Methods

Monte Carlo simulations are based on statistical mechanics, and samples from phase space from a particular ensemble. The name 'Monte Carlo' arises from the fact that random numbers are used extensively in the calculation. Two types of Monte Carlo simulations are used in the work described in this thesis, Canonical Monte Carlo and Grand Canonical Monte Carlo. The elements of each method are outlined below.

If one wished to calculate a particular property, Q , in a particular ensemble (say the canonical ensemble, described later), then the average value of Q could be written as

$$\langle Q \rangle = \int Q(X)P(X)dX \quad \text{Eq. 2.28}$$

where X represents all states of the system, and P is the Boltzmann weighted factor:

$$P(X) = \frac{\exp\left[-\frac{U}{k_B T}\right]}{\int \exp\left[-\frac{U}{k_B T}\right]} \quad \text{Eq. 2.29}$$

where U is the internal energy of the system, T is the temperature and k_B is Boltzmann's constant.

Making random moves, such as translations and rotations, to the system and sampling different configurations could solve the above integrals. However, only low energy configurations would make a significant contribution to $P(X)$, and so proper sampling has not been achieved, as only a small number of configurations will contribute to $P(X)$. The Metropolis method^{11,14} provides a solution to this by accepting contributions to $P(X)$ if the move made has a probability of occurring that is proportional to the Boltzmann factor.

Random moves are made to particles in the system. If the energy of the new configuration is lower than that of the old configuration, then it is accepted immediately.

If the energy of the new configuration is higher than that of the old configuration, then the Boltzmann factor of the energy difference between the two configurations is calculated. This is then compared to a random number between 0 and 1. If the Boltzmann factor is higher than the random number, the configuration is accepted, else the new configuration is rejected, and the system reverts back to the previous configuration for another iteration. The procedure therefore allows moves to states of higher energy and to escape from local minima, allowing the sampling to take place over a wider area of space.

For Grand Canonical Monte Carlo simulations, the sampling is from the Grand Canonical ensemble, which is described later in this chapter. The pressure is fixed, but the number of molecules is allowed to vary. This means that as well as translation and rotation, moves

involving the creation and destruction of molecules are allowed, and these moves also have associated probabilities of occurring.

The probability of creating a molecule, P_c is

$$P_c = \min \left[1; \exp \left(-\frac{\Delta E}{k_b T} - \ln \frac{(N_i + 1)k_b T}{f_i V} \right) \right] \quad \text{Eq. 2.30}$$

where f is the fugacity and N represents the current number of molecules in the system and the probability of destroying a molecule is

$$P_c = \min \left[1; \exp \left(-\frac{\Delta E}{k_b T} + \ln \frac{N_i k_b T}{f_i V} \right) \right] \quad \text{Eq. 2.31}$$

Grand Canonical Monte Carlo is useful for the calculation of adsorption isotherms. There are a number of practical considerations when Monte Carlo methods are applied to sorption in zeolites; for example, one should take into account the possibility of the creation of molecules in unrealistic situations. For instance, in the case of faujasite-structured zeolites, placement of most sorbates in the sodalite cages must be excluded as it would generally not be possible for them to enter and reside within the cage.

Statistical Ensembles

Computer simulations can be performed under various conditions (or constraints). There are a number of standard ensembles in which simulations are performed, details of which follow.

The microcanonical ensemble: In this ensemble, N , the number of particles is kept constant during the simulation, along with the cell volume, V , and the energy of the system, E . The microcanonical ensemble is also known as the NVE ensemble, and traditionally molecular dynamics simulations are performed under this ensemble.

The canonical ensemble: Also called the NVT ensemble, the number of particles, N , the volume, V , and the temperature, T , of the simulation is kept constant during the simulation.

The grand canonical ensemble: Volume, temperature and chemical potential are kept fixed in this ensemble, and it is also called the μ VT ensemble. Simulations performed under this ensemble are performed under fixed pressure.

Associated with each ensemble is a probability density function (or distribution function) that gives the probability density i.e. the probability of finding a certain configuration in phase space. During a molecular dynamics simulation it is necessary to reproduce the distribution function for the ensemble in which the simulation is being performed. This can

be done by modification of the motion of the particles in the system. There are three main ways of doing this:¹⁷

1. Stochastic Methods: A thermal bath can be mimicked by randomly re-selecting a particle's velocity from the Boltzmann distribution. This is done at various intervals, and keeps the probability density within the canonical ensemble.
2. The Extended System method is where one or more additional degrees of freedom are added, acting as external constraints (e.g. a heat reservoir). This produces distributions from NVT or NPT ensembles.
3. In the Constraint Method the velocities are scaled by a factor $(T/T_j)^{1/2}$ after each time step. T is the actual temperature at that time, and T_j is the desired temperature. This keeps the temperature constant thus mimicking the NVT ensemble. Hoover *et al.*^{17,19} and Evans^{17,20} have investigated this method, and molecular dynamics codes such as DLPOLY, and Monte Carlo codes use their equations to mimic the NVT ensemble.

Electronic Structure (or Quantum Mechanical) Methods

Some problems in computational chemistry or physics cannot be solved by using classical methods, due to the fact that these methods do not explicitly treat the electronic degrees of freedom. Therefore problems such as the calculation of NMR spectra, studies of transition states and general studies of the electronic effects of intermolecular or interionic

interactions must be studied using electronic structure methods. These methods fall into two broad categories, namely ab initio ('from the beginning') and semi-empirical methods. Both types will be outlined, as both types are used in this thesis (chapter 6).

Brief Background to Electronic Structure Methods and Hartree Fock Theory

Quantum mechanical techniques are aimed at finding the solution to the time independent form of Schrödinger's equation,

$$H \Psi = E \Psi \qquad \text{Eq. 2.32}$$

where H is the Hamiltonian operator, from which the kinetic energy and potential energy of the electrons and nuclei may be derived. E is the energy (and eigenvalue), and Ψ , the wavefunction, represents the spatial coordinates of the particles in the system in the time independent form. The square of the wavefunction is the probability of finding electrons in a certain region of space.

The Schrödinger equation is generally acknowledged to be exactly solvable for the hydrogen atom only, as this atom has only one electron. As with all computational techniques, approximations are used in order to make the calculations of more complex systems than the hydrogen atom possible within a reasonable time. A major approximation is the separation of nuclear and electronic motions. The nuclei are considered to be much more massive than the electrons, so the electrons can instantaneously adjust to any change in the positions of the nuclei (the Born-Oppenheimer approximation). This means that the electronic wavefunction depends only on the nuclear positions, and not on their momenta.

Therefore, as a result, two Schrödinger equations can be written, one describing the electronic motions, and the other one describing the nuclear motions along the potential energy surface, which is a solution of the electronic wavefunction.²

In the case of polyelectronic systems, the ‘many electron wavefunction’ is set up as a combination of one electron wavefunctions (electron orbitals). These orbitals have to change sign when two electron coordinates are interchanged (the antisymmetry principle). This is in accordance with the Pauli principle, which states that no two electrons can have the same set of quantum numbers. The antisymmetry requirement is fulfilled by representing the total wavefunction as a Slater Determinant – essentially a matrix with the columns representing one electron wavefunctions and the rows representing the electron coordinates. Such a matrix mathematically preserves the physics of a system.²

According to the variational theorem, the wavefunction used will give a higher energy than the true wavefunction due to the fact that a number of approximations are made in calculating it. The Hartree-Fock method involves finding the optimum molecular orbital coefficients for the used wavefunction via the means of a ‘self consistent field method’ (SCF), but under the constraint that the molecular orbital remains orthonormal. A method of solving this type of problem is offered by the use of Lagrange multipliers. The Hartree-Fock equation is:

$$FC = SC\varepsilon \qquad \text{Eq. 2.33}$$

F represents the Fock matrix, which contains information on the kinetic energy of the electron, the electron-electron repulsion (exchange operator) and the nuclear-electron interaction (Coulomb operator). S represents the overlap integral between two orbitals and C is the matrix of the molecular orbital coefficients. ϵ is an eigenvalue matrix. The equation is solved via the SCF method, which attempts to improve the MO coefficients iteratively until convergence. The method is also known as the Roothaan-Hartree-Fock method, as the equations were also proposed by Roothaan and Hall simultaneously.

Basis Sets

Basis sets are essentially a collection of wavefunctions (or atomic orbitals) that describe the electrons in an atom. There are two common types of orbitals.

1. Slater type orbitals (STOs), which have the form:

$$\chi_{\zeta, n, l, m}(r, \theta, \varphi) = N Y_{l, m}(\theta, \varphi) r^{(n-1)} e^{-\zeta r} \quad \text{Eq. 2.34}$$

2. Gaussian type orbitals (GTOs) of the form:

$$\chi_{\zeta, n, l, m}(r, \theta, \varphi) = N Y_{l, m}(\theta, \varphi) r^{(2n-2-l)} e^{-\zeta r^2} \quad \text{Eq. 2.35}$$

As can be seen from the above two functions, a Gaussian type orbital depends on an r^2 term in the exponential, whereas STOs do not. This makes GTOs inferior to STOs. Although Slater type orbitals give good descriptions of electron densities, they are difficult to evaluate and computationally more expensive than GTOs. Therefore, a significant number of ab initio programs use basis sets based on Gaussian-type orbitals. However, a GTO does not give a true description of the electron density around a nucleus (a consequence of the r^2

term), and so therefore more GTOs are needed in a basis set in order to overcome this deficiency (a rough guideline is that three times as many GTOs as STOs are required to reach the same level of accuracy in a calculation). However, the relative ease with which GTOs can be evaluated is a factor in their extensive use in ab initio calculations.

The level of accuracy of an ab initio calculation is dependent on the size of the basis set used. The smallest number of orbitals required to accommodate all of the electrons in an atom in their ground state is known as a minimal basis set. An example is the STO-3G basis set which is a contraction of 3 Gaussian functions to represent a STO. Doubling the number of basis functions for each orbital yields a double zeta basis set, so called because of the ζ exponent in the orbital functions, and because the number of functions have doubled.

Diffuse functions are basis functions with small exponents and are used in order to treat cases where there might be excited states, anions, or any other cases where loosely bound electrons are present. They are also used to describe polarisation. These types of functions are used in the double zeta basis set.

One should bear in mind that increasing the number of functions in a basis set will also mean an increase in computational cost. One might solve this by consideration of the fact that the valence electrons are involved in chemical bonding, whereas the core electrons are not, and therefore are relatively unaffected by the chemical environment. Split valence basis sets are used to counter this problem. For example, in the case of a double zeta basis set, only the functions describing the valence electrons are doubled. Another example is

the 3-21G basis set, where 3 primitive (individual) Gaussians are used to describe the core electrons and the valence electrons are described by two contracted Gaussian and a diffuse function.

The next level of improvement in basis sets are polarised basis sets. Here d orbitals are added to non-hydrogen atoms, allowing the electron density to polarise in energetically favourable directions. An example of such a basis set is the 6-31G* basis set. 6 Gaussian primitives are used for the core orbitals, and the valence electrons are treated using 3 Gaussians for the inner valence orbitals and 1 for the outer valence orbitals. The star signifies the d orbitals for the non-hydrogenic atoms. Polarisation for hydrogen atoms can be treated using the 6-31G** basis set, which includes a set of p functions for the hydrogen atoms.

Density Functional Theory

One of the reasons for the growth in the popularity of this method has been its advantages of computational speed over Hartree-Fock theory based methods. Furthermore, another attractive feature of this method is the fact that electron correlation is explicitly taken into account in the calculations, unlike in Hartree-Fock methods. Also, the discovery of more accurate approximations to the exchange-correlation density functional has contributed to the boom in the usage of density functional theory to calculate the properties of materials and other chemical systems.

The underlying principle of Density Functional Theory is that the energy of the system in the ground state can be expressed as a functional of the electron density, $\rho(\mathbf{r})$, as proposed by Hohenberg and Kohn.⁴

The total energy of the system is defined as

$$E[\rho] = E_{ne} + E_{ee} + E_K + E_{XC} \quad \text{Eq. 2.36}$$

where E_{ne} is the energy due to the nuclei-electron interactions, E_{ee} is the energy due to interactions between the electrons, E_K is the kinetic energy of the electrons, and E_{XC} is an exchange–correlation term, which represents a major difference between Hartree Fock and Density Functional Theory. In Hartree-Fock, the electron exchange term is included and calculated exactly, whereas electron correlation is not. E_{ee} is also known as the Hartree energy and can be defined as the Coulombic interaction of a system of non-interacting electrons. As for Hartree-Fock methods, the nuclear interaction energy can be separated from those due to electronic interactions using the Born-Oppenheimer approximation, and so express the energy as:

$$E(\rho) = \int V_N(\mathbf{r})\rho(\mathbf{r})d\mathbf{r} + V_e(\rho) \quad \text{Eq. 2.37}$$

V_N is the potential due to the nuclei and V_e includes the Hartree energy, kinetic energy of the electrons, and the exchange correlation term.

Now, the variational principle can again be invoked here in order to calculate the ground state energy of the system. The energy calculated from a function of the electron density will always be greater than the true energy. Therefore the problem is one of minimising the energy function with respect to the changes in the electron density.

As in Hartree-Fock theory, this is achieved via the use of Lagrange multipliers, an elegant method of solving constrained optimisation problems. The Lagrange multiplier method leads to a set of canonical (Kohn-Sham) orbitals. In Kohn and Sham's method²¹, the electron density is represented as if it was derived from a single Slater determinant with orthonormal orbitals thus enabling the energy to be optimised using a set of one-electron orbital equations. The resulting eigenvalue equation is known as the Kohn-Sham equation.

$$E_i \Psi_i = \left[-\frac{\nabla^2}{2} + V_N + V_{ee} + V_{xc} \right] \Psi_i \quad \text{Eq. 2.38}$$

One of the major goals of research in Density Functional Theory is to find a functional that can represent the exchange-correlation term exactly. Such a functional would lead to the calculation of the exact ground state energy. Functionals available so far fall under the umbrella of one of two schemes: Local Density Approximation or Generalised Gradient Approximation.

Local Density Approximation (LDA) states that E_{xc} at any point only depends on the electron density at that point.

$$E_{xc} = \int \rho(r) \epsilon_{xc}(\rho(r)) dr \quad \text{Eq. 2.39}$$

where ϵ_{xc} is the exchange-correlation energy per electron, which has already been determined for a uniform gas. LDA is a generally successful method, reproducing geometries well, although it has been found to overestimate binding energies. This can be disadvantageous for calculations of thermodynamic properties such as heats of adsorption. A variant on the LDA method is the Local Spin Density Approximation (LSDA). In LSDA, the individual spin densities are incorporated in a more explicit fashion than the LDA version of the method, thus allowing a better representation of open shell systems. For closed shell systems, the LDA and LSDA are equivalent.

Improvements to the LDA method should not consider the electron density as a uniform electron gas. The Generalised Gradient Approximation (GGA) attempts to correct for the shortfalls of the energy calculations of LDA by using the gradient of the electron density as well as the density itself. The energy is expressed as

$$E_{xc}^{GGA} = E_{xc}^{LDA} + E_x(\rho'(r)) + E_c(\rho'(r)) \quad \text{Eq. 2.40}$$

E_x and E_c are correction terms for the exchange and correlation energy respectively, and are calculated from the first derivative of the electron density, ρ' .

Semi Empirical Methods

Semi-empirical computational methods are considered as “in between” the methods based on classical mechanics and those based on quantum mechanics. Indeed these methods share common ground with both of their ‘neighbours’. Experimentally determined parameters are employed in semi-empirical methods, as is the case with classical methods. The same basic theoretical assumptions are made in semi-empirical methods as for quantum mechanical methods. However the level of approximation used is far more extensive. This means that computational time is much reduced, due to the fact that the evaluation of the large number of terms used in *ab initio* work is avoided. The method instead relies on experimentally determined parameters, thus still resulting in chemically useful accuracy.²

The methods are based on the Hartree-Fock method, except that in semi empirical methods the valence electrons are treated explicitly, and only a minimal basis set is used to describe them. The core electrons are accounted for by reducing the nuclear charge, so in effect the core electrons are assumed to screen the nucleus.

As mentioned, the Hartree-Fock equations are solved in semi empirical methods, except that approximations are made in the construction of the Fock matrix. A major feature is that the overlap between different pairs of orbitals is set to zero. This is known as the Zero Differential Overlap approximation. The overlap matrix, S , is reduced to a unit matrix and one-electron integrals are set to zero. Furthermore, another consequence of the ZDO approximation is that many of the two electron integrals present in the Fock matrix are

neglected. The remaining integrals are treated using experimentally derived parameters. Each different semi-empirical method has its own level of parameterisation, and defines how many integrals are to be neglected. A brief description of some common methods follows.²

NDDO: Neglect of Diatomic Differential Overlap. This method makes no further approximations apart from those described for the ZDO approximation. All three- and four-centre two-electron integrals are neglected.

INDO: Intermediate Neglect of Differential Overlap. In INDO, the NDDO approximations are made, but many two-centre two-electron integrals are neglected as well. This method is intermediate between NDDO and CNDO.

CNDO: Complete Neglect of Differential Overlap. Only a small number of one- and two-centre two-electron integrals remain (the Coulomb integrals). The atomic orbitals are assumed to be spherical when evaluating the two-electron integrals.

MINDO/3: Modified INDO: This is an attempt to parameterise INDO and gives quite reasonable results. It uses a set of parameters based on pairs of bonded atoms to approximate the two-electron repulsion integrals.

Modified Neglect of Diatomic Orbitals (MNDO) and Austin Model 1 (AM1)

Two other methods developed by Dewar and Thiel^{2,22} are available, and were used in the electronic structure calculations described later in this thesis: MNDO^{2,22} and AM1²³. Both of these methods are parameterisations of the NDDO model. The parameterisation is in terms of atomic variables, referring to the nature of a particular single atom only. Both methods consider only valence s and p functions and are taken as Slater type orbitals. Overlaps of one electron integrals are parameterised by reduced nuclear charges and the two electron integral. Two electron integrals are calculated explicitly, thereby differing from the ZDO approximation. Hence the reason why the method includes the word ‘modified’ in its name. The two models also include core-core repulsions. This is the repulsion between the reduced nuclear charges, and treated using a modified version of the ‘exact’ equation:

$$Z_a' Z_b' / R_{ab} \quad \text{Eq. 2.41}$$

where Z_a' and Z_b' are the charges, and R_{ab} is the separating distance. However, a problem arises due to the many approximations made in the NDDO model. The nuclear-nuclear repulsions are not cancelled by the electron repulsion terms at long distances, resulting in a net repulsion between uncharged molecules or atoms. Each method (AM1 and MNDO) has its own functional to deal with this problem. MNDO has limitations such as it is unable to predict H bonds, and over-predicts activation energies in general. It may also over-predict bond lengths and under-predict angles in some systems. AM1 is a successor to the MNDO model, and the method was developed in order to overcome the systematic errors in the MNDO model. The problems with MNDO are said to be due to the overly repulsive core-

core interaction parameters. In the AM1 model, Gaussian functions are present in the core-core functional, and the model contains entirely new parameters. However, there are cases when MNDO is more suitable than AM1, and the work described in chapter 6 serves as an example. More details can be found in that chapter and references therein.

Population Analysis: Mulliken Population Analysis

Having performed electronic structure calculations, one might wish to extract information on the charge distribution within the system. Mulliken population analysis is a popular method of assigning charges to atomic centres in a system. In the Mulliken method, the basic philosophy is to separate the electron densities associated with a particular bond into atomic contributions. However, because it is not obvious how one might split electron density that is spread over space into particular atomic contributions, the method is somewhat arbitrary. The density matrix is used, with the diagonal elements making up the areas where the electron density, $P_{\mu\mu}$, is located¹¹. The off-diagonal elements represent the overlap population, $\phi_{\mu}\phi_{\nu}$, and this is shared equally between the two atoms with which the atomic orbitals ϕ_{μ} and ϕ_{ν} , are associated. The net charge, q_A is then calculated by subtracting the electronic charge from the nuclear charge, Z_A , using the following equation:

$$q_A = Z_A - \sum_{\mu A}^n P_{\mu\mu} - \sum_{\mu A}^n \sum_{\nu \neq \mu}^n P_{\mu\nu} S_{\mu\nu} \quad \text{Eq. 2.42}$$

The method does have a number of shortcomings. The method of charge partitioning is a shortfall, since it splits the charge equally between atoms with no consideration of the electronegativities of each atom. It is also very basis set dependent, and so the size of the basis set will have an effect. If a large number of basis functions are used, then a reasonable wavefunction to describe an atomic orbital might be obtained. However, in the case of atoms with p, d and f orbitals, which are spread quite far from their associated nucleus, the electrons will still be assigned to the atom where the atomic orbital is centred, even if the electron is far from the nucleus and closer to another atom.

Despite its shortcomings, the technique is still very useful, since trends in changes of charge density can be gleaned from information on Mulliken charges. However, one must be careful to only compare calculations that use the same basis set.

Chapter 2 References

- (1) Richards, W. G.; Grant, G. H. *Computational Chemistry*; Oxford University Press, 1995.
- (2) Jensen, F. *Introduction to Computational Chemistry*; John Wiley and Sons Ltd, 1999.
- (3) Dick, B. G.; Overhauser, A. W. *Phys. Rev* **1958**, *112*, 90.
- (4) Hohenberg, P.; Kohn, W. *Phys. Rev.* **1964**, *B864*, 136.
- (5) Braithwaite, J. S.; C.R.A., C.; Gale, J. D.; Harding, J. H.; Ngoepe, P. E. *J. Mat. Chem* **2000**, *10*, 239.
- (6) Barker, C. M.; Gleeson, D.; Kaltsoyannis, N.; Catlow, C. R. A.; Sankar, G.; Thomas, J. M., *Physical Chemistry Chemical Physics* **2002**, *4*, 1228.
- (7) Simperler, A.; Bell, R. G.; Philippou, A.; Anderson, M. W. *J. Phys. Chem. B* **2002**, *106*, 10944.

- (8) Slater, B.; Catlow, C. R. A.; Williams, D. E.; Stoneham, A. M. *Chem. Commun.* **2000**, 14.
- (9) Sutton, A. P. *Electronic Structure of Materials*; Oxford University Press, 1994.
- (10) Gale, J. D. *Journal of the Chemical Society-Faraday Transactions* **1997**, 93, 629.
- (11) Leach, A. R. *Molecular Modelling: Principles and Applications*; Longman, 1996.
- (12) Press, W. H.; Teukolsky, S. A.; Vetterling, W. T.; Flannery, B. P. *Numerical Recipes*, 2nd ed.; Cambridge University Press, 1992.
- (13) MSI. DISCOVER Theory and Methodology. In *Biosym Manuals*, 1993; Vol. 1.
- (14) Allen, M. P.; Tildesley, D. J. *Computer Simulation of Liquids*; Oxford Science Publication, 1987.
- (15) Ewald, P. P. *Ann. Phys.* **1921**, 64, 253.
- (16) Woodley, S. M., Private Communication.
- (17) Demontis, P.; Suffritti, G. B. In *Modelling of Structure and Reactivity in Zeolites*; Catlow, C. R. A., Ed.; Academic Press, 1992.
- (18) Verlet, L. *Phys. Rev. Lett.* **1967**, 98, 159.
- (19) Hoover, W. J.; Ladd, A. J. C.; Moran, B. *Phys. Rev. Lett* **1982**, 48, 1818.
- (20) Evans, D. J. *J. Chem. Phys.* **1983**, 78, 3297.
- (21) Kohn, W.; Sham, L. J. *Phys. Rev.* **1965**, 140, A1133.
- (22) Dewar, M. J. S.; Thiel, W. *J. Am. Chem. Soc.* **1977**, 99, 4899.
- (23) Dewar, M. J. S.; Zoebisch, E. G.; Healy, E. F.; Stewart, J. J. P. *J. Am. Chem. Soc.* **1985**, 107, 3902.

**Chapter 3: Molecular
Dynamics of Cation Motion
Upon CHCl_3 Adsorption**

Introduction

This chapter documents the molecular dynamics simulations of chloroform adsorbed in zeolite NaY at various temperatures.

Molecular dynamics is a well-established technique for studying diffusive processes, having successfully been utilised in the past for the study of zeolites and other materials such as minerals, perovskite oxides and amorphous solids, including the simulation of diffusion and migration of cations, and of framework stability. For instance, molecular dynamics has been used to study the behaviour of sodium cations in hollandite, a porous manganese oxide. Work by Cormack¹ has revealed the cation migration mechanism in materials such as sodium silicate glasses.

In terms of zeolite science, diffusive processes are an important part of the study of zeolite properties because reactant molecules must reach active sites before any catalytic chemistry can take place. Computational studies in this area have mainly focused on the diffusion of organic molecules such as methane, butane and benzene and other hydrocarbons, as these are industrially important. However, simulations using argon, krypton and xenon as probe molecules can also give us useful information on molecular diffusion in zeolites, as shown in studies by Calmiano² and Yashonath *et al.*^{3,4}, as well as Mosell⁵. The importance of and interest in such studies is reflected in the number of works published over the last 15 years. Studies on benzene diffusion in NaY by Yashonath *et al.*⁶ and Bull *et al.*⁷ have elucidated the migration paths and diffusion coefficients of methane and benzene in zeolite Y.

In previous works reporting the simulation of sorbate molecules in zeolite systems,

there has been little mention of cation motion and migration. A feature of early molecular dynamics work (and some recent studies) was the use of a fixed zeolite framework. Computational limitations at the time meant that a fixed framework needed to be used. Studies of molecular diffusion in zeolite A have concluded that the diffusion coefficients for these molecules are not significantly affected by the framework vibrations and that mutual thermalisation of the guest molecules is sufficient for them to pass through any potential barriers to diffusion, e.g. the apertures of supercages^{6,8}. Earlier work detailing the diffusion of methane in silicalite reached the same conclusion. A number of authors studying diffusion of guest molecules in other zeolites have concluded that diffusion constants are not affected by whether the framework is flexible or not^{9,10}, for instance, work by Demontis *et al.* on methane in silicalite-1¹¹. This study was conducted with both a rigid and a flexible framework, and the authors concluded that the diffusion coefficients were not greatly influenced by the framework flexibility, although a flexible framework would affect dynamical properties, such as the damping of the velocity autocorrelation function⁸. It has been suggested that the zeolite lattice vibrations have a small influence on the diffusion of guest molecules that are relatively small, and a greater influence on larger molecules that are closer in size to the zeolite pores⁸.

The molecular dynamics technique has also been applied to the study of proton and cation motion in framework materials such as perovskite oxides and in the zeolite materials. Both hydrated and dehydrated zeolites have been studied in the past, and the cases where the zeolite framework has been treated both as rigid and flexible have been considered.

Sodium cations in zeolite A have been studied by Faux¹², and Lee *et al.*¹³ and Shin *et al.*¹⁴ Simulations on dehydrated zeolite NaA have also been performed by Demontis and Suffritti¹⁵. Shin *et al.*¹⁴ and Lee *et al.*¹³ use unusually small charges for the zeolite and cations which will affect the Coulomb sum when calculating the long range electrostatic contributions to the total energy. Furthermore, the diffusion coefficients calculated by Lee *et al.* could be deemed to be inaccurate due to the short simulation time over which the mean square displacements were calculated (4 ps).

Studies by Faux *et al.*¹⁶, and later by Faux¹² on Na cations in zeolite A have concluded that Na cations sited in six rings are immobile in hydrated and dehydrated Na zeolite A. Other cations, sited in 8 rings and 4 rings exhibited diffusive characteristics. These findings may give some qualitative idea of the sodium-oxygen interactions in zeolite six rings, although their model of Na in a six ring is questionable. The position of the Na cation at the six-ring site was unusual, as the model predicted the cation to lie in the plane of the six-ring. Such a position is at odds with crystallographic studies and would probably be energetically unstable, as indicated by energy minimisation calculations of cation positions described in a later chapter of this thesis.

Also, the fact that these cations were immobile in the presence of water could be construed as an inadequacy in the forcefield parameters for the water-sodium interactions. Extraframework cations in zeolite structures are held at their sites by coordination to oxygen atoms. In anhydrous zeolites they are not very mobile, although they are mobile in hydrous zeolites as water enhances their mobility. Hence the use of cation-containing zeolites as ion exchangers, a property facilitated by the presence of water molecules.

As in the case of simulation studies of molecular diffusion through zeolite pores, some works available on cations in zeolite employs a rigid framework model. Although a number of molecular dynamics studies have suggested that a flexible framework does not make a big difference to the diffusion of guest molecules in zeolites, it could be argued that when studying cation motion in zeolites, the effect of a flexible framework should be included as the cations are located closer to the framework than the guest molecules. For example, sodium cations are coordinated to framework oxygen atoms. Therefore the effect of the vibrations of the framework on those of the cation would be more significant. Inclusion of a flexible zeolite framework might have the effect of thermalisation of the cations in a similar way that it is proposed for molecular diffusion. The term 'thermalisation' is taken to mean the ability of a species to lose its excess kinetic energy when moving from a region of high potential energy to one of lower potential energy, in this case energy transfer from cations to the framework¹⁷. In view of this, a rigid framework might therefore mean that the cations would have unrealistically high velocities, and might well affect the diffusion constants of these species.

The purpose of the molecular dynamics work described here was principally to investigate the question of the cation migration evident from experimental studies of halocarbon molecules adsorbed in dehydrated NaY and NaX zeolite.

The Forcefield

The forcefield used in the molecular dynamics simulations made use of newly developed parameters to describe the interactions between the zeolite framework and the extraframework cations. These were of the Buckingham type and developed by fitting to the potential energy surfaces of various sodium-substituted zeolites in order to reproduce the experimentally derived zeolite structure upon optimisation using the GULP¹⁸ program. The sorbate-sorbate and sorbate-zeolite nonbonding potentials were of the Lennard-Jones 12-6 form, and were taken from the publication of Mellot and Cheetham¹⁹. These parameters had been obtained by fitting to the experimental heats of sorption of methane and argon in FAU, mordenite and ZSM-5. The intrasorbate bonding and three body terms were represented by modified *cvff* parameters²⁰. These were described using harmonic bond terms to describe the chemical bonding within the molecules, and a three body harmonic term to describe bond angle interactions. Three body terms were also included for the various tetrahedra in the framework, O-Al-O and O-Si-O. These were based on the screened harmonic function, a function used to include the effects of interatomic distance on the angle bending interactions. The equation to describe the energy for the screened three body interactions between atoms *i*, *j* and *k* with an angle of θ_{jik} is:

$$V(\theta_{jik}) = \frac{1}{2} K (\theta_{jik} - \theta_0)^2 \exp [-(r_{ij}/\rho_1) + (r_{ik}/\rho_2)]$$

ρ_1 and ρ_2 are adjustable parameters and r_{ij} and r_{ik} represents the distances between atoms *i* and *j*, and between *i* and *k*.

The partial charges on the zeolite and sorbate atoms were those used by Mellot and Cheetham¹⁹. The framework charges are those adopted by a number of authors, including Kramer and Auerbach²¹. In the case of the zeolite framework atoms, the charges were derived from ab initio calculations and the results of x-ray diffraction experiments. The charges of the atoms making up the guest molecules were derived from ab initio calculations.

The parameters used to treat interactions of the sorbate molecules with the zeolite framework include only the interactions with the framework oxygen atoms. This practise is adopted in many simulations involving zeolites. It is generally assumed that due to the fact that the silicon and aluminium atoms are in the centre of the TO_4 tetrahedra, they do not have any significant short-range interaction with the sorbate molecules. Put another way, the short-range interaction between molecule and framework is parameterized into the sorbate-O interaction. The partial charge of the T atom still interacts with the sorbate molecules. This reduces the number of variable parameters and saves on computation time. One more notable aspect of the forcefield is the distinction between Al and Si atoms. In a number of early studies, an average T atom model has been used. More recent studies have distinguished between the two, as such a treatment would allow for a more accurate reproduction of experimental results. The potential parameters and partial charges used are listed in tables 3.1-3.6.

Si	2.400
Al	1.400
O	-1.200
Na	1.000
H	0.180
C	-0.102
Cl	-0.026

Table 3.1: Partial charges on the atoms in MD simulation

		A (eV)	ρ (Å)	C (eV Å ⁶)
O	Si	30023.000	0.162100	12.840
O	Al	26998.000	0.162200	12.840
O	O	894.60000	0.324400	0.0000
O	Na	8200.0000	0.218000	11.800

Table 3.2: Buckingham terms for the framework-framework and framework-cation interactions

		ϵ (eV)	r_0 (Å)
C	O	0.750232E-02	3.25
H	O	0.780134E-02	2.70
Cl	O	0.142532E-01	3.43
C	C	0.222836E-02	3.75
H	C	0.230329E-02	3.36
C	Cl	0.479530E-02	3.79
H	Cl	0.495729E-02	3.39
Na	Cl	0.183103E-01	2.90
Cl	Cl	0.103230E-01	3.82
H	Na	0.983246E-03	3.10
C	Na	0.114095E-02	3.69

Table 3.3: Lennard-Jones parameters for the sorbate-sorbate, zeolite-sorbate and cation-sorbate interactions

		k (eV)	r_0 (Å)
C	Cl	27.2511	1.761
C	H	29.5612	1.105

Table 3.4: Harmonic bond terms from cvff forcefield for bonding within the chloroform molecules

			k (eV.rad ⁻²)	θ_0 (°)	ρ_1 (Angs)	ρ_2 (Angs)
O	Si	O	12.100	109.47	1.7	1.7
O	Al	O	2.2000	109.47	1.7	1.7

Table 3.5: Three body terms for the T atoms in the zeolites framework

			k (eV)	θ_0 (°)
C	Cl	Cl	8.6730	109.50
C	H	Cl	11.622	107.10

Table 3.6: Harmonic three body terms for chloroform

Monte Carlo Simulations

Monte Carlo docking simulations were performed in order to study the various docking conformations possible for chloroform adsorbing on NaY zeolite. MSI's Cerius² version 3.8 software (Sorption Module) was used for the simulations. A model structure of the sorbate molecule, CHCl₃, was built using the molecule library and 3D Sketcher facility within Cerius². Using the Sorption module available within the software suite, the Canonical Monte Carlo (or 'Fixed Loading') simulations were run for 100 iterations at a temperature of 300 K. A real space cutoff of 12 Angstroms was used for the Ewald summation, with a reciprocal space cutoff of 0.353 Å⁻¹. The system was then energy minimised, with the zeolite framework and cations fixed in space. The procedure was repeated fifty times for each sorbate molecule, in order to sample a greater area of the phase space. 'Dummy' americium atoms were placed inside the sodalite cages in order to prevent the insertion of sorbate molecules inside these cages, as this would result in an unrealistic situation. The molecules would not be able to enter

the sodalite cages in reality, as this would mean traversing a six ring, which would be impossible due to the size of the molecule in relation to the six ring opening.

Grand Canonical Monte Carlo simulations ('Fixed Pressure') were also performed for a range of pressures between 0.02 kPa and 100 kPa at a temperature of 330K. This was to simulate the adsorption isotherm for CHCl_3 in NaY zeolite.

Molecular Dynamics Simulations

The zeolite was loaded with 40 chloroform molecules using a Monte Carlo algorithm as implemented in Accelrys Cerius2 (the amount of sorbate being roughly equal to the equilibrium loading at 1 atmosphere and at 300K)²². Prior to the molecular dynamics simulations, the entire system underwent energy minimisation using the GULP code, at constant pressure but with the constraint that the cell remained cubic. The new framework potential parameters were found to reproduce the powder x-ray diffraction structure report by Fitch *et al.*²³ to a high degree of accuracy. The lattice parameters and volume before and after the minimisation are shown in table 3.7. The minimised cell dimensions were then kept fixed during the MD runs. MD was conducted using the program DL_POLY²⁴, in the NVT ensemble using the Evans thermostat for at least 500 picoseconds on a SGI Origin 2000 computer. During an initial 50 ps equilibration period, the Na cations were held fixed in their energy minimised positions. Analysis of subsequent MD runs showed that this did not affect the conservation of energy during the simulation. All components of the system were treated as fully flexible during the MD simulation. The molecular dynamics simulations were also repeated for a sorbate loading of 10 molecules per unit cell. Configurations, forces and velocities of the atoms

were saved every 1 picosecond. Mean Square Displacement plots were calculated for the cations and sorbate molecules. Further simulations were performed for a shorter time of 200 picoseconds for both the unloaded zeolite and NaY loaded with 40 chloroform molecules, writing the information on configurations, forces and velocities every 0.02 picoseconds. This was for the purpose of calculating velocity autocorrelation functions and their power spectra in order to predict the vibrational frequencies of the cations.

Parameter	Experimental Value	Simulated Value	Difference	Units	Percent
Volume	15206.81	15240.93	34.12	Å ³	0.22
a	24.77	24.80	0.02	Å	0.07

Table 3.7: Simulated and experimental values of the NaY zeolite lattice parameters and volume after optimisation with the new potentials listed in table 3.2 . The zeolite was constrained to remain cubic, but there is little change in the volume and lattice parameter after energy minimisation in GULP.

Results

Canonical Monte Carlo Simulations

Visual inspection of the configurations generated by the Canonical Monte Carlo simulations (figures 3.1 to 3.3) indicate that some of the configurations calculated by the Monte Carlo simulation are similar to those proposed by Cheetham and Mellot¹⁹. Furthermore, all of the docking configurations obtained fit into one of the schemes suggested by Bosch *et al.*²⁵ (see figure 1.6 in chapter 1 of this thesis). Cheetham and Mellot also compare their configurations with those of Kaszkur *et al.*²⁶, who proposed two configurations for chloroform adsorbed in the zeolite cage. One configuration had

the hydrogen atom on the chloroform molecule pointing towards the zeolite framework, and the second configuration was with the hydrogen atom pointing towards the centre of the supercage. The configurations calculated by the Monte Carlo simulations are mostly those where the hydrogen atom are pointing towards the zeolite framework, at distances that would suggest hydrogen bonding between the hydrogen and the framework oxygen.

In order to sample the ensemble thoroughly, a longer simulation of 500000 iterations under the same conditions of pressure and temperature resulted in a configuration where the hydrogen atom was pointing towards the centre of the zeolite supercage. Figure 3.1 shows the orientation of the chloroform molecule in relation to the zeolite for this simulation. As can be seen, the hydrogen atom does not point to any framework oxygen and is too far away to interact with them. The sorption interaction occurs via an electrostatic interaction between the chlorine atoms and a sodium cation in this case. The energy calculated for this simulation was -52.9 kJ/mol. This is comparable to the experimental heat of -53.2 kJ/mol for chloroform sorption quoted by Mellot *et al.*²⁷. This configuration is similar to the one proposed by Kaszkur *et al.*²⁶, and is similar to the configuration labelled as Species IV in figure 1.4 (see chapter 1, page 19). Other low energy configurations also resemble various configurations proposed by Bosch *et al.*²⁵ (see figures 3.2 and 3.3). The resulting configuration of one run is similar to Species II, with the chloroform in a position where it can interact with the sodium cation, and a possible hydrogen bond with a framework oxygen atom. Another simulation yields the configuration of Species I, with the halogen atoms pointing away from the framework towards the centre of the supercage, and the hydrogen pointing to an oxygen atom, at a distance of 2.36 Angstroms. Both are shown below in figures 3.2

and 3.3, and have adsorption energies of -70.0 kJ/mol and -65.4 kJ/mol respectively. It should be noted that although the molecule has been energy minimized with respect to the zeolite framework, the final configurations do not take into account the motion of the cations, as these were held fixed during the Monte Carlo runs.

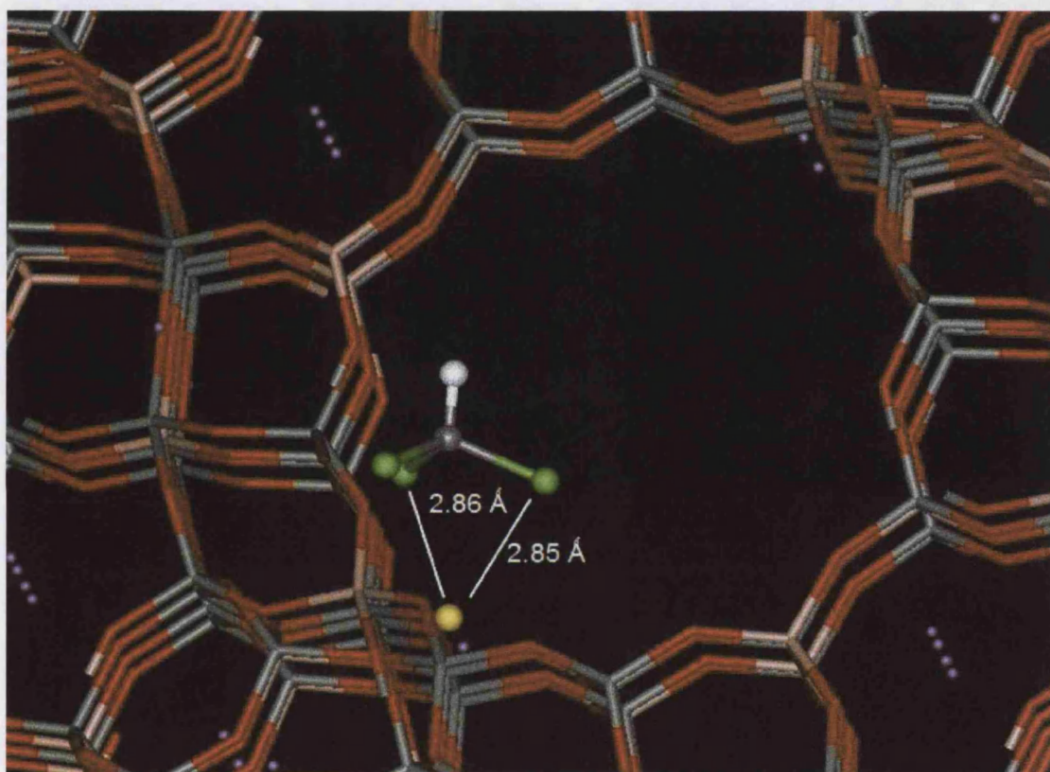


Figure 3.1: The final configuration of the Monte Carlo run of 500000 iterations. The green spheres represent the chlorine atoms and the yellow sphere represents a sodium cation involved in an electrostatic interaction with two chlorine atoms.

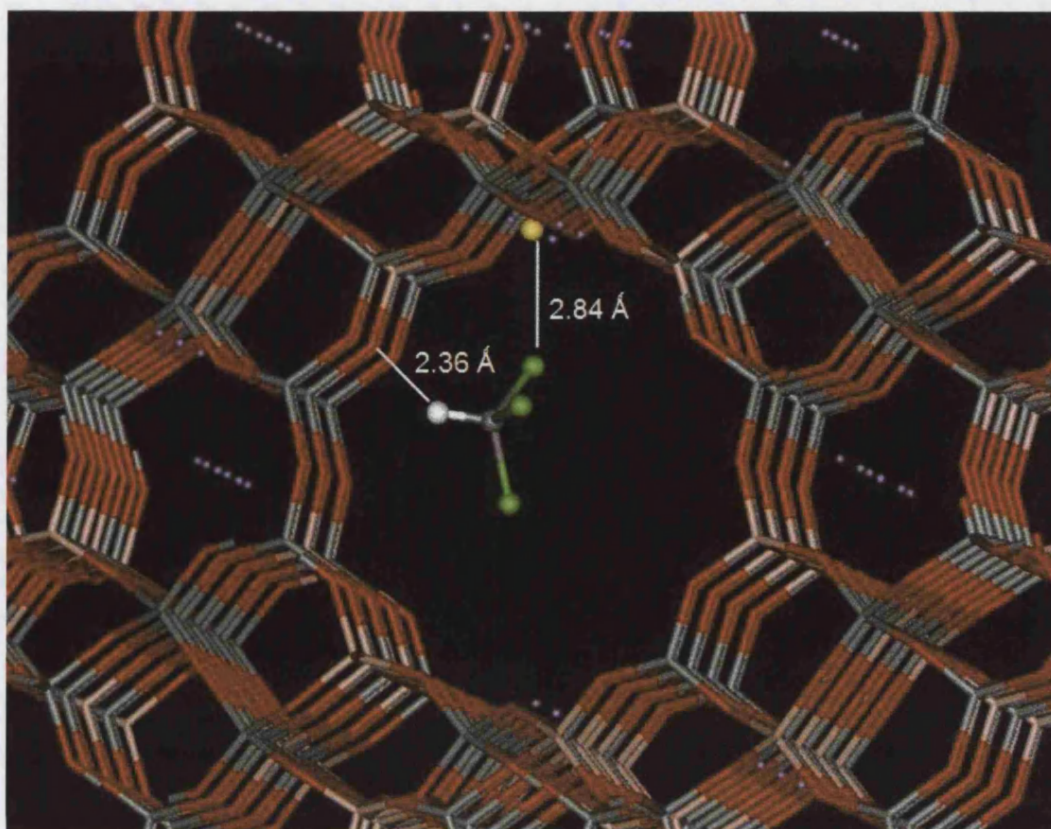


Figure 3.2: The configuration showing the dual interaction whereby the molecule is bound to the zeolite via a hydrogen atom weakly interacting with a framework oxygen atom, and via an electrostatic interaction between a chlorine atom (green spheres) and a sodium cation (the specific sodium is represented by a yellow sphere). The hydrogen atom on the CHCl₃ molecule is represented by a white sphere.

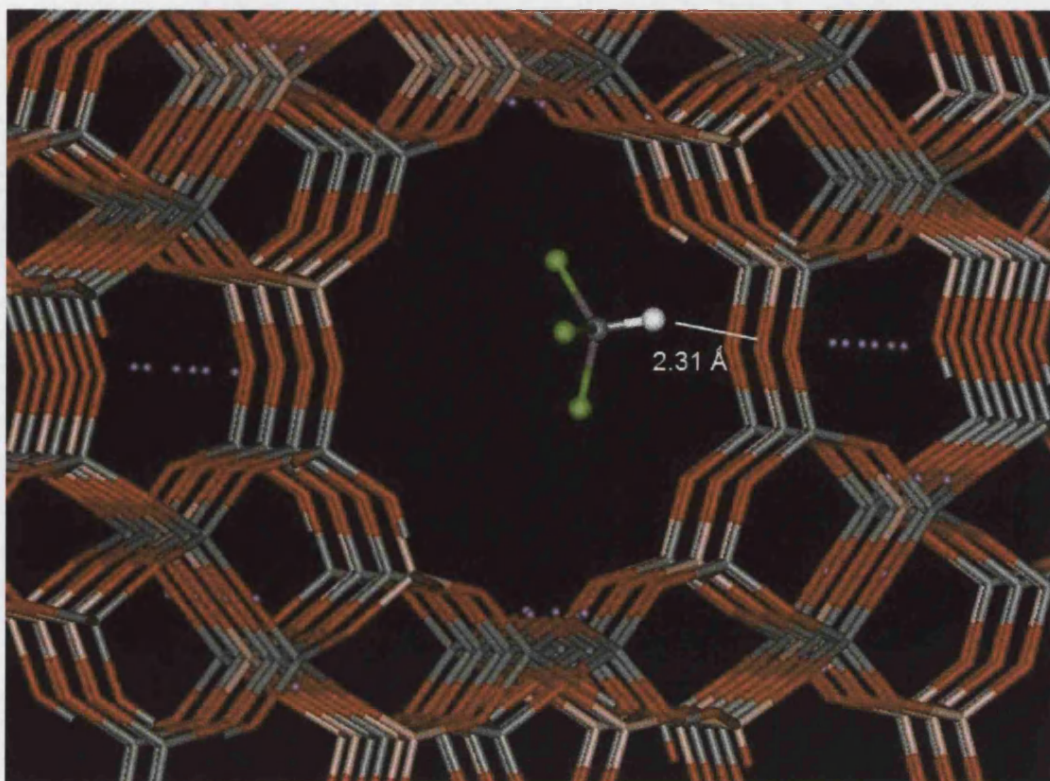


Figure 3.3: A Monte Carlo generated configuration showing the hydrogen atom (white sphere) on a CHCl_3 molecule interacting with an oxygen atom on the zeolite framework.

Simulation of the Adsorption Isotherm for CHCl_3 in NaY

The results of the isotherm simulation are shown below in table 3.8, and the isotherm plot is shown in figure 3.4. As can be seen, the form of the isotherm is similar to the experimentally determined one, despite the fluctuations in the average loading at the different pressures. The results compared well with those of Kawai *et al.*²², as the maximum loadings for the calculated isotherm was between 37 and 44 molecules per unit cell, calculated at pressures between 0.02 kPa and 100 kPa, whereas the maximum for the experimentally measured isotherm is about 39 molecules per unit cell.

Pressure (kPa)	Ave. Loading	Mass of molecules (g)	No. of mmols	No. of mmols/g
0.02	37.359	7.406E-21	6.204E-20	2.927
0.05	39.082	7.747E-21	6.490E-20	3.062
0.07	40.293	7.987E-21	6.691E-20	3.157
0.1	40.716	8.071E-21	6.761E-20	3.190
0.2	38.696	7.671E-21	6.426E-20	3.032
0.4	41.566	8.240E-21	6.902E-20	3.257
0.5	42.238	8.373E-21	7.014E-20	3.310
1	43.782	8.679E-21	7.270E-20	3.431
2	40.448	8.018E-21	6.717E-20	3.169
5	44.134	8.749E-21	7.329E-20	3.458
7	43.936	8.709E-21	7.296E-20	3.443
10	45.499	9.019E-21	7.555E-20	3.565
15	37.520	7.438E-21	6.230E-20	2.940
20	45.724	9.064E-21	7.593E-20	3.583
30	46.627	9.243E-21	7.743E-20	3.654
40	43.773	8.677E-21	7.269E-20	3.430
50	44.869	8.894E-21	7.451E-20	3.516
60	43.529	8.629E-21	7.228E-20	3.411
70	42.871	8.498E-21	7.119E-20	3.359
80	42.029	8.332E-21	6.979E-20	3.293
100	44.077	8.738E-21	7.319E-20	3.454

Table 3.8: Table of results of the isotherm simulation for chloroform sorption on NaY zeolite

Mass of Zeolite cell	2.12E-20	g
Mass of chloroform molecule	1.98E-22	g

Table 3.9: Masses used to covert molecules/unit cell to mmol/g

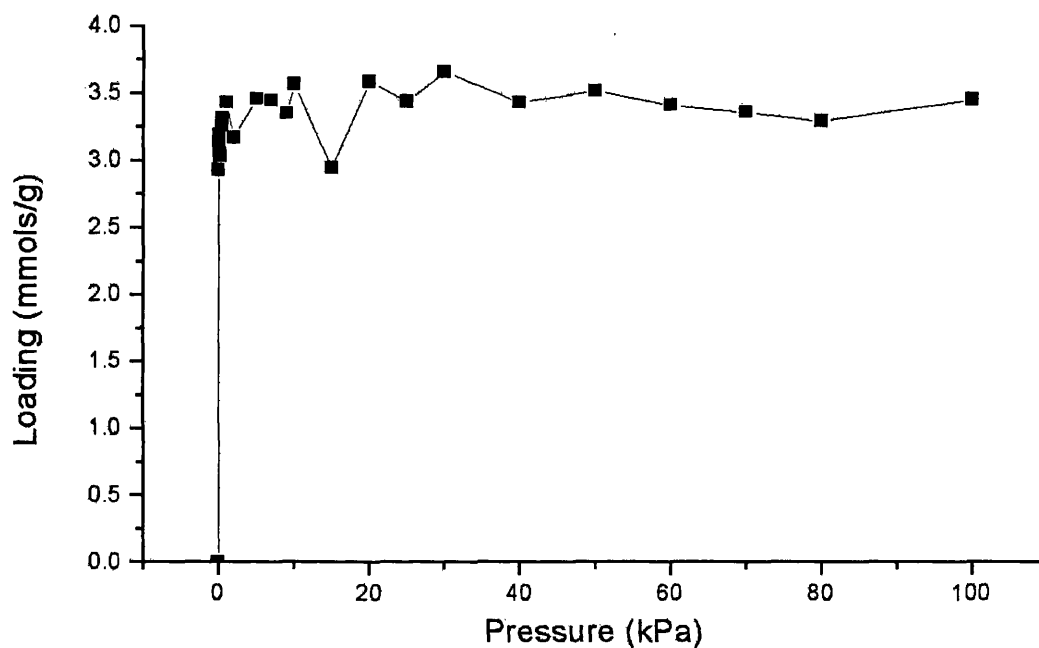


Figure 3.4: The calculated isotherm plot for chloroform sorption in NaY zeolite.

Molecular Dynamics: Bare Zeolite

Molecular dynamics simulations by Jaramillo and Auerbach²¹ using interatomic potentials derived by themselves have already indicated that the Na cations in unloaded NaY are essentially immobile at 300K and at 1000K. Simulations using our own models and potential parameters at 270K, 300K, 390K and 700K have largely confirmed this observation. Although some small cation displacements at the SII site are observed at

higher temperatures (390K and 700K) in the bare zeolite, there was no appreciable migration occurring for the cations in sites filled in NaY, as reflected in the Mean Square Displacement (MSD) plots shown as figure 3.5. The MSD scale (y axis) shows that although SII cations are seen to migrate, the motion is on a very small scale, and involves a small proportion of cations moving to a different site (close to the SIII' site). The temperature of the simulations is likely to cause the cations to explore neighbouring local minima. Analysis and observation of the trajectory shows that cations in all three crystallographic sites, SI, SI' and SII, oscillate about their mean positions, thus concurring also with the findings of Faux, Smith and Forester¹⁶, and in later work by Faux, albeit for a different zeolite, that the cations located at six ring sites are immobile in unloaded zeolites. Reservations regarding some aspects of these models and simulations have been expressed earlier in this chapter. The simulations of Jaramillo and Auerbach²⁸ also showed that cations sited at the six rings were immobile, and that only SIII' cations in NaX were mobile to any extent, these cations being located near four rings.

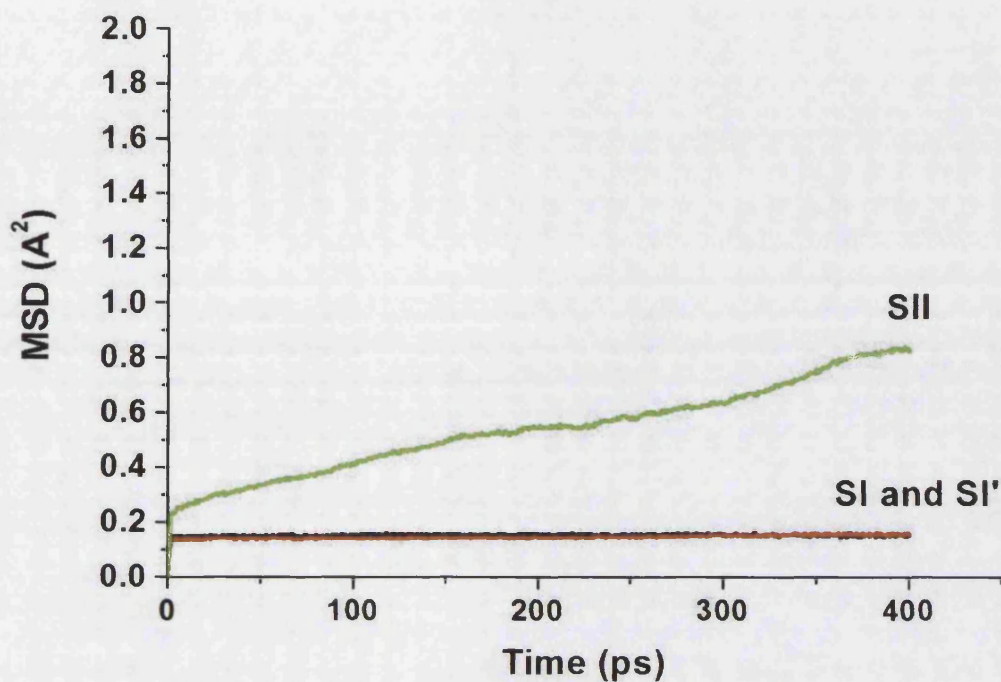


Figure 3.5: MSD plots for the sodium cations at 390K in unloaded NaY.

Simulations using a rigid zeolite framework were also carried out for at least 500 ps. As discussed earlier in this chapter, it is generally considered that the use of a rigid framework has little effect on diffusion coefficients when compared to those calculated from simulations utilising a flexible framework model. These conclusions were derived from studies of molecular diffusion however, as opposed to cation diffusion in zeolites.

Analysis of the MSD plots calculated from the resulting trajectory shows that SI and SI' cations are not mobile, and the qualitative features of the MSD for these cations are much the same as for the case where the framework is flexible. This is shown in figure 3.6. As will be shown in a later chapter in this thesis, there are energetic barriers to be overcome if a cation is to successfully traverse a zeolite six ring and enter the supercage. For SII cations though, the small displacements observed with a flexible

framework are larger in this case, in the region of 2.8 - 3.0 Å², as shown in the MSD plot for the cations in this simulation. A study of the trajectory reveals the fact that some of the SII cations move 3 to 4 angstroms away from their original position. An explanation could be that the cations are simply able to explore a flat region of the potential energy surface in this case, and thus the observation could be more akin to a 'minimisation' as opposed to a diffusive phenomenon. A more detailed study is required to quantify the effect on the velocity autocorrelation function and its dampening over time and effect on vibrational frequencies, although the difference in diffusion coefficients calculated for the SII cations lends some support to the argument that cation motion is affected by whether or not the framework is flexible in the simulation.

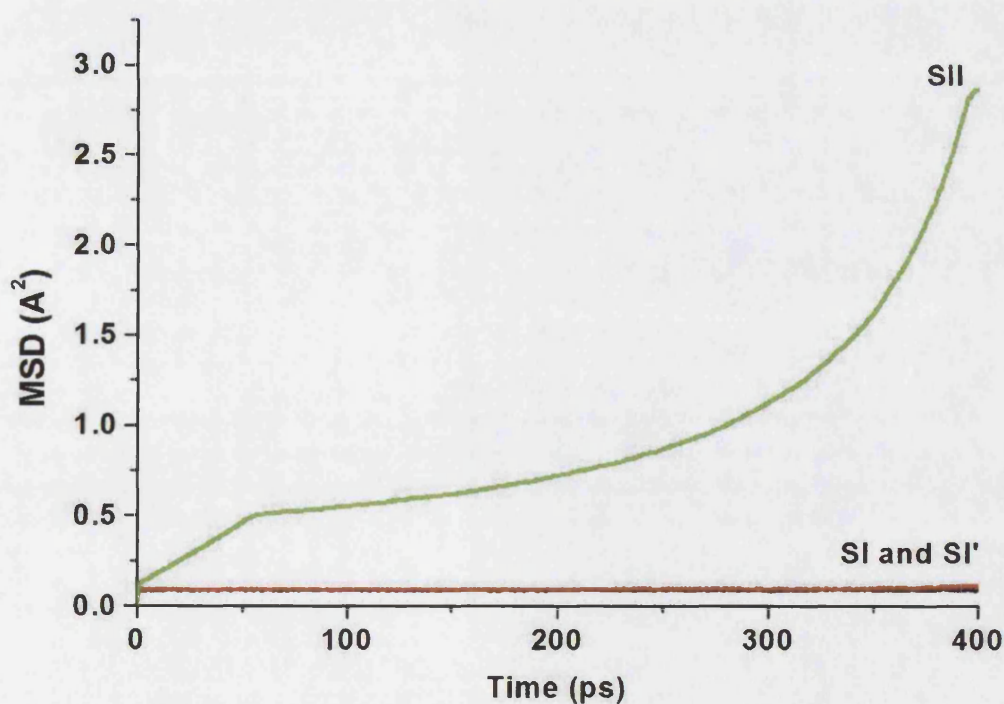


Figure 3.6: MSD plot for SII, SI' and SI cations for a simulation of unloaded NaY at 390K. The framework atoms were held fixed for the duration of this simulation.

Cation Motion in Chloroform Loaded NaY Zeolite

The results of the MD simulations presented here show that there is migration of the cations upon chloroform adsorption. Different types of motion are observed depending both on the location of the cation and on the time elapsed. It is important to note that many of the cation migrations appear to be irreversible within the timescale of the simulation in that they involve migration from sites inaccessible to the sorbate molecules into the larger cavities of the zeolite pore system. Therefore results of the simulation evolve over the passage of time, rather than representing a steady-state situation. The results presented are for the simulations run at 270K, 330K and 390K. There are four types of motion observed during the simulation:

1. Migration of SII Cations → Supercage

Some cations located in the SII site migrate from their positions at the edge of the supercage towards the centre. In the simulation cell this part of the zeolite is crowded with chloroform molecules, and interaction of the polar molecule with the cations would explain the migration of these particular cations with the Na^+ being more favourably solvated by the chloroform molecules than by the zeolite framework. In certain instances it is also observed that a SI' cation (see below) starts to move into the supercage prior to any substantial migration of nearby SII cations. Therefore electrostatic repulsion between sodium ions may also contribute to SII motion. For instance at 390K, a SI' cation moves to within 3.9 Å of a SII cation interacting with a sorbate molecule. This is similar to the simultaneous migration suggested by MD calculations on HFC-134 in NaY by Auerbach *et al.*²⁸. However not all migrations

occurred in this way. The SII cations begin their migration early on in the simulation at all temperatures simulated; the Mean Square Displacement (MSD) plots calculated for these particular cations reflect this (see figures 3.7 and 3.8). The plots show that there are continuous migrations over a period of 70-90 ps together with shorter hops. The SII cations do not move back toward their initial positions and tend to become less mobile after a certain period of time, as seen in the decreasing scale of the MSD plots in successive timeframes in figures 3.7 and 3.8. The original SII are held in new positions by a dual interaction between the oxygen atoms near two SIII' sites, and by the chloroform molecule. It is important to note that throughout this work the characterisation of SI, SI' and SII cations refers only to their locations at the start of the simulation and not necessarily their position at any subsequent time. The cation motion during the rest of the simulation may be described as thermal vibrations. Radial distribution function plots for the SII cations and chlorine atoms were calculated between 0 and 100ps of simulation and between 100 and 200 ps of simulation, and these are shown as figures 3.9 and 3.10. Although the peaks of the two plots are very close together, integration of the plots shows that there is an increase in the area from the former to the latter mentioned plots between 0 and 4.5 Angstroms, as represented by area A in the figures, suggesting that the SII cations get closer to the chlorine atoms over the passage of time, which would be consistent with the fact that they are moving away from their original SII sites. There is a corresponding decrease in area between the distances of 4.5 and 6.8 Angstroms from the RDF plot for the initial time period to the second time period, shown as area B in the figures (see tables 3.10 and 3.11). Figure 3.11 illustrates the movement of SII cations over the initial 100 ps of production in the simulation.

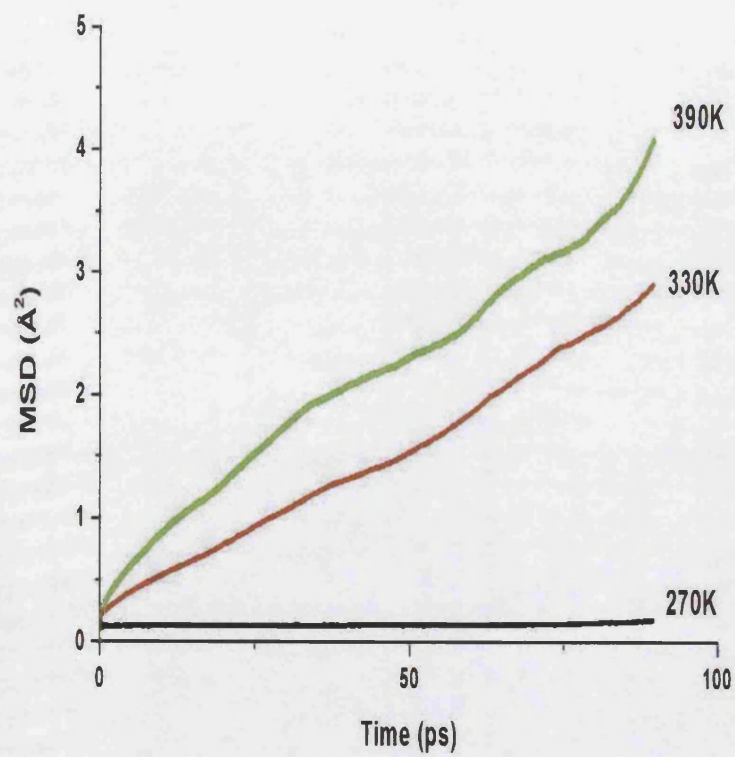


Figure 3.7: MSD plot for SII cations from 0 to 100 ps of MD simulation

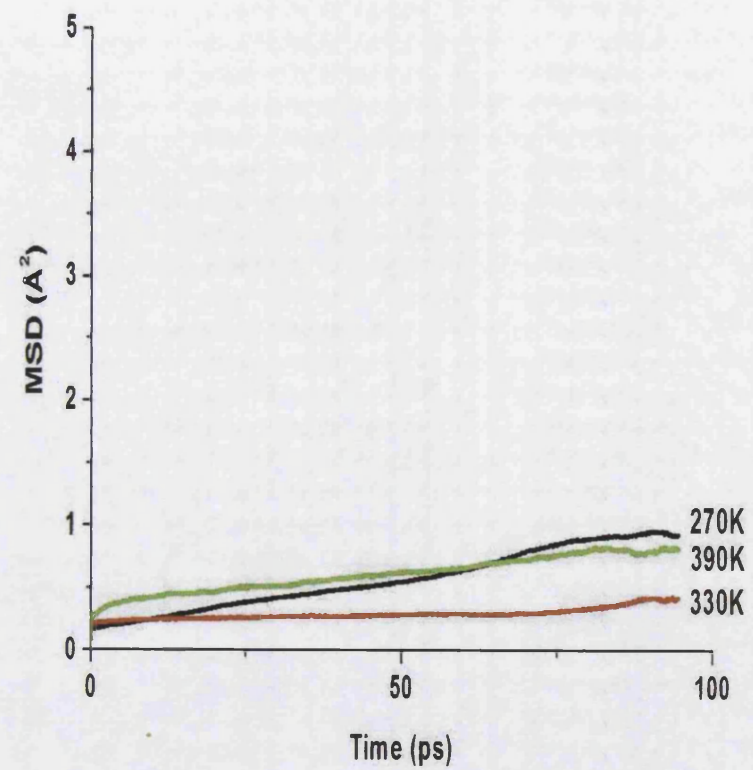


Figure 3.8: MSD plot for SII cations from 100 to 200 ps of MD simulation

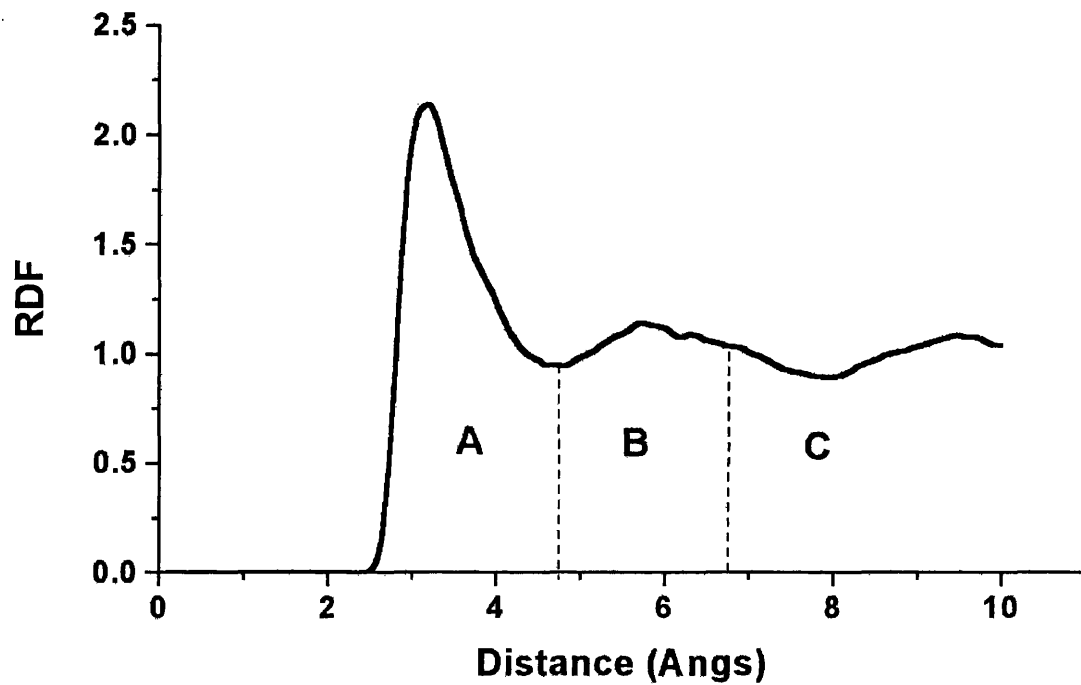


Figure 3.9: Radial Distribution Function plot for SII cations and Cl atoms between 0 and 100 ps of MD simulation.

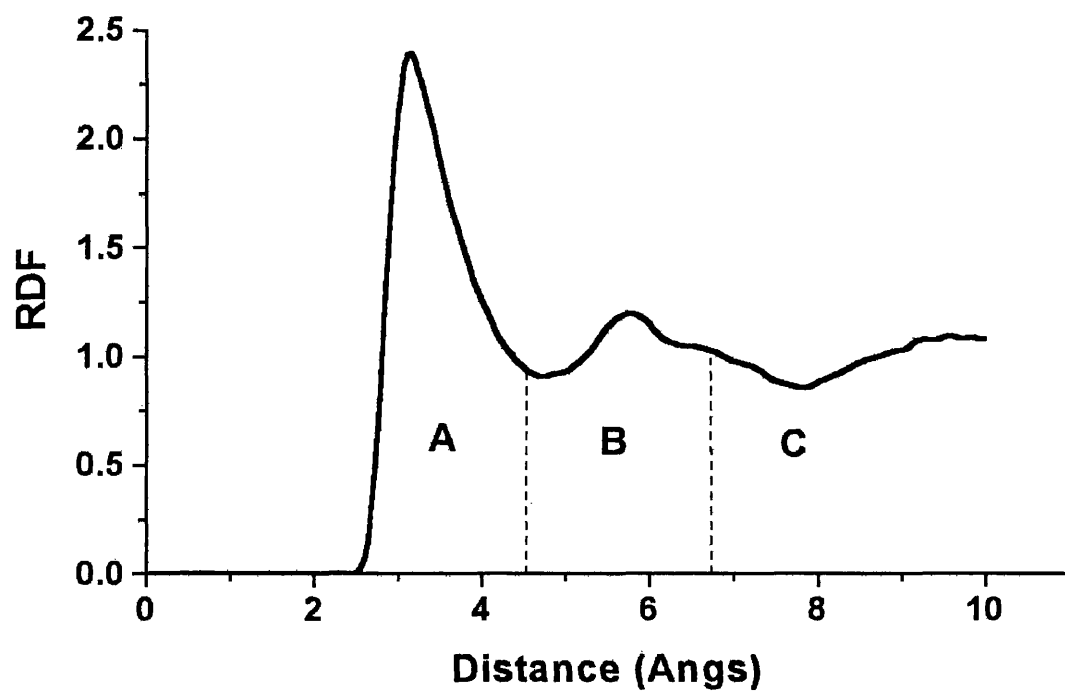


Figure 3.10: Radial Distribution Function plot for SII cations and Cl atoms between 100 and 200 ps of MD simulation.

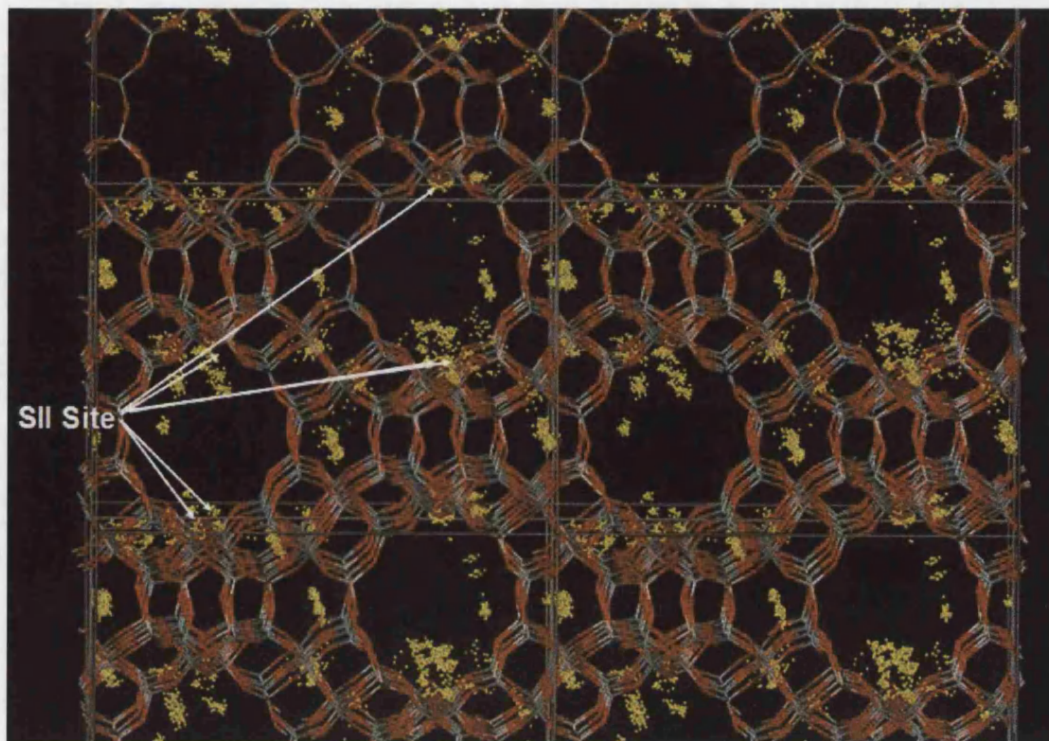


Figure 3.11: Movement of sodium cations from SII sites towards the middle of the zeolite supercage over the initial 100 ps of MD simulation. A number of simulation cells are shown in this diagram, and the SII sites are indicated in one of the cells by the white arrows. The chloroform molecules are not shown in this diagram for clarity.

2. Migration of SI' Sited Cations → SII Sites

Some cations in site I' are observed to migrate from their position in the sodalite cage into the supercage and take up position in a vacant SII site, in the manner reported by Grey *et al.*²⁹ using x-ray diffraction and NMR experiments, and as shown from the calculated MD trajectory in figure 3.16. This involves the cation traversing a zeolite 6-ring; a process predicted to have a high activation energy³⁰. Recent work using molecular dynamics has indicated that such motion also occurs upon sorption of HFC-134 and HFC-134a. It was reported that the cation motion was SI' to SII' to SII²⁸. Although the cations do pass through SII' on the way out of the sodalite cage, the amount of time spent there is small, possibly due to a low energy barrier to jump from SII' to SII. Calculations by ourselves, described in chapter 5 of this thesis, using the defect energy minimisation technique with the Mott Littleton scheme have shown the presence of a potential energy well on both sides of the six ring facing the supercage, corresponding to SII and SII' sites. The jump from SII' to SII had a low energy barrier, hence the ease of transition shown in our MD simulations. The number of cations migrating is dependent on the temperature of the simulation, with seven SI' cations per unit cell being seen to migrate into the supercage at 390K over 500ps.

At 270K two SI' cations per unit cell migrate over the simulation timescale with the remainder oscillating in the sodalite cage. At 330K, this number increases to three cations per unit cell. The process of a SI' cation migrating to a SII site happens within a time period of about 5 picoseconds, and takes the form of a short "hop" across a six-ring into the supercage. The MSD plot for SI' cations over this initial period, shown in figure 3.12, shows only the very short timescale "hops" consistent with this migration, except

for the 390K run, where the cations are seen to diffuse over a longer timescale within the first 100 ps of MD, this being consistent with the diffusional type motion seen for the SII cations in the supercage. On the MSD plots the 'hops' are deemed to be the initial 'jump' at 0 ps from 0 Å² to a low MSD value. Otherwise the cations are essentially immobile for the first 100 picoseconds at 330K and at 270K. This is in contrast to the motion of the SII cation in the first 100 picoseconds at these temperatures. A possible explanation could be that certain SII sites need to be vacated first in order to permit the SI' cations to migrate into them. Also the SII diffusion within the supercage may have a lower energy barrier than diffusion of cations within the sodalite cage, as no six ring needs to be traversed for migration from SII → SIII', for example. After 100 picoseconds a combination of short "hops" and more continuous diffusion is observed, as shown by the MSD plot in figure 3.13. This represents both migration to the SII site, and diffusion of the former SI' cations now in the supercages. From the trajectory, it is evident that some cations migrate into vacant SII sites in the first 100 picoseconds, and also to recently vacated SII sites as also seen at the lower temperatures. Radial distribution functions for SI' cations and Cl atoms calculated from 0 to 100 ps and 100 to 200 ps indicates that there is an increase in 'population' between 0 and 4.5 Angstroms from former time period to the latter (area A in figures 3.14 and 3.15). This points to the possibility of migration of SI' cations into the supercage. This is the only way that these cations could get closer to the chlorine atoms. The area of region B also increases slightly (see tables 3.10 and 3.11), and there is a decrease in the area of region C in this case. This means that the sodium – chlorine distances become smaller over the period of simulation within which the RDF plots were taken. When taken along with the MSD plots, this points to possible migration of these cations to get closer to, and interact with the chloroform molecules.

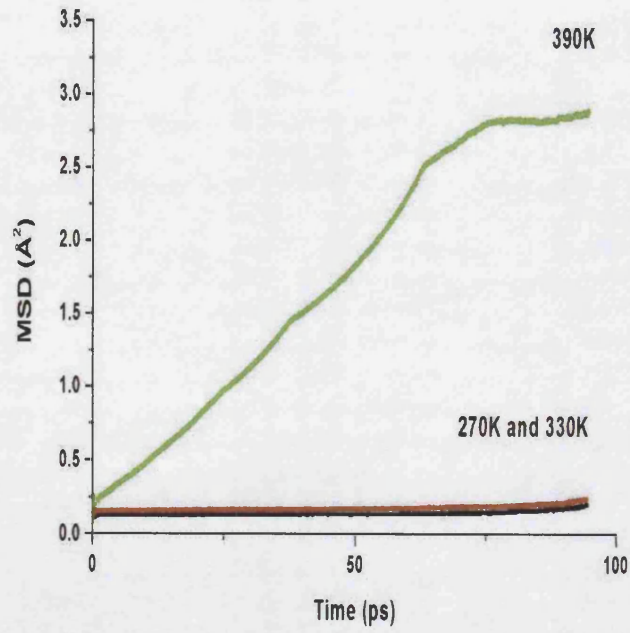


Figure 3.12: MSD plot for SI' cations from 0 to 100 ps of MD simulation.

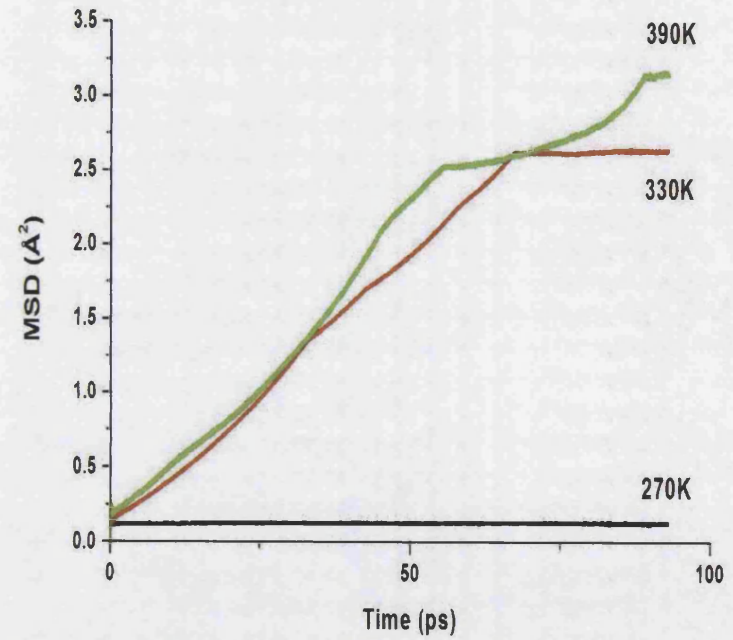


Figure 3.13: MSD plot for Site I' cations between 100 and 200 ps of MD simulation.

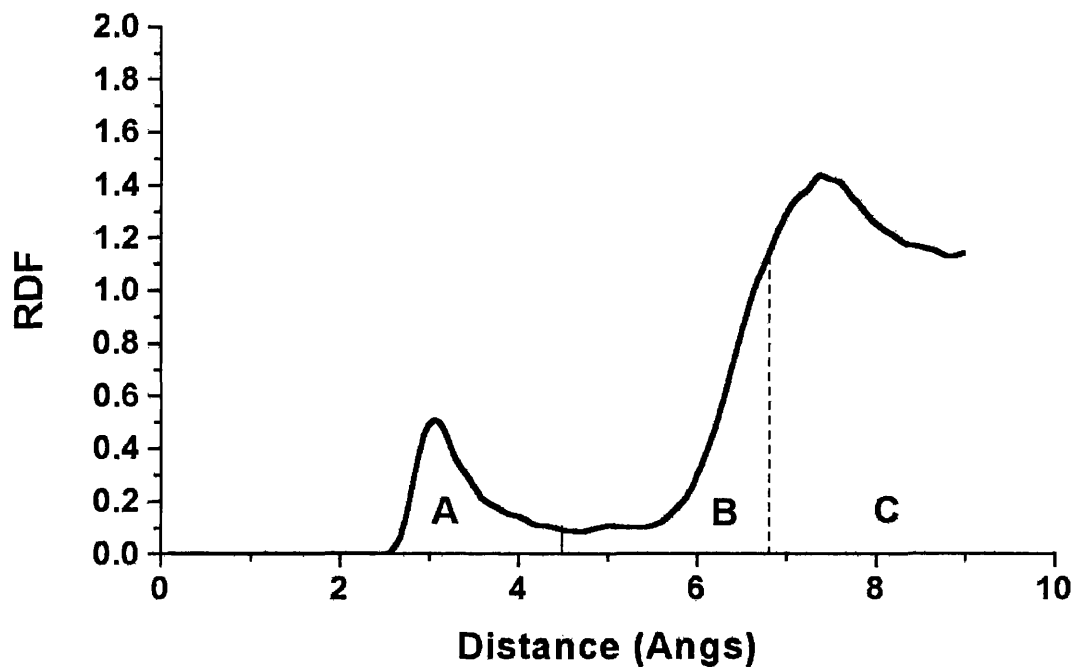


Figure 3.14: Radial Distribution Function plot for SI' cations and Cl atoms between 0 and 100 ps of MD simulation

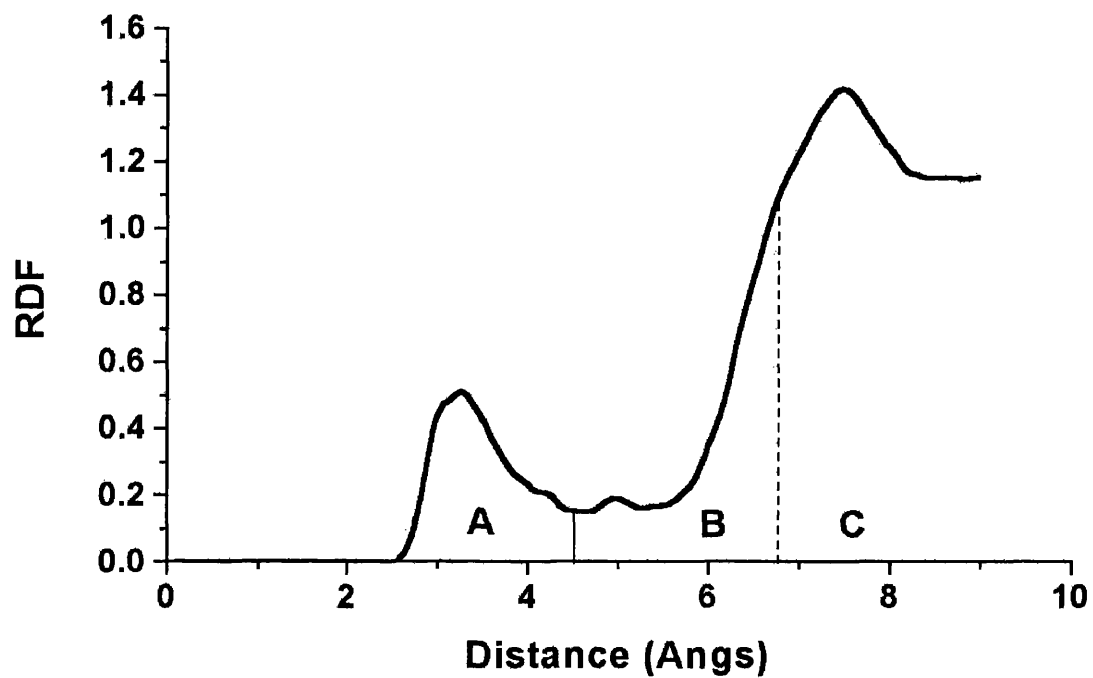


Figure 3.15: Radial Distribution Function plot for SI⁺ cations and CL atoms between 0 and 100 ps of MD simulation

	0 – 100 ps	100 – 200 ps
SII - CI	2.71	2.87
SI' - CI	0.45	0.58

Table 3.10: Areas of region A from figures 3.9,3.10 and 3.14, 3.15

	0 – 100 ps	100 – 200 ps
SII - CI	2.42	2.41
SI' - CI	0.09	0.15

Table 3.11: Areas of region B from figures 3.9,3.10 and 3.14, 3.15

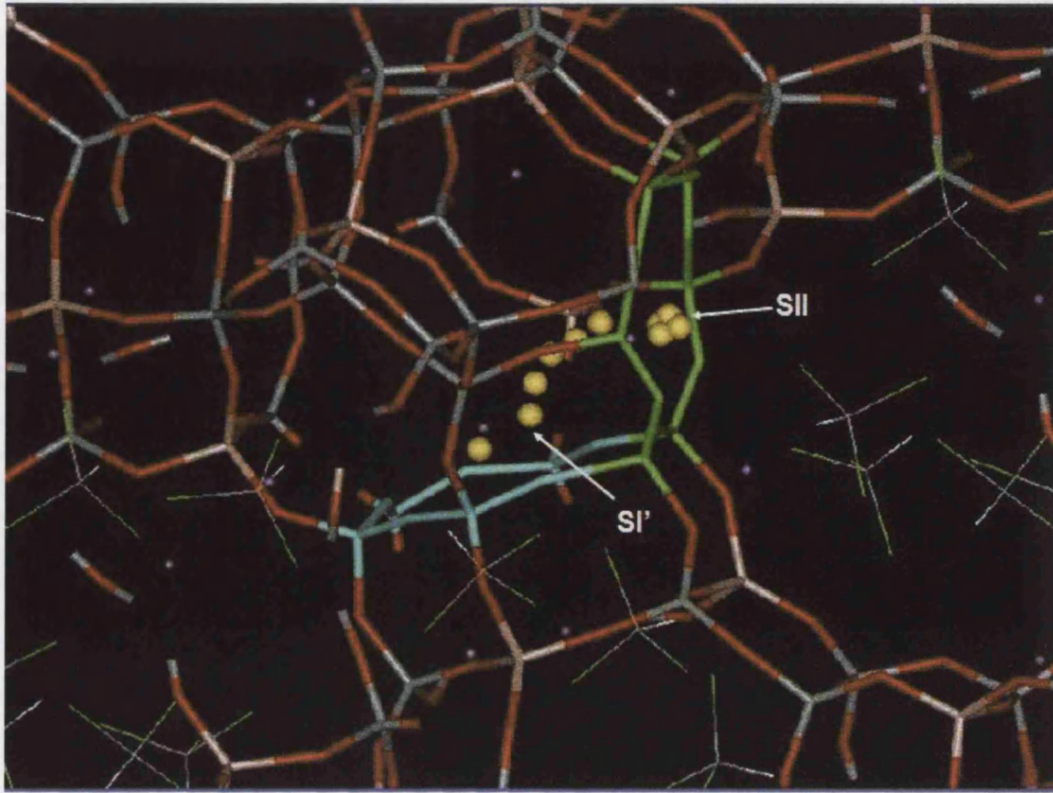


Figure 3.16: Migration path of sodium cation (yellow balls) from a SI' site to a SII site. The blue ring represents the six ring associated with the SI' site. The green ring highlights the six ring facing the supercage, containing the SII site. The cluster of yellow spheres shows the cations thermally vibrating in an equilibrium SII position.

3. Migration of SI' cations to vacant SI' Sites

The third type of motion observed involves the concerted migration of SI' cations. When one SI' cation vacates its site and hops into the supercage, a second SI' cation from a site within the same sodalite cage is sometimes observed to migrate across the cage and take up the original position of a cation that has migrated into the supercage. This has been observed to occur in the simulation at 330K and takes place over a timescale of 5 picoseconds.

4. Migration of SI cations to vacant SII Sites

Analysis of the trajectories reveals that the SI cations are more mobile after adsorption than in unloaded NaY. Some SI cations are observed to migrate out of their original position in the double six ring between the sodalite cages, and into a nearby SI' site. This accords with the observation by Bosch *et al.*²⁵ that there is a decrease in site I population upon adsorption and occurs over a longer time period than the SI' hopping motion. SI cations are immobile during the first 100 ps of MD at 270K and 330K in that there is no diffusive motion, as shown in figure 3.17. At 390K however the cations are seen to migrate. Between 100 and 200 ps of simulation, the cations still do not exhibit diffusive motion at 270K, although they are seen to be more mobile at 330K during the same time period. This is reflected in the MSD plot in figure 3.18. Some cations hop into a SI' site after 100 ps of simulation having initially been seen to oscillate in the double six ring. Having entered the sodalite cage the cations are also seen to diffuse in the sodalite cage. During the simulation at 390K, some SI cations that have hopped into

SI' sites can be seen to diffuse into the supercage, via a vacant SII site, in the manner suggested for the SI' cations.

Diffusion of these cations towards the centre of the supercage has not been observed in the simulations to the same extent as for the other cations, although longer simulation times may be necessary to observe this. The relative mobilities of the cations at 330K are shown in figures 3.19 and 3.20. The different types of motion described can be seen in figure 3.21.

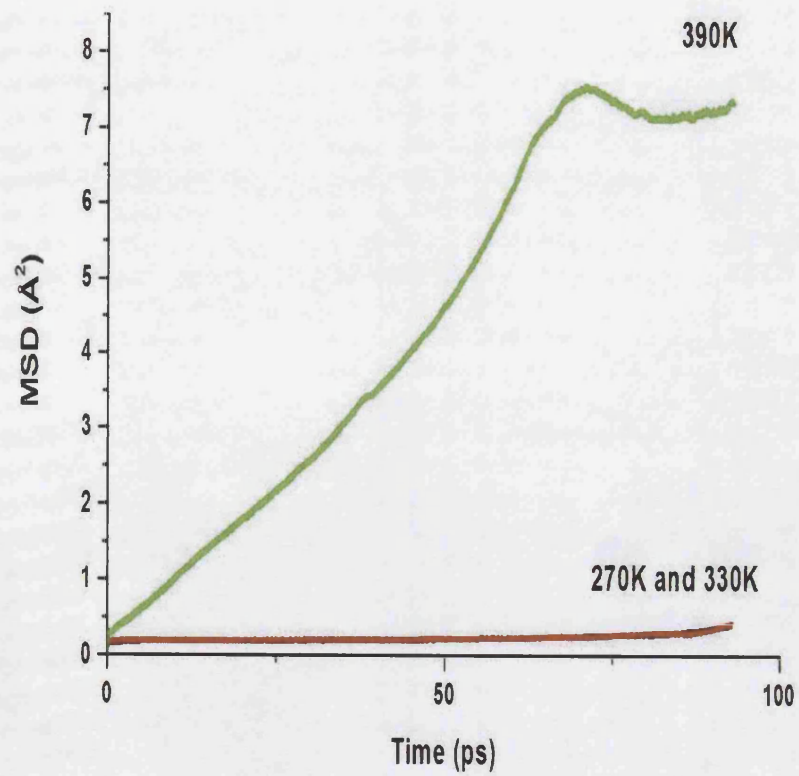


Figure 3.17: MSD plot for SI cations between 0 and 100 ps of MD simulation at 270K, 330K and 390K.

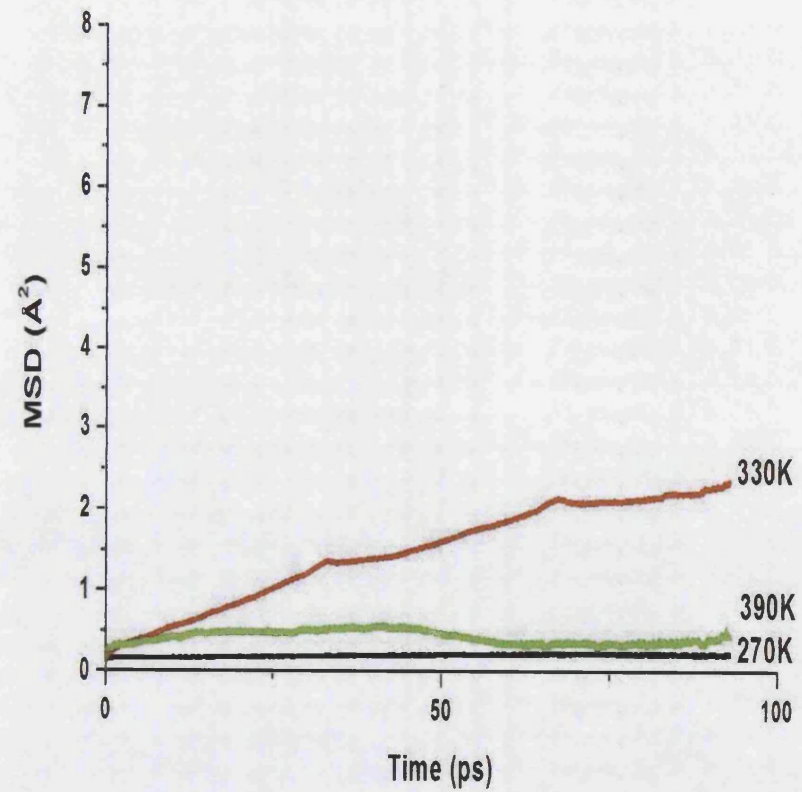


Figure 3.18: MSD plot for SI cations between 100 and 200 ps of MD simulation at 270K, 330K and 390K.

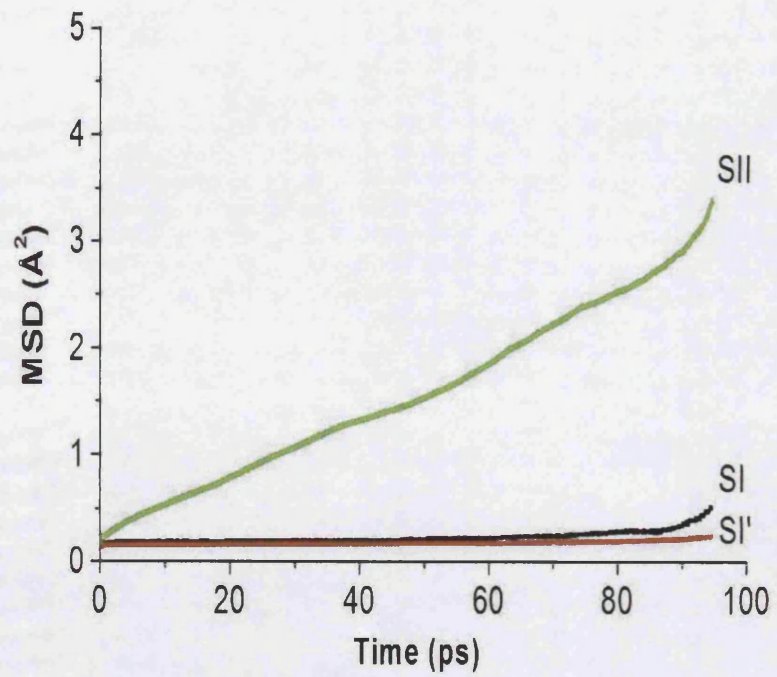


Figure 3.19: MSD plot for all cations between 0 and 100 ps of MD simulation at 330K.

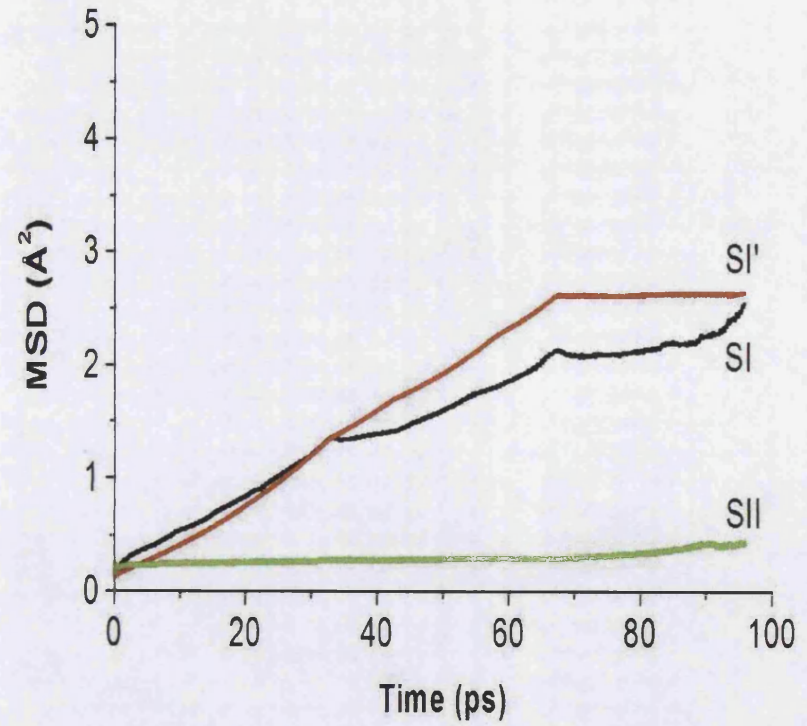


Figure 3.20: MSD plot for all cations between 100 and 200 ps of MD simulation at 330K.

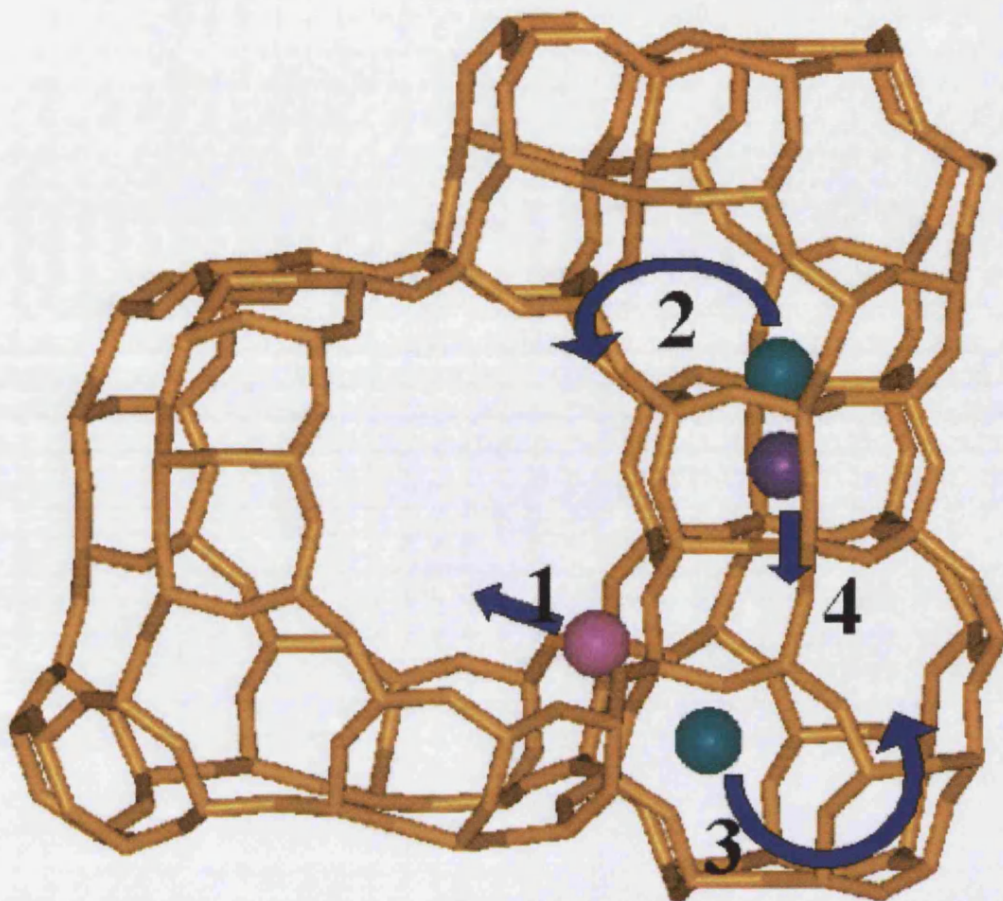


Figure 3.21: Graphic showing the various cation motions described. 1. Motion of SII cations towards the centre of the supercage. 2. Hopping of SI' cation into a site II position in the supercage. 3. Migration of SI' cation across the sodalite cage into another SI' site. 4. Hopping of the SI cation into a SI' position.

Loading of 10 Molecules per Unit Cell

The simulations were also performed with ten chloroform molecules per unit cell in order to study the effect on the cations at a lower loading. At all of the simulated temperatures the cations were found to be comparatively immobile. Some cations were seen to migrate between sites, but these were restricted to certain SII and SI' cations, exhibiting SII \rightarrow middle of supercage and SI' \rightarrow SII migration. The fact that these were largely the same cations that migrated during molecular dynamics with a higher sorbate loading could indicate that the local framework composition has a role in determining the migration of these cations, related to the local composition of the preferred adsorption sites in the zeolite. The migration observed was on a smaller scale to that occurring with forty molecules per unit cell, suggesting that local framework configurations may play a part in determining cation migration in conjunction with the sorbate - cation interactions. The aforementioned suggestion that Coulombic interactions between cations play a large part in determining the cation distribution could be illustrated by the simulations, as some SII cations that are displaced from their sites on a six ring are followed by SI' cations close by.

Movement of Chloroform Molecules

The diffusion of the chloroform molecules is correlated to the loading and temperature, as expected. It is reported in some other studies of molecular diffusion in zeolites using the molecular dynamics technique that the rate of diffusion increases with loading. At low to intermediate loadings, it is believed that co-operative effects between molecules are believed to increase diffusivity in zeolites. In the case of chloroform, for the

simulations performed, the reverse is observed. Although intermediate numbers of sorbate molecules have not been studied, it is possible that the diffusion rates of the molecules would follow the expected trend should they be considered, up to a point where the supercage is 'saturated', thereby rendering the molecule relatively immobile. At 40 molecules per unit cell, this is the case.

At a loading of 40 molecules per unit cell, the chloroform molecules in the simulation cells are observed to diffuse at a lower rate than at a loading of 10 molecules per unit cell. However, in general, diffusion coefficients calculated for molecular dynamics simulations with 10 and 40 sorbate molecules in sodium zeolite Y are lower than those calculated for other, less polar hydrocarbons in zeolite Y and other zeolites. For instance, Yashonath *et al.*⁴ performed molecular dynamics of methane diffusing in both zeolites A and Y^{6,31}. The diffusion coefficients reported for the sodium zeolite Y case matched well with experimental data, and were faster than those calculated and reported in this thesis for chloroform. There are a number of possibilities to account for this. The molecules studied by these authors were not as polar as chloroform, in the sense that the dipoles were not as large as the dipole between the H atom and C atom in the chloroform molecule. Therefore, the electrostatic interaction with the framework basic sites is more significant for chloroform than for the other molecules in question and so some molecules are held due to the fact that they are adsorbed, thus colliding and blocking other diffusing sorbate molecules. Also, in the simulations described, the number of sorbate molecules in the cell is 40 molecules, and repulsion between the molecules would restrict such diffusive motion, as would collisions between the sorbates. The orientation of some of the polar sorbate molecules are such that a hydrogen bonding interaction is liable to take place between the partially positively

charged hydrogen atom and the basic framework oxygen. Monte Carlo simulations by ourselves (described earlier in this chapter) and others indicate that these interactions may take place with oxygen atoms situated on a four ring facing the zeolite supercage (where a SIII or SIII' site would be in zeolite X). Some of the molecules in molecular dynamics simulations are orientated in such a way, and at such a distance, as to allow interaction with a cation and framework oxygen atoms, in the scheme II proposed by Bosch *et al.*²⁵, as shown in figure 3.22. This would help to explain the rapid and early motion of the SII cations with a loading of 40 molecules per unit cell, and the fact that a smaller number of cations move during molecular dynamics on a system containing only 10 sorbate chloroform molecules.

However, in the system containing 10 molecules of chloroform, the diffusion coefficients show that diffusion of the molecules is generally faster than in the more highly loaded systems. A reasonable explanation for this could be that in the case of the simulation with 40 molecules per unit cell, more collisions between the molecules are possible, which would restrict any diffusive motion.

Temperature (K)	Approximate Diffusion Coefficient (m ² s ⁻¹)
270	4.72 x 10 ⁻¹⁰
330	5.54 x 10 ⁻¹⁰
390	1.29 x 10 ⁻⁹

Table 3.12: Diffusion coefficients for 10 molecules diffusing through NaY zeolite

Temperature (K)	Approximate Diffusion Coefficient (m ² s ⁻¹)
270	2.55 x 10 ⁻¹²
330	2.92 x 10 ⁻¹²
390	5.98 x 10 ⁻¹¹

Table 3.13: Diffusion coefficients for 40 molecules diffusing through NaY zeolite

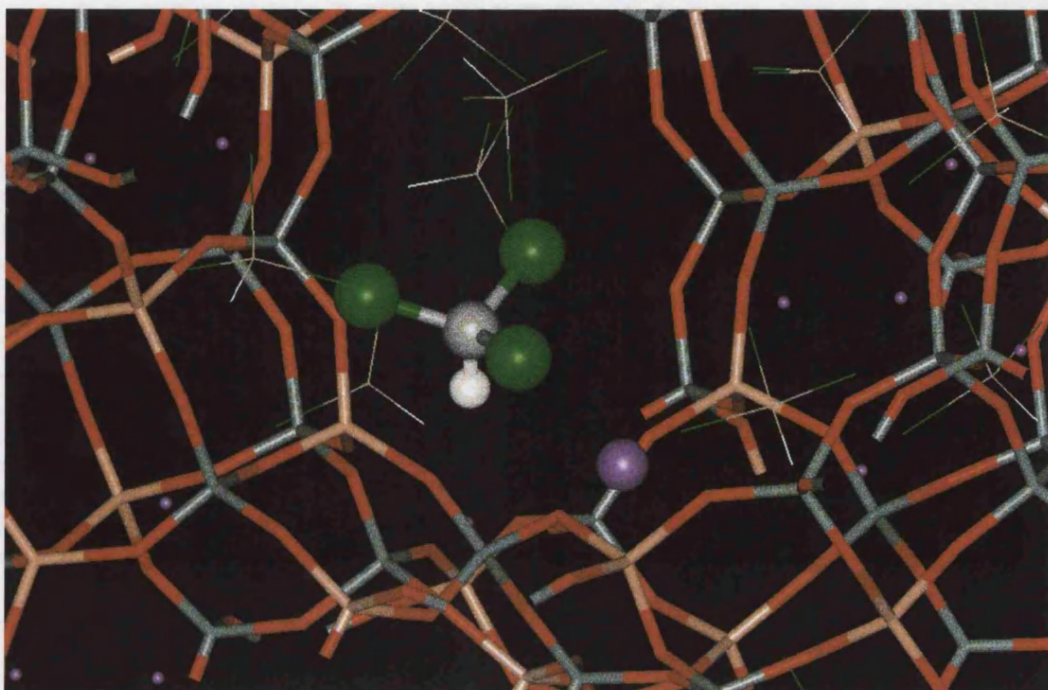


Figure 3.22: Orientation of a chloroform molecule adsorbed in NaY. The orientation is similar to one proposed by Bosch et al, where the hydrogen (white) can interact with a framework oxygen atom (red), and the chlorine (green) interacts with a sodium cation (purple).

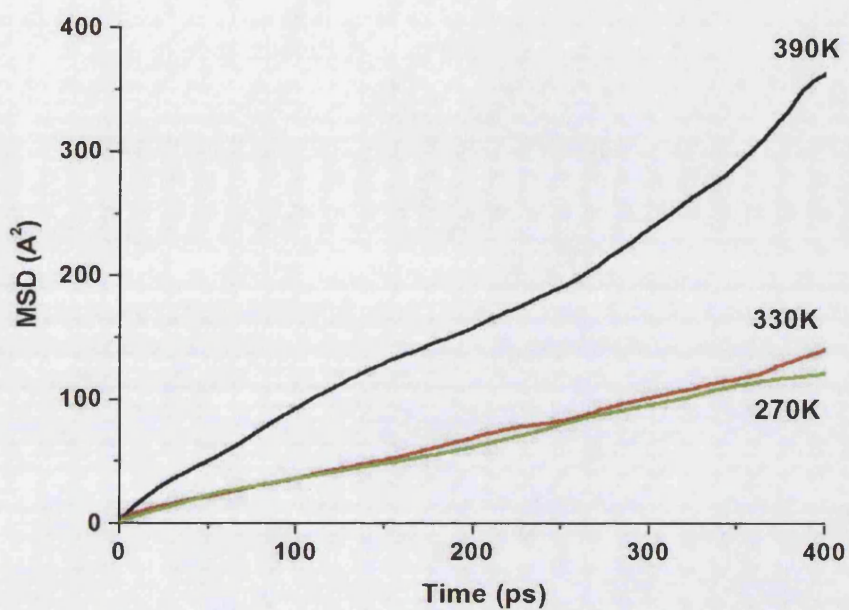


Figure 3.23: MSD plot for carbon atoms for the MD simulations at 390K, 330K and 270K with a loading of 10 molecules per unit cell.

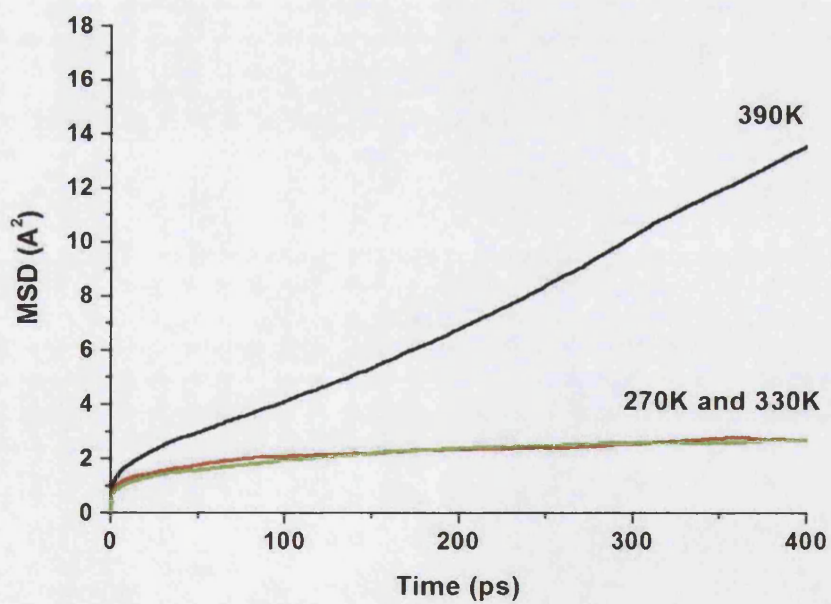


Figure 3.24: MSD plot for carbon atoms for the MD simulations at 390K, 330K and 270K with a loading of 40 molecules per unit cell.

Effect of a Rigid Framework on Cation Motion in Sorbate Loaded NaY

As previously mentioned in this chapter, it is believed by some authors that the use of a rigid framework in molecular dynamics of sorbate diffusion in zeolites would have little effect on the diffusion coefficients of the sorbates⁹. Arguments have been put forward in this thesis that this would not be true for the extraframework cations, evidenced by the observation of the unorthodox behaviour of the SII cations in unloaded zeolite NaY. Simulations performed with a loaded zeolite further bolster the evidence produced that cation motions are affected by the framework vibrations.

Some of the SII cations are, as mentioned above, observed to migrate away from their sites towards the centre of the supercage or towards an SIII' site upon adsorption of chloroform. However, an analysis of the trajectory reveals that the SII cations are largely immobile in the simulation where the zeolite framework is held fixed at all times, which is a contradiction to the results of the molecular dynamics incorporating a flexible framework.

The diffusion coefficient for the chloroform molecules is calculated to be approximately $5.33 \times 10^{-11} \text{ m}^2\text{s}^{-1}$. This is faster than the molecular diffusion for the flexible zeolite case by one order of magnitude, and a possible explanation could be that coupling with the zeolite framework was not possible in this case, thereby precluding the possibility of kinetic energy exchange, or that the lack of migration of the cations means that coupling with them was not possible either.

Evacuation of the Sorbates

Having performed simulations for at least 600 picoseconds, the sorbates were deleted from the simulation cell, and the simulations were rerun at 390K and 700K in order to study any possible redistribution of the cations. The simulations were run under the same conditions as for the sorbate-loaded cases, and for at least 500ps.

Analysis of the trajectories indicated that the migration of a cation from a SII site back to a SI' site is possible. The mean square displacements for these cations reflect the observation that over the simulation period, there is significant movement by some of the cations occupying SII positions that formerly occupied SI' positions. The fact that only these cations are seen to traverse the six ring and enter the sodalite cage may indicate the relative stabilities of cations held in six rings of differing aluminium content. SI cations (or cations that were SI cations before adsorption) are relatively immobile during this simulation.

For the simulation at 700K, some cations that had been extracted from SII positions due to interactions with the polar sorbate molecules are observed to return to their original positions, indicating that the configuration whereby the cation is coordinated with either two oxygen atoms, or near a SIII' site is not necessarily stable at 700K in a bare zeolite. A reason for this is that the potential energy surface in this area is relatively flat. This accords with the finding by Jaramillo and Auerbach that SIII' sites are mobile in NaX. Interestingly enough, this is only observed at the six ring where there are more than one aluminium atoms present. The relative mobilities of the SII cations after sorbate evacuation at 390K and 700K as calculated from the MD runs is shown in figure 3.25.

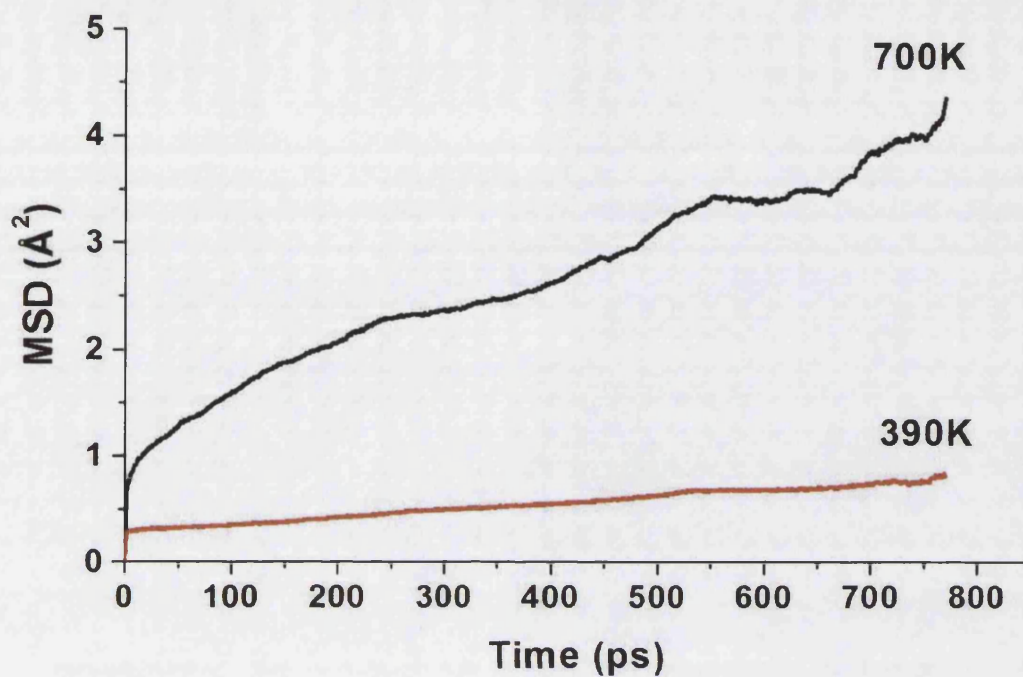


Figure 3.25: MSD plot for SII cations at 700K and 390K after sorbate evacuation.

Prediction of Vibrational Frequencies

Extra simulations were performed for both the sorbate loaded and unloaded zeolite, with the positions, forces and velocities being saved every 20 steps (equating to 20 fs). The frequency of saving the trajectory gives a time period between frames that is much smaller than the period of vibration for the sodium cations, and so therefore the velocity autocorrelation function (VACF) and the corresponding Fourier transform (or power spectrum) could be calculated and compared to experimental vibrational spectroscopy data. The simulations were run for 200 picoseconds after a 50 ps equilibration period.

In light of the results of molecular dynamics calculations using a rigid zeolite framework described earlier in this chapter, a flexible zeolite framework was employed in both simulations. One should bear in mind that when comparing vibrational spectra calculated from VACFs with infra red spectroscopic data, only a qualitative comparison should be made, due to the fact that we do not include quantum corrections in our calculations. Ideally, VACF power spectra should be compared to inelastic neutron scattering data. However, the lack of availability such spectra for sodium cations in zeolites means that IR spectra would have to be used in this case.

Predictions for NaY in the Loaded and Unloaded Zeolite

The velocity autocorrelation functions for the molecular dynamics simulation of the unloaded zeolite and loaded zeolite were calculated and their corresponding Fourier transforms are shown as figures 3.26-3.31. The graphs shown are for each of the cation sites, SI, SI' and SII. The simulations were run for long enough that the VACF were damped to zero.

Comparisons are made with experimentally measured infra red spectra by Jacobs³² and by Ozin's group³³⁻³⁶. Sodium cation vibrations at SI sites are assigned to frequencies of 160 cm^{-1} by both authors. Comparisons with our calculated power spectrum show that for the SI cations a peak is predicted at 169 cm^{-1} in the unloaded zeolite molecular dynamics simulations. However, the other peaks visible from our prediction, notably a peak at 78 cm^{-1} have not been assigned to SI cations in experimental works studied, although it could simply represent an anomaly due to the Fourier transform algorithm used. A qualitative glance at the predicted spectra by Krause *et al.*³⁷ for these cations

reveals peaks at approximately 150 cm^{-1} and 175 cm^{-1} . However, the relative intensities of the peaks are not representative of the experimental spectra, as our calculations do not make use of vibrational selection rules. Other factors to be considered are the forcefield potential parameters, as it has been shown by Jousse *et al.*³⁸ that different forcefields will give significantly different calculated vibrational spectra.

SI' cation vibrations are experimentally assigned to a peak at 109 cm^{-1} , which is matched by our calculations with a peak at 104 cm^{-1} . The spectra for the SII cations are experimentally determined to have a peak at a frequency of 190 cm^{-1} by Ozin *et al.*, or 187 cm^{-1} by Jacobs *et al.*³². A shoulder at approximately 225 cm^{-1} is assigned by Jacobs *et al.*³² as an 'E mode' of the SII cations. In the simulations reported here, a peak at 195 cm^{-1} is observed, and also present is a small shoulder at approximately 234 cm^{-1} , thereby matching the experimental findings to a degree.

Upon adsorption of chloroform molecules, new peaks are visible in the spectra for each cation type, and this may be reflecting to some extent the cation migration described earlier in this chapter. The spectrum for the SI cations indicates that a peak is formed at 104 cm^{-1} , and this could be assigned to SI cations that have migrated into SI' sites. Also, a shoulder at 182 cm^{-1} seen in the spectrum for the loaded case may be due to the fact that a SI cation is seen to migrate to a SI' site and then on to a SII site in the MD trajectory. In the spectrum for SI' cations (or those that were formerly located at SI' sites), one would expect to see a new peak at a frequency characteristic of SII cations. In fact, a small shoulder is visible at 188 cm^{-1} , although this is dominated by the peak at 201 cm^{-1} , which is unassigned. However, this is close to the SII vibrational frequency. The qualitative features of the loaded and unloaded case are quite similar, although the

peak at 51 cm^{-1} has disappeared in the loaded case, and the peaks at 91 cm^{-1} and 110 cm^{-1} in the unloaded case is seen as a full peak at 97 cm^{-1} in the loaded zeolite's spectrum. However lack of INS data for the cations makes interpretation of the power spectra difficult. SIII' frequencies were not assigned in the experimental works studied, and so therefore it is difficult to assign this peak 'swap' to migration between SII \rightarrow SIII'. Other peaks also appear in the loaded case, for example at 175 cm^{-1} in the SI' and SII spectra, which could all reflect changes in the cation's environment.

The general trend in the spectra is that there is a shift towards higher frequencies as the zeolite is loaded with chloroform molecules, with the disappearance of some of the lower frequency peaks. A possible reason for this might be because of a decoupling between the sodium cations and the zeolite framework, as some of the cations are pulled away from their sites.

However it is difficult to unambiguously assign all of the peaks by matching to experimental IR data as the power spectrum was calculated with no selection rules imposed, only the total velocity vectors were used. Furthermore, a large number of peaks are present that could simply represent 'noisy data'. That being said, there are a number of peak shifts between the unloaded and loaded cases for all the cations which could very well be due to changes in the exact cation environment. It could also be that a number of the peaks simply represent the coupling of the cation vibrations to those of the zeolite framework, especially since a number of common peaks are visible in all of the calculated spectra, whether the zeolite was loaded or not. Thus the spectra are too 'noisy' to unambiguously interpret and assign.

However, on a final note regarding the spectra for the cations in zeolite Y (and zeolite A), in terms of assigning peaks for specific cation sites, it has been suggested by Krause *et al.*³⁷ that one cannot assign a specific band to a vibration due to a specific cation site, possible for the reason suggested above.

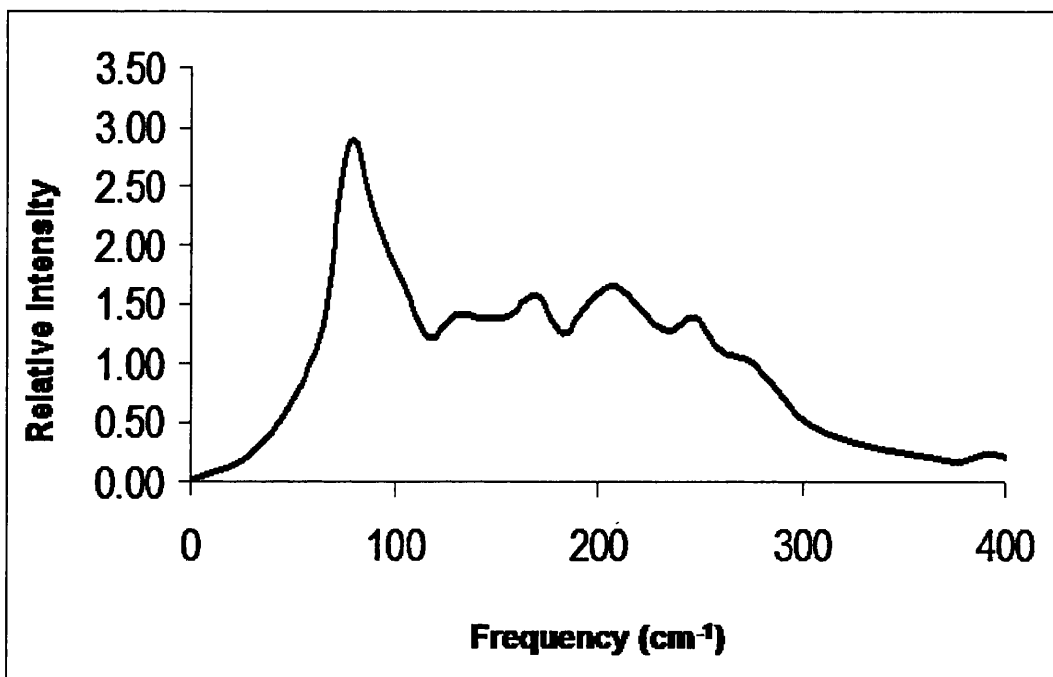


Fig 3.26: Power spectrum of SI cations in unloaded NaY

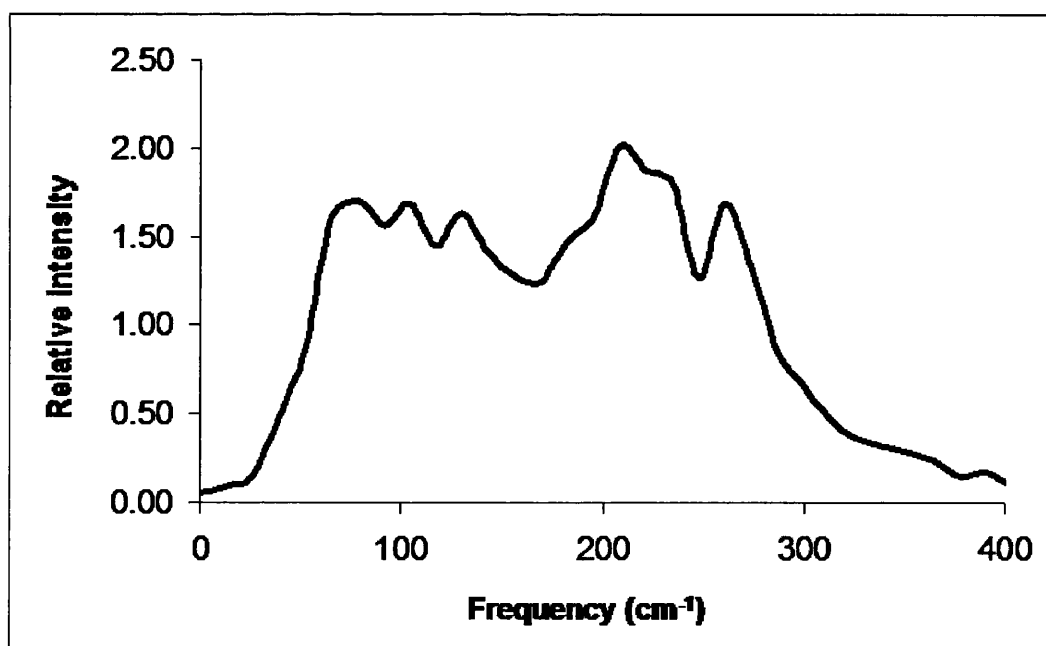


Fig 3.27: Power spectrum of SI cations in chloroform loaded NaY

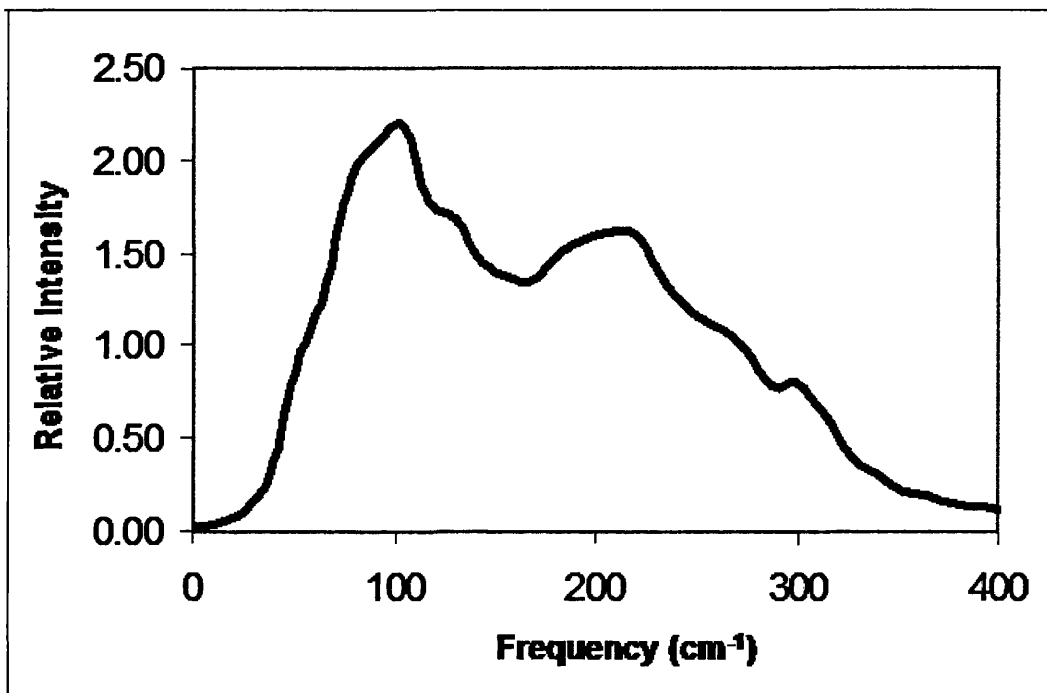


Figure 3.28: Power spectrum of SI' cations in unloaded NaY

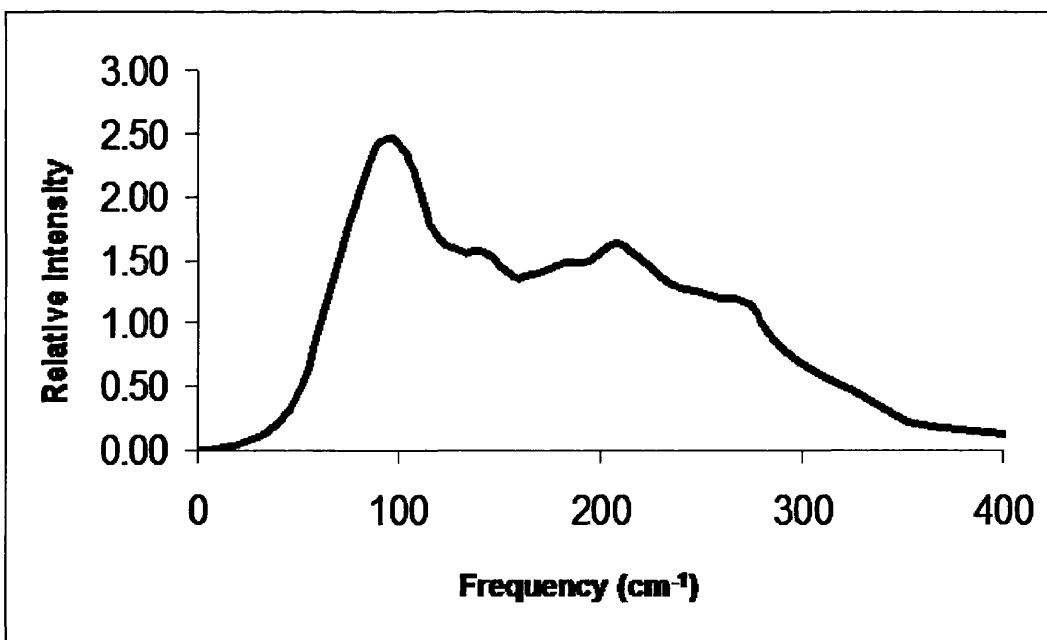


Figure 3.29: Power spectrum of SI' cations in chloroform loaded NaY

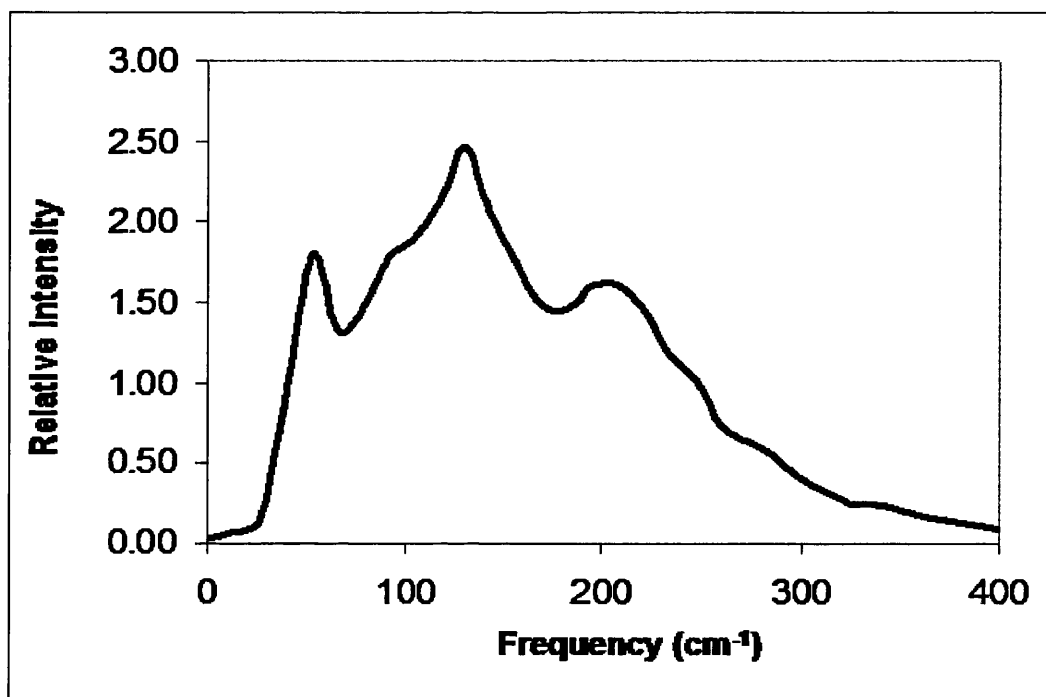


Figure 3.30: Power spectrum of SII cations in unloaded NaY

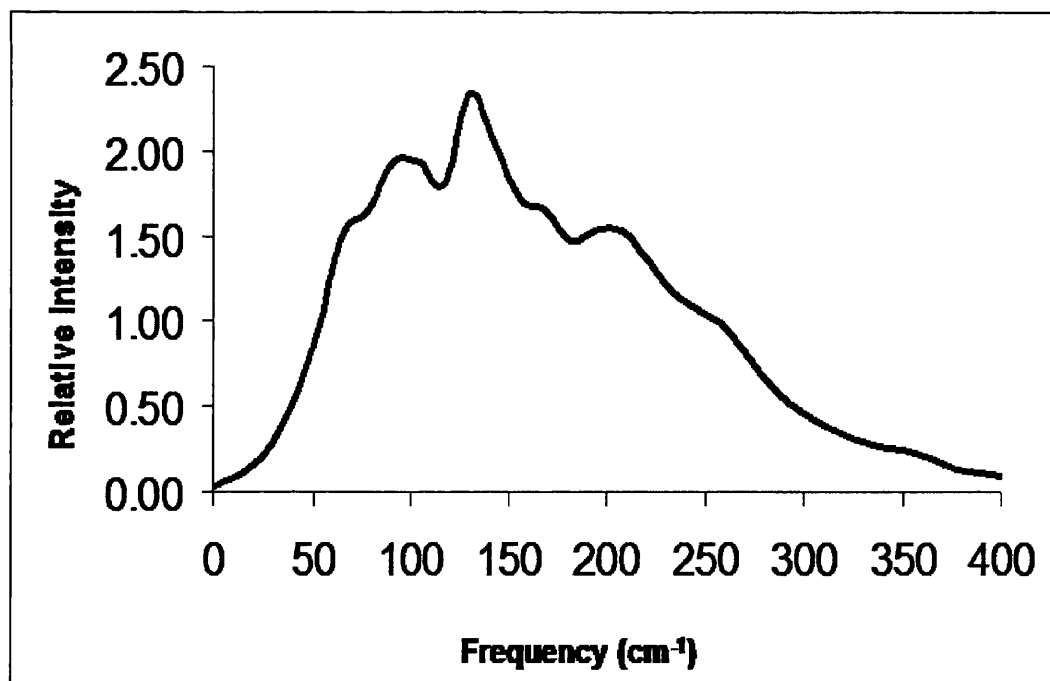


Figure 3.31: Power spectrum of SII cations in chloroform loaded NaY

Conclusions

Molecular dynamics simulations indicate that at temperatures of 270K, 330K and 390K, the Na cations in NaY become mobile upon chloroform sorption. The timescale on which the migrations occur depends on the original siting of the cation and the temperature of the simulation. The SII cations are observed to migrate towards the centre of the zeolite supercage, as they are drawn out by the presence of the chloroform molecules. The SI' cations are seen to migrate in two ways: (1) SI' cations hop from their sites into adjacent SII sites in the supercage; (2) SI' cations move to fill those SI' sites vacated by migration into the supercage. Some SI cations are seen to migrate into nearby SI' sites, and subsequently exhibit similar behaviour. At 390K some SI cations are observed to migrate into the zeolite supercage and fill vacant SII sites.

Otherwise SI cations simply oscillate within the double six ring, evidence of which is shown in the trajectories calculated from the simulation. SI and SI' cations that migrate into the supercage are not observed to diffuse towards the centre of the supercage in the manner of the SII cations over the timescale of the simulation in the case of chloroform adsorption. There is the possibility that this phenomenon may occur over longer simulation times.

The extent and rate of diffusion of the chloroform molecules depends on the temperature and loading. At high loadings, for example 40 molecules per unit cell, the diffusive motion is very sluggish. This is reflected by the MSD plots and possibly explained by the fact that collisions between the molecules in such a crowded supercage would be a hindrance to long range diffusive motion. 'Blockages' may also occur due

to the fact that some molecules would be adsorbed and interact strongly with the framework (which would increase collisions between migrating and adsorbed molecules).

Simulations were performed with the sorbate molecules evacuated from the cell after a period of simulation in which the cations had shifted. The results indicate that although the cations in a bare zeolite are immobile, this is not the case when they have been displaced from their positions as determined by x-ray diffraction. A possible explanation for this is that the cations coordinated by two oxygen atoms, a configuration achieved after the displacement of a SII cation by interactions with polar sorbates, is not as stable as a position where the cation can coordinate with six oxygen atoms. Recent MAS NMR work by Sanchez-Sanchez *et al.*^{39,40} has suggested migration of Li and Na cations upon adsorption of pyrrole in LiNaY and LiNaX zeolites. The mechanism proposed was similar to that described in this work, with the migration of SII cations away from their crystallographic sites due to interactions with the sorbate molecules, and migration of SI' cations into vacant SII sites.

The inclusion of a flexible framework has been deemed to be important when treating the dynamics of the extraframework cations due to the coupling between the cations and the framework. Also, contrary to a number of other works, this work has indicated that the diffusion coefficients of guest molecules are affected by whether or not the zeolite framework is treated as being rigid or flexible in the simulations.

Attempts to calculate the vibrational spectra have been made, and it is concluded that although some peaks observed in experimental IR spectroscopy are reproduced,

assigning frequencies from VACF data is difficult, due to inadequacies in the technique in that selection rules are not taken into account, and that therefore some peaks are masked by other dominant vibrations. Dipole autocorrelation functions may be better served for the purpose of the IR prediction.

In these simulations, we have assumed that no reaction occurs between the molecule and the zeolite framework. The work of Sanchez-Sanchez *et al.*⁴¹ shows that a reaction between the chloroform molecule and the zeolite framework does occur when considering both zeolites NaX and NaY. For this reaction, the authors report that carbon dioxide and a methoxy species are liberated, followed by decomposition of the framework. In the case of zeolite Y however, this reaction occurs very slowly, even at 423K. Our simulations cannot include these possibilities however, as the technique does not allow treatment of electronic degrees of freedom.

Chapter 3 References

- (1) Yuan, X. L.; Cormack, A. N. *Journal of Non-Crystalline Solids* **2001**, 283, 69.
- (2) Calmiano, M. D. Computer Simulation of Molecular Sorption in Zeolites, University College London, 2001.
- (3) Yashonath, S.; Demontis, P.; Klein, M. L. *Chemical Physics Letters* **1988**, 153, 551.
- (4) Yashonath, S.; Demontis, P.; Klein, M. L. *Journal of Physical Chemistry* **1991**, 95, 5881.
- (5) Mosell, T.; Schrimpf, G.; Hahn, C.; Brickmann, J. *Journal of Physical Chemistry* **1996**, 100, 4571.
- (6) Demontis, P.; Suffritti, G. B. *Chemical Reviews* **1997**, 97, 2845.
- (7) Bull, L. M.; Henson, N. J.; Cheetham, A. K.; Newsam, J. M.; Heyes, S. J. *Journal of Physical Chemistry* **1993**, 97, 11776.
- (8) Auerbach, S. M. *International Reviews in Physical Chemistry* **2000**, 19, 155.

- (9) Kärger, J.; Vasenkov, S.; Auerbach, S. M. Diffusion in Zeolites. In *Handbook of Zeolite Catalysts and Microporous Materials*; Dutta, P. K., Ed.; Marcel Dekker, Inc, 2002.
- (10) Clark, L. A.; Ye, G. T.; Gupta, A.; Hall, L. L.; Snurr, R. Q. *Journal of Chemical Physics* **1999**, *111*, 1209.
- (11) Demontis, P.; Fois, E. S.; Suffritti, G. B.; Quartieri, S. *Journal of Physical Chemistry* **1990**, *94*, 4329.
- (12) Faux, D. A. *Journal of Physical Chemistry B* **1998**, *102*, 10658.
- (13) Lee, S. H.; Moon, G. K.; Choi, S. G.; Kim, H. S. *J. Phys. Chem* **1994**, *98*, 1561.
- (14) Shin, J. M.; No, K. T.; Jhon, M. S. *J. Phys. Chem* **1988**, *92*, 4533.
- (15) Demontis, P.; Suffritti, G. B.; Quartieri, S.; Fois, E. S.; Gamba, A. *Journal of Physical Chemistry* **1988**, *92*, 867.
- (16) Faux, D. A.; Smith, W.; Forester, T. R. *Journal of Physical Chemistry B* **1997**, *101*, 1762.
- (17) Hernandez, E. R. R. Computational Studies of Diffusion in Zeolites. PhD, UCL, 1994.
- (18) Gale, J. D. *Journal of the Chemical Society-Faraday Transactions* **1997**, *93*, 629.
- (19) Mellot, C. F.; Cheetham, A. K. *Journal of Physical Chemistry B* **1999**, *103*, 3864.
- (20) Hagler, A. T.; Lifson, S.; Dauber, J. J. *Amer. Chem. Soc.* **1979**, *101*, 5122.
- (21) Jaramillo, E.; Auerbach, S. M. *Journal of Physical Chemistry B* **1999**, *103*, 9589.
- (22) Kawai, T.; Yanagihara, T.; Tsutsumi, K. *Colloid. Polym. Sci.* **1994**, *272*, 1620.
- (23) Fitch, A. N.; Jobic, H.; Renouprez, A. *Journal of Physical Chemistry* **1986**, *90*, 1311.
- (24) Smith, W.; Forester, T. R. *Journal of Molecular Graphics* **1996**, *14*, 136.
- (25) Bosch, E.; Huber, S.; Weitkamp, J.; Knozinger, H. *Physical Chemistry Chemical Physics* **1999**, *1*, 579.
- (26) Kaszukur, Z. A.; Jones, R. H.; Couves, J. W.; Waller, D.; Catlow, C. R. A.; Thomas, J. M. *Journal of Physics and Chemistry of Solids* **1991**, *52*, 1219.
- (27) Mellot, C. F.; Cheetham, A. K.; Harms, S.; Savitz, S.; Gorte, R. J.; Myers, A. L. *Journal of the American Chemical Society* **1998**, *120*, 5788.

- (28) Jaramillo, E.; Grey, C. P.; Auerbach, S. M. *Journal of Physical Chemistry B* **2001**, *105*, 12319.
- (29) Grey, C. P.; Poshni, F. I.; Gualtieri, A. F.; Norby, P.; Hanson, J. C.; Corbin, D. R. *Journal of the American Chemical Society* **1997**, *119*, 1981.
- (30) Catlow, C. R. A.; Bell, R. G. *Solid State Ionics* **1994**, *70*, 511.
- (31) Yashonath, S.; Thomas, J. M.; Nowak, A. K.; Cheetham, A. K. *Nature* **1988**, *331*, 601.
- (32) Jacobs, W. P. J. H. Spectroscopic Studies of the Proton-Ammonia Interaction in Zeolite Y. PhD, TU Eindhoven, 1993.
- (33) Baker, M. D.; Godber, J.; Helwig, K.; Ozin, G. A. *Journal of Physical Chemistry* **1988**, *92*, 6017.
- (34) Godber, J.; Ozin, G. A. *Journal of Physical Chemistry* **1988**, *92*, 4980.
- (35) Godber, J.; Baker, M. D.; Ozin, G. A. *Journal of Physical Chemistry* **1989**, *93*, 1409.
- (36) Ozin, G. A.; Baker, M. D.; Godber, J.; Gil, C. J. *Journal of Physical Chemistry* **1989**, *93*, 2899.
- (37) Krause, K.; Geidel, E.; Kindler, J.; Forster, H.; Bohlig, H. *Journal of the Chemical Society-Chemical Communications* **1995**, 2481.
- (38) Jousse, F.; Vercauteren, D. P.; Auerbach, S. M. *Journal of Physical Chemistry B* **2000**, *104*, 8768.
- (39) Sanchez-Sanchez, M.; Blasco, T. *Chemical Communications* **2000**, 491.
- (40) Sanchez-Sanchez, M.; Blasco, T. *Journal of the American Chemical Society* **2002**, *124*, 3443.
- (41) Sanchez-Sanchez, M.; Blasco, T.; Rey, F. *Physical Chemistry Chemical Physics* **1999**, *1*, 4529.

**Chapter 4: CCl₂F₂ and
CHF₃ Molecules Adsorbed
in NaY Zeolite: A Monte
Carlo and Molecular
Dynamics Study**

Introduction

Continuing the same theme as the molecular dynamics work described in chapter 3, this chapter describes the simulations of two small halocarbon molecules adsorbed in NaY zeolite. CCl_2F_2 , dichloro,difluoromethane, is also commonly known as CFC-12. It was used as a refrigerant in the past, and is said to be partly responsible for the stratospheric ozone depletion observed in the past few decades¹. It is still formed as a side product during the synthesis of its replacement, HFC-134, and so therefore it would be prudent to study and develop materials that aid in its sorption. Fluoroform is an acidic molecule that can be used to probe the basic properties of zeolites.²

Very few studies are reported in the literature on the dynamics of these types molecules in zeolites. Jaramillo *et al.*³ and Grey *et al.*⁴ have studied the dynamics and effects of HFC-134 and HFC-134a in zeolites NaY and NaY, using both molecular dynamics and a combination of experimental techniques (MAS NMR and x-ray diffraction). Their findings mirror those described in chapter 3, in the sense that cation motion is predicted when polar molecules are adsorbed in the zeolite. The authors report the same kind of cation motion as reported in this thesis, and as proposed by some experimental studies, some of which have already been reviewed elsewhere in this thesis. Early work using the Monte Carlo method by George *et al.*⁵ has given an idea of the kind of interactions that might take place when such molecules are adsorbed into zeolite Y, and other zeolites such as sodium mordenite. An unusual aspect of the work of those authors is that the molecules were allowed to be placed inside the sodalite beta cages by the algorithm. In reality, it is generally believed that molecules cannot be resident in such

cages, as they would have to traverse a six-ring in order to enter the cage, which would not be possible, purely due to the relative sizes.

Methodology

The methodology employed for the work detailed in this chapter is the same as that for chapter 3. A Grand Canonical Monte Carlo algorithm was used to insert the sorbate molecules into the zeolite. Americium atoms were placed in the centre of the sodalite cages to act as “dummy” atoms. This was in order to prevent the unrealistic situation of the halocarbon molecules being placed inside such cages, as the molecules would not be able to pass through a six-ring and enter the cage in a real system, due to their relative size as compared with that of the ring. This strategy makes use of the fact that the Monte Carlo program uses the van der Waals overlap of atoms as an initial selection criterion for a particular configuration before considering energetic factors. In order to make a direct comparison with the work reported in chapter 3 of this thesis, configurations with 10 and 40 molecules per unit cell were selected from the adsorption isotherm derived from the Monte Carlo runs. A study of docking conformations was also performed with only one molecule adsorbed in the zeolite cell. Prior to the molecular dynamics, the americium atoms were deleted from the system. Molecular dynamics simulations of CHF_3 and CCl_2F_2 were carried out using the DLPOLY⁶ code in the NVT ensemble. Temperatures of 270K, 330K and 390K were chosen and the system was studied at molecule loading of 40 molecules per unit cell and 10 molecules per unit cell. The forcefield consisted of Buckingham terms to treat the zeolite framework-framework interactions and to treat the cation-oxygen interaction, as described in chapter 3. The molecule-cation and molecule-framework interactions were

treated using Lennard-Jones 12-6 parameters derived from the work of Mellot and Cheetham⁷. The partial charges for the molecules are shown in tables 4.1 and 4.2. The forcefield parameters are shown in tables 4.3 to 4.7. The effects of using a flexible framework to model the dynamics of such molecules and cations in zeolites have been tested and described in the previous chapter. As a consequence of those findings, the framework and molecules were allowed to be flexible in the following calculations.

Atom	Partial Charge
C	0.21000
F	-0.08600
Cl	-0.01900

Table 4.1: Partial charges for the atoms in the CCl₂F₂ molecule

Atom	Partial Charge
C	0.71900
F	-0.24500
H	0.01600

Table 4.2: Partial charges for the atoms in the CHF₃ molecule

	ϵ (eV)	r_0 (Å)
Na - F	4.49E-03	2.50
O - F	3.56E-03	3.03
C - F	1.20E-03	3.39
Cl - F	2.56E-03	3.70
F - F	2.56E-03	3.02
F - H	1.24E-03	2.99

Table 4.3: Lennard-Jones parameters for the non bonded interactions between the sorbate molecule's constituent atoms and the cation / framework oxygen atom, and also the sorbate – sorbate interactions.

	K (eV)	r_0 (Å)
C - F	43.0171	1.363
C - Cl	27.2511	1.761

Table 4.4: Harmonic bonding parameters for the CCl_2F_2 molecule

	K (eV)	r_0 (Å)
C - F	43.0171	1.363
C - H	29.5612	1.105

Table 4.5: Harmonic bonding parameters for the CHF_3 molecule

	K (eV)	Θ_0 (Degrees)
Cl - C - Cl	8.67300	109.50
F - C - Cl	8.67300	109.50

Table 4.6: Harmonic bonding parameters for the CCl₂F₂ molecule

	K (eV)	Θ_0 (Degrees)
F - C - F	8.67300	109.50
F - C - H	5.37710	107.10

Table 4.7: Harmonic bonding parameters for the CHF₃ molecule

Results and Discussion

Docking of the Molecules

A number of the low energy configurations of CHF₃ molecules adopt a very similar configuration to that of the chloroform molecule when docked into the same zeolite. This is not too surprising, since the two different types of molecule polarise in the same manner (i.e. the charge is distributed in the same manner; positively charged hydrogen and negatively charged halogen atoms). However, the distance between the hydrogen and the framework oxygen atom is typically shorter than that in the chloroform case, because of the greater positive charge on the hydrogen atom.

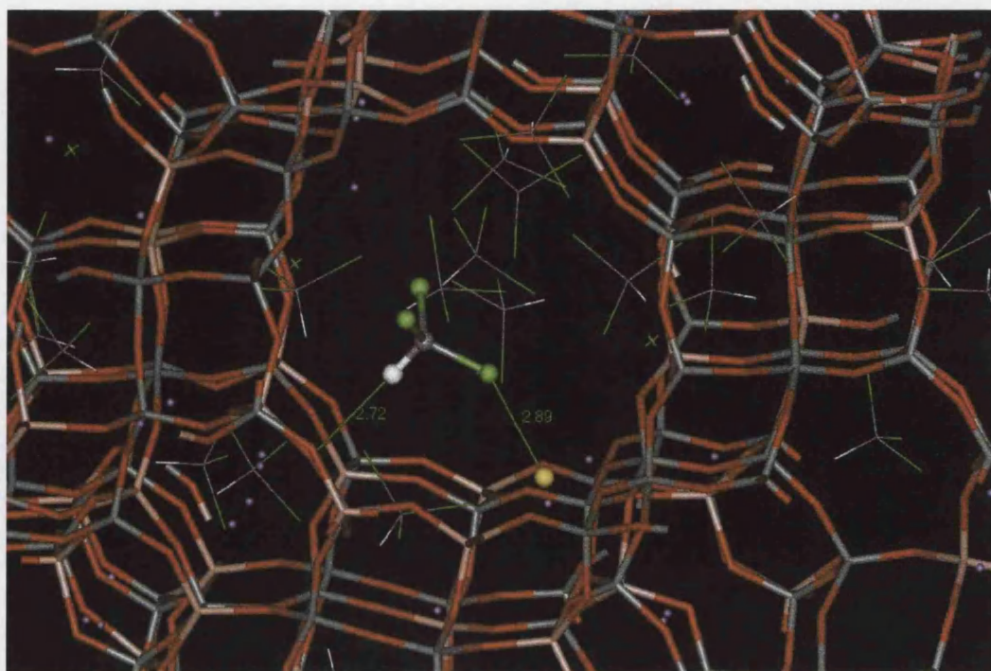


Figure 4.1: A low energy docking configuration of a fluoroform molecule. The molecule of interest is represented by the ball and stick model, with the green spheres representing the fluorine atoms. The white sphere is the hydrogen atom which can be seen to be interacting with a framework oxygen atom (red) at a distance of 2.72 Å. The yellow sphere represents a sodium cation in a SII site.

However, in the case where only one CHF_3 molecule was docked, the lowest energy case was found to be that where the fluorine atom is interacting with a sodium cation, and the hydrogen atom is approximately 3.9 Å from the nearest oxygen (which is part of the six ring containing the SII cation site). This is akin to docking ‘Species III’, as proposed by Bosch *et al.*², and shown in figure 1.6 (page 34). This could therefore be an indicator of the strength of such electrostatic interactions.

For the dichlorodifluoromethane case, only the fluorine atoms are close to the sodium cations, as this is really the only realistic strong attractive interaction. Analysis of the

frames sampled from the Monte Carlo simulations show that there are no chlorine atoms within 3 Å of any sodium cation, with the exception of one, which is 2.89 Å away. No molecules were found inside the sodalite beta cages, due to the presence of the ‘dummy’ atoms (americium atoms in this case). As already mentioned, it has been reported that the energetics of the docking of CFC-12 molecules inside the sodalite cage are lower than when it docks inside the supercage. We assert that it would not be possible for the molecule to traverse a six-ring in order to enter the cages. A scenario does exist however that makes it possible for such configurations to be formed, and that is if the sodalite cage was cleaved open at the external surface of the zeolite and the molecule was adsorbed into it at that location. We did not consider such an event as the study was of bulk sorption and diffusion.

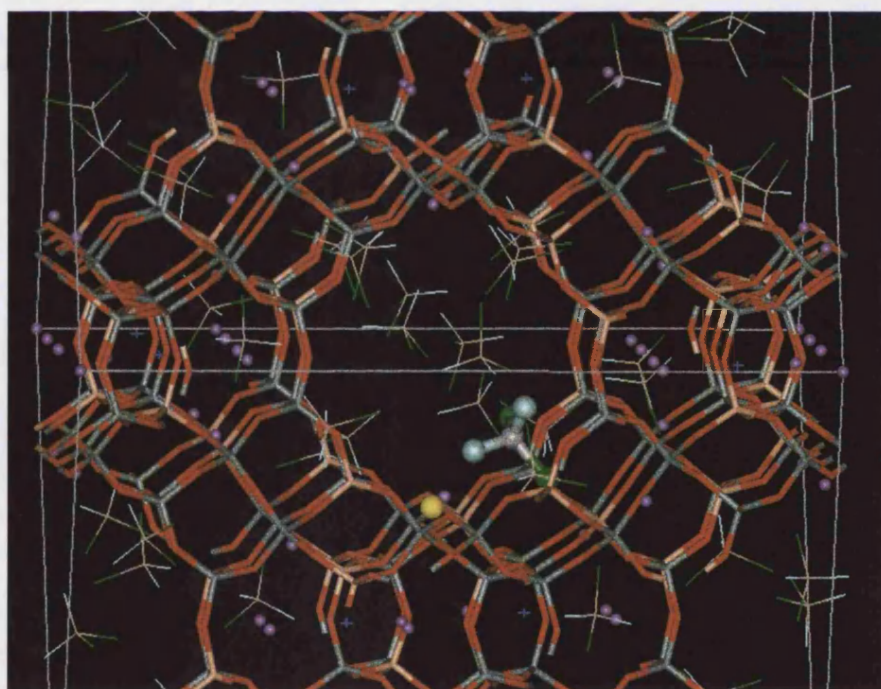


Figure 4.2: A low energy docking configuration of a CFC-12 molecule. The molecule of interest is represented by the ball and stick model. The yellow sphere represents a sodium cation in a SII site.

Cation motions

Analysis of the trajectories of both the CCl_2F_2 and CHF_3 simulations reveal that the cation motion occurring upon the adsorption of the said molecules is very similar to that proposed in chapter 3 of this thesis for the chloroform molecules, that is migration of SII cations to the middle of the supercage or to SIII' sites, and migration of $\text{SI}' \rightarrow \text{SII}$ sites. In the case of the fluoroform molecules, the molecular dynamics trajectory shows a phenomenon that is not observed when chloroform is adsorbed, at least not within the simulation timescale: the migration of an SI' cation \rightarrow SII site \rightarrow middle of the supercage or to a site close to SIII'. Therefore, this could be an indication of the size of the electrostatic effects of the molecule on the extent of cation motion over certain periods of time. The migration mechanism is similar to that observed in the chloroform case, although events generally occur on a shorter timescale. For example, comparing the scale of mean square displacement of SI' cations in the fluoroform case with those in the chloroform loaded case, one can see that in the fluoroform case, the mean square displacements are larger for the time period of 0 to 100 picoseconds of simulation, shown as figure 4.3. Observation of the dynamics trajectory for these cations discloses the fact that some SI' cations are mobile in the first 100 picoseconds of simulation, more so than when the zeolite is loaded with chloroform (see figure 3.12 in chapter 3). This would also mean an increase in migration rate of the SII cations, as they block the only feasible sodalite cage exit for the SI' cations and so would have to vacate their sites first. The SII cations vacate their sites and embark on their respective migrations within the first 50 picoseconds of the simulation. This allows for SI' cation movement at an earlier time during the simulation. This is evident from the MSD plots shown in figures 4.3 to 4.5. A possible reason for this is that stronger electrostatic interactions are possible between fluorine and the sodium cations than the electrostatic

interactions between chlorine and sodium cations. This is reflected in the forcefield, where the fluorine atoms in the fluoroform molecule are assigned a much larger negative charge than the chlorine atoms in chloroform.

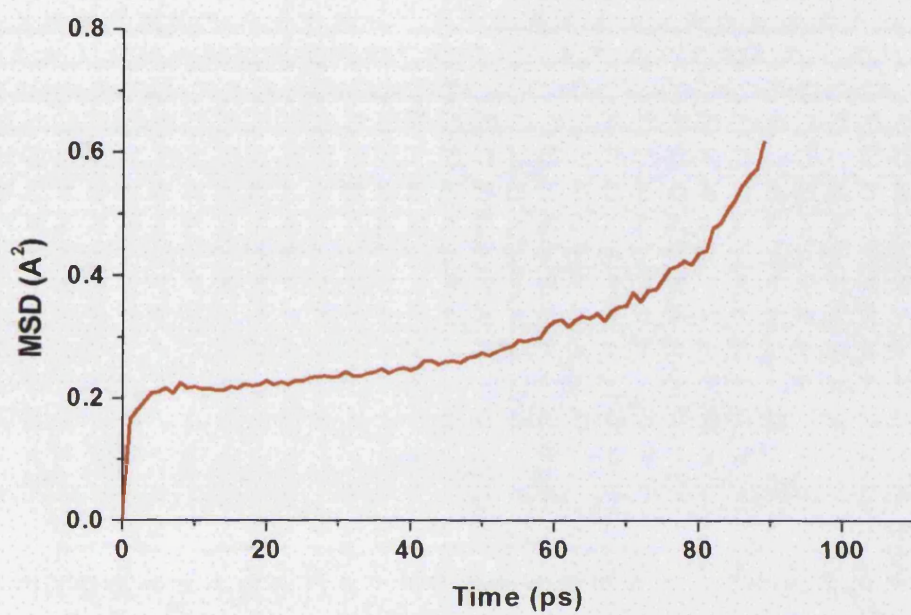


Figure 4.3: MSD plot for the SI' cations between 0 and 100 ps of simulation of NaY zeolite loaded with 40 molecules of CHF_3

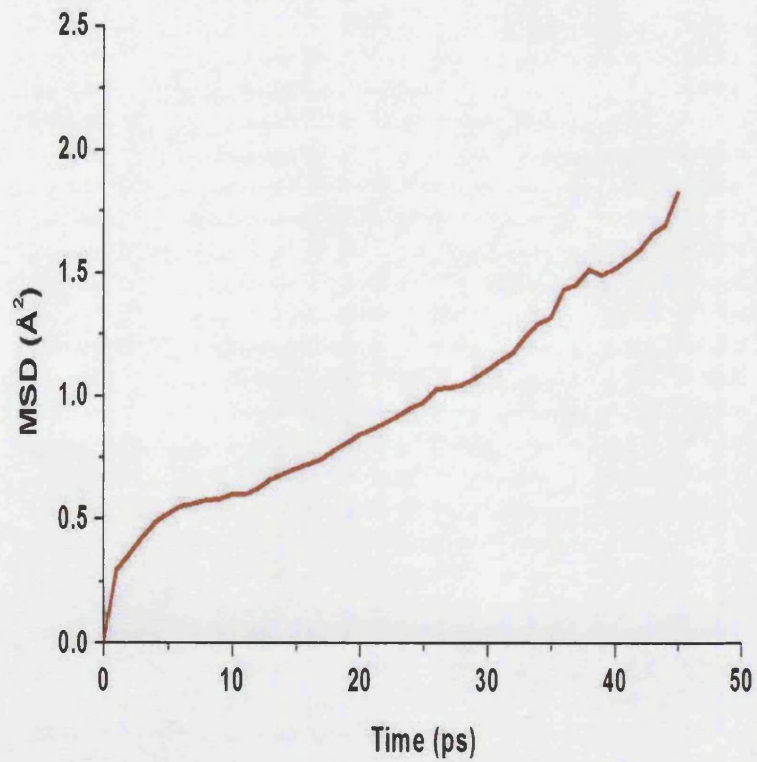


Figure 4.4: MSD plot for the SII cations between 0 and 50 ps of simulation of NaY zeolite loaded with 40 molecules of CHF_3

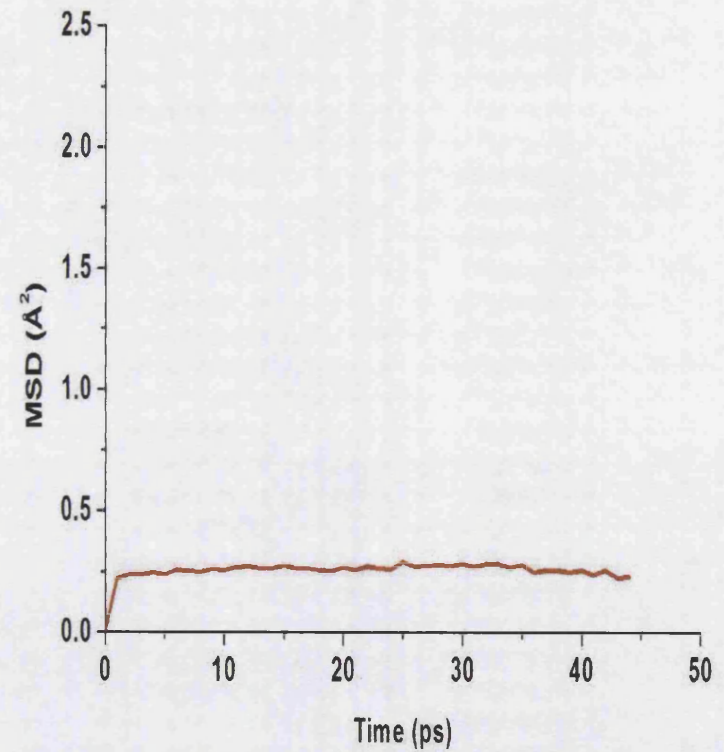


Figure 4.5: MSD (in \AA^2) plot for the SII cations between 50 and 100 ps of simulation of NaY zeolite loaded with 40 molecules of CHF_3

The cation migration upon adsorption of CFC-12 molecules is less marked than that of the fluoroform case in that it happens on a larger timescale. An intuitive explanation for this could be that the dipole would be smaller for this molecule relative to chloroform and fluoroform. In CFC-12, both chlorine and fluorine are competing for electrons from the carbon atom, and hence the smaller dipole. In fluoroform and chloroform, the electronegativity of the hydrogen is small, and so there is less competition for charge from that atom. However this effect cannot be explicitly modelled using the classical molecular dynamics technique due to the fact that the charges of on each atom remain constant (although some of the effects are implicitly included within the interatomic potentials).

However, indications from the MSD plots for the cations for simulations involving this molecule are that the migration happens in the same order as for the chloroform molecule i.e. SII \rightarrow SII', followed by SI' \rightarrow SII, with cation rearrangement within the sodalite cages (SI \rightarrow SI' and SI' \rightarrow SI' motion).

It can be seen from the radial distribution functions that the fluorine atoms are able to get closer to the cations than the chlorine atoms in the CFC-12 molecule. Indeed, the adsorbed geometry indicates that the more significant interaction between molecule and cation is likely to come from the fluorine atoms in CFC-12. This is indicated in the radial distribution function plots for F – SII cation and for Cl – SII cation distances (see figures 4.6 and 4.7). Another feature is the fact that again, the F – Na distance is shorter than the Cl – Na distance for the chloroform case (see chapter 3, figures 3.9 and 3.10).

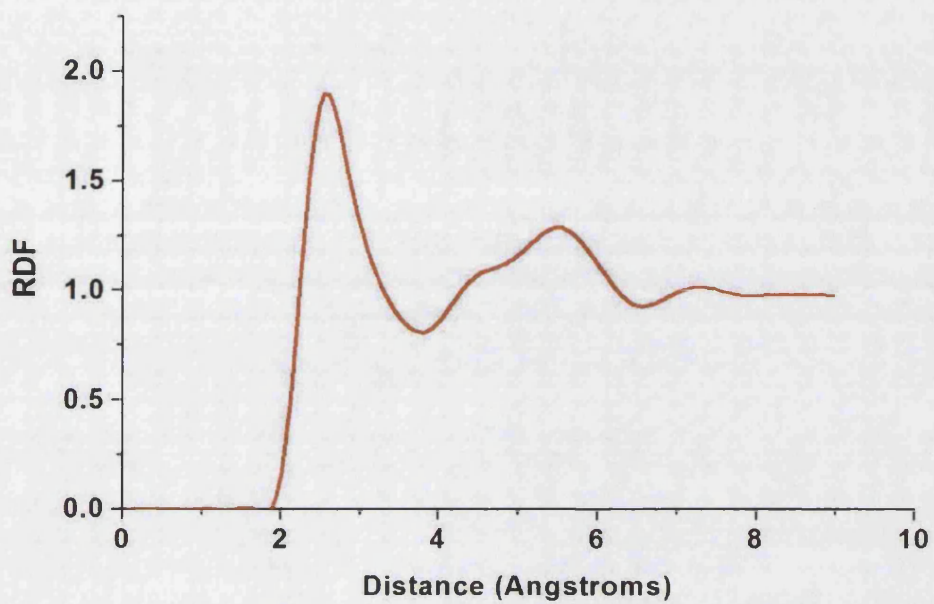


Figure 4.6: RDF plot for the F – Na interaction during the MD simulation of CCl_2F_2 adsorbed in zeolite NaY.

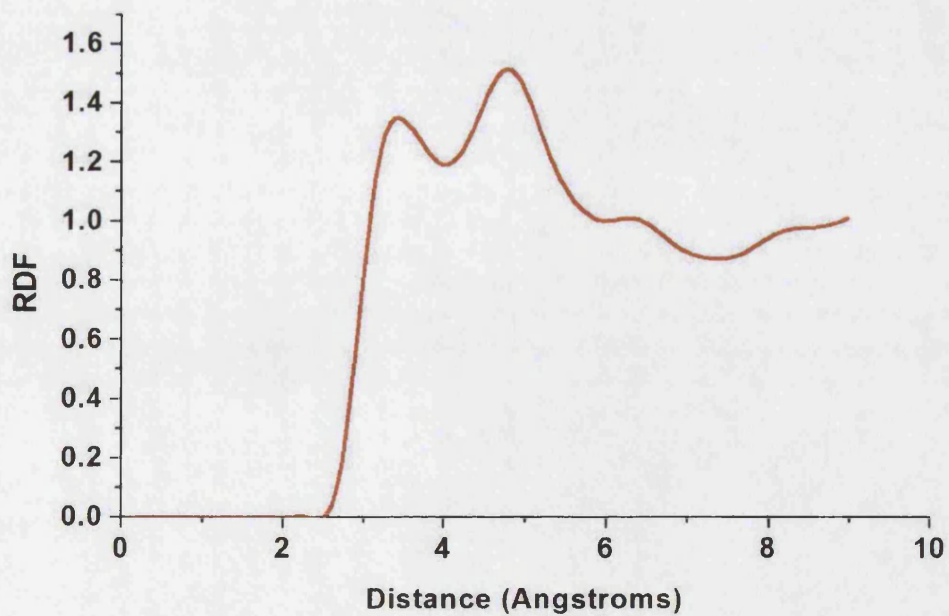


Figure 4.7: RDF plot for the Cl – Na interaction during the MD simulation of CCl_2F_2 adsorbed in zeolite NaY.

Despite all however, one might also argue that strongly acidic molecules such as fluoroform might very well react with the zeolite framework. Although this is a possibility, the molecular dynamics technique cannot treat such a scenario. One would have to apply electronic structure techniques and transition state searches in order to look into this particular problem. A conclusion from the NMR study by Sanchez-Sanchez, Blasco and Rey⁸ is that chloroform will decompose over basic zeolites X and Y. Although this possible consequence of halocarbon adsorption in zeolite Y was not mentioned in the NMR and IR study of CHCl_3 and CHF_3 by Bosch *et al.*², one would intuitively propose that the same type of reaction might occur in the case of fluoroform.

Molecular Motions

Comparison of the molecular motion shows that the fluoroform has a higher diffusion coefficient than chloroform or dichlorodifluoromethane at a loading of 40 molecules per cell. One might explain this by the fact that the fluoroform is smaller than the other two molecules that were simulated, and when comparing similar loadings and temperatures, it might be the case that there are fewer collisions between the fluoroform molecules than between the chloroform or dichlorodifluoromethane molecules. This could also be due to there being more fluoroform molecules interacting with the zeolite at any one time when compared to either of the other two molecules. In fact, inspection of the corresponding frames between the simulations shows that this is the case between fluoroform and chloroform, because more of the fluoroform molecules interact with sodium cations solely, as opposed to a combination of cation – halogen and hydrogen – oxygen interactions. After 500 ps of simulation time at 330K for example, 26

fluoroform molecules have fluorine atoms that are within a distance of 3.2 Å to a sodium cation (whether originally SII or SI'). In contrast, at the same point in time during the chloroform simulation, only 17 molecules have chlorine atoms that are within a distance of 3.2 Å. This is shown in figure 4.8. The number of H—O distances that are below 2.6 Å fluctuates as the simulation progresses, as shown in figure 4.9. For example, at the beginning of the CHF₃ simulation, there are 8 molecules with a H atom interacting with a framework oxygen at or below a distance of 2.6 Å. This number is 13 molecules after 500 ps of simulation, although there is an increase and decrease followed by another increase during the simulation prior to 500 ps. This 'fluctuation' is observed for the chloroform case, with there being little change in the number of molecules whose halogen—cation distances are below 3.2 Å between the beginning and end of the simulation. This could be an indication of the relative strength of the halogen—Na interaction over the H—O interaction. In any case, the molecules can still be considered to be bound to the internal surface of the zeolite, with more fluoroform molecules being adsorbed than chloroform.

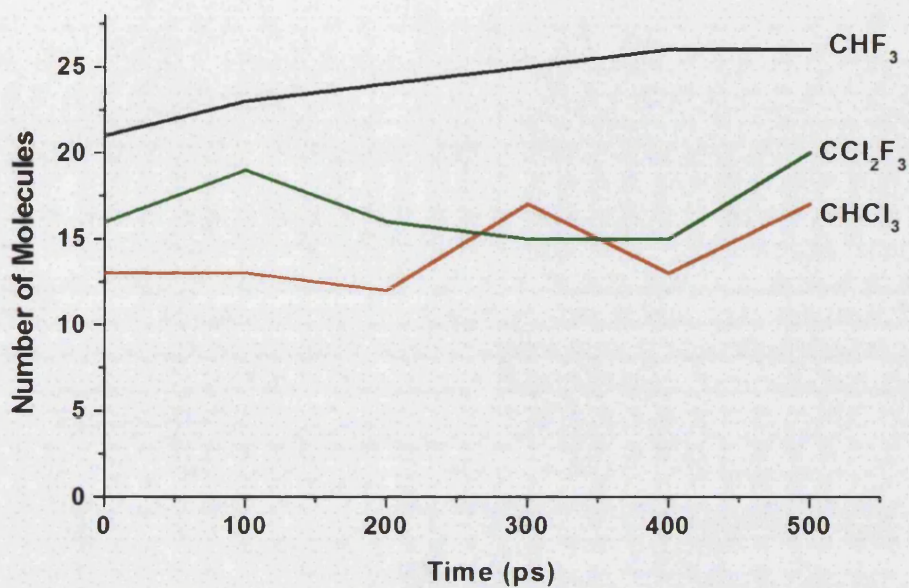


Figure 4.8: Plot of number of sorbate molecules with halogen atoms that are within 3.2 Å of a cation for each molecule simulated over 500 picoseconds

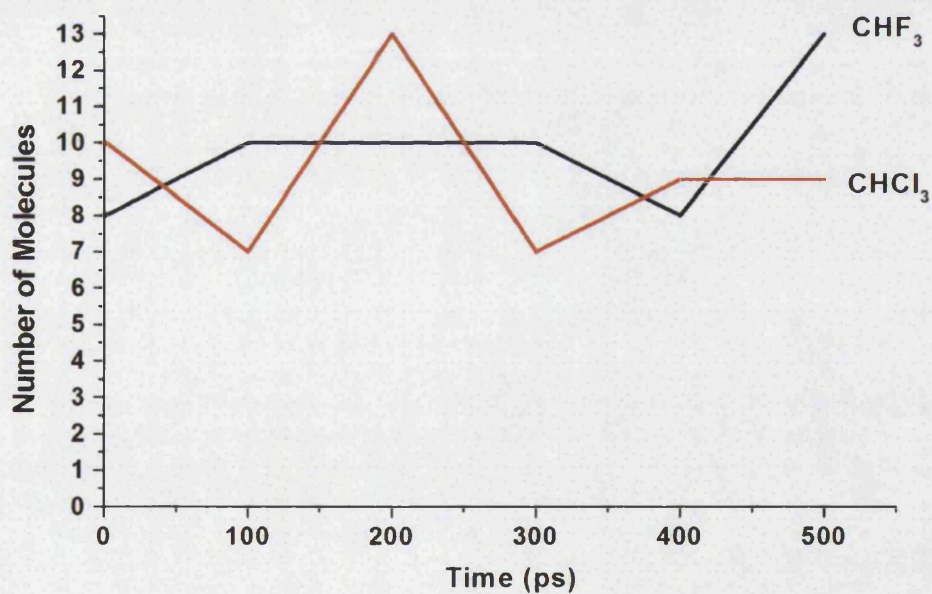


Figure 4.9: Plot of number of sorbate molecules with hydrogen atoms that are within 2.6 Å of a framework oxygen atom for each molecule simulated over 500 picoseconds

In the case of dichlorodifluoromethane, as mentioned before, only the fluorine atoms interact with the sodium cations, with the exception of one molecule, where a chlorine atom is seen to be docked at 2.9 Å from a cation. However, during the course of the simulation this distance increases as the said molecule rotates, and a fluorine atom on the same molecule interacts with a cation instead. Therefore the mode of docking changes during the course of the simulation, in that the molecule is able to ‘flip’ to allow the more favourable fluorine – cation interaction to take place. Although the dichlorodifluoromethane molecules are calculated to diffuse slower than the fluoroform molecules at a loading of 40 molecules per cell for reasons proposed above, with 10 molecules in each cell the opposite is true. The diffusion coefficient calculated from the simulation of 10 CFC-12 molecules shows that the CFC-12 molecules move faster than the fluoroform molecules at the same loading. Inspection of the trajectories and of the docking configurations shows that at this loading, more fluoroform molecules can be considered to be bound to the zeolite than CFC-12 molecules. This is either via halogen – cation interactions, hydrogen – oxygen interactions or a combination of both. In fact, after 500 picoseconds, only one fluoroform molecule is far enough away from the cations and zeolite framework so as to be considered as not bound to the zeolite, whereas only 5 molecules are bound in the case of CFC-12. The diffusion coefficients for CHF₃ and CFC-12 are given in tables 4.8 and 4.9 respectively.

Temperature (K)	10 Molecules per Unit Cell	40 Molecules per Unit Cell
	Diffusion Coefficient (m^2s^{-1})	Diffusion Coefficient (m^2s^{-1})
270	1.26E-10	1.26E-10
330	4.65E-10	4.65E-10
390	6.80E-10	9.49E-10

Table 4.8: Diffusion coefficients for CHF₃ diffusing in NaY zeolite

Temperature (K)	10 Molecules per Unit Cell	40 Molecules per Unit Cell
	Diffusion Coefficient (m^2s^{-1})	Diffusion Coefficient (m^2s^{-1})
270	4.42E-10	2.32E-10
330	3.25E-9	9.70E-11
390	3.68E-9	1.87E-10

Table 4.9: Diffusion coefficients for CCl₂F₂ diffusing in NaY zeolite

Conclusions

The results presented in this chapter have helped to confirm the findings in the previous chapter that the extraframework cations are mobile upon the sorption of polar halocarbon molecules. As in the case of the simulations involving chloroform, two types of interactions are observed in the fluoroform simulations, namely a $\text{H}_{\text{sorbate}} - \text{O}_{\text{zeolite}}$ and a halogen — cation interaction. The decrease in the number of the $\text{H}-\text{O}$

interactions and the fact that this trend is not observed for the halogen — cation interactions may indicate the relative strengths of these interactions and possibly the mode of adsorption of these molecules.

In the case of the dichlorodifluoromethane simulations, only halogen — cation interactions are realistically possible to aid in adsorption. The results of these simulations indicate that the F—Na interaction is more favourable than the Cl—Na. Only one Cl—Na interaction was observed at the beginning of the simulations, and by the end of the simulation, the molecule involved had flipped and was adsorbed via a F—Na interaction.

Again, as in the case of the simulations involving chloroform adsorbed on NaY (chapter 3), we assume that no reaction between the molecule and zeolite framework takes place. Fluoroform adsorbed on NaY has been studied by IR and NMR spectroscopies, and the fact that a reaction might take place was not discussed. However, a slow reaction was reported by Sanchez-Sanchez et al. between chloroform and zeolite NaY at 423K. One might propose that a similar reaction might occur in the fluoroform case, perhaps at a faster rate due to the enhanced acidity of the fluoroform molecule as compared to chloroform. In any case, the molecular dynamics technique would not be suitable to treat this possibility, and in order to do so, one would have to resort to electronic structure techniques.

Chapter 4 References

- (1) Manzer, L. E. *Science* **1990**, *249*, 31.
- (2) Bosch, E.; Huber, S.; Weitkamp, J.; Knozinger, H. *Physical Chemistry Chemical Physics* **1999**, *1*, 579.
- (3) Jaramillo, E.; Grey, C. P.; Auerbach, S. M. *Journal of Physical Chemistry B* **2001**, *105*, 12319.
- (4) Grey, C. P.; Poshni, F. I.; Gualtieri, A. F.; Norby, P.; Hanson, J. C.; Corbin, D. R. *Journal of the American Chemical Society* **1997**, *119*, 1981.
- (5) George, A. R.; Freeman, C. M.; Catlow, C. R. A. *Zeolites* **1996**, *17*, 466.
- (6) Smith, W.; Forester, T. R. *Journal of Molecular Graphics* **1996**, *14*, 136.
- (7) Mellot, C. F.; Cheetham, A. K. *Journal of Physical Chemistry B* **1999**, *103*, 3864.
- (8) Sanchez-Sanchez, M.; Blasco, T.; Rey, F. *Physical Chemistry Chemical Physics* **1999**, *1*, 4529.

**Chapter 5: Calculation of
the Energetic Barriers to
Na Cation Motion through
Zeolite Y Six Rings (SI' to
SII)**

Introduction

Work presented in previous chapters of this thesis has shown that the extraframework cations in zeolite Y are immobile in the absence of polar sorbates, but exhibit “diffusive” or migration properties upon adsorption of such sorbates, depending on the nature of the site in question. Migration from the SI' to SII site is believed to have a high energy barrier, so such a migration would require the cation to have sufficient energy, kinetic or otherwise, to enable it to make the transition.

The work presented in this chapter makes use of the defect energy minimisation technique, using the Mott-Littleton scheme¹, for modelling defects in solids. A number of studies of solid oxides have been performed using this method. Work on proton conduction in perovskite oxides by Islam^{2,3}, Gale and Catlow^{4,5} serve as notable examples of such studies. The technique has traditionally been used in the past to study migration of charges throughout solid ionic lattices. These processes have usually involved defects within the structure, such as vacancies and interstitials, and the migration of these defects played a critical role in the chemistry associated with the material under study. The success of this methodology, when applied to the study of the energetics of the movement of charged species throughout a solid material, has meant that the applications have been extended to other similar problems, not necessarily involving defects. This has included the site to site migration of extraframework cations within zeolite structures.

The technique is a static minimisation technique, where the energetics of a migrating ion are studied by moving the said ion along a migration path (perhaps pre-determined

by a time-dependent technique such as molecular dynamics), representing the species as an “interstitial”. The ion is held fixed in this position and each ‘frame’ is then energy minimised. A “vacancy” is created at the initial ‘perfect’ lattice position, and this maintains charge neutrality.

In the field of zeolite science, Catlow and Bell⁶ have performed computational studies on sodium halide sodalites in order to calculate the energy barrier encountered by sodium cations migrating across six rings in sodalite. The values obtained compared favourably with experimentally determined values. Grey *et al.*⁷ also utilised the Mott Littleton method. In this work the defect energy minimisation scheme was used to study the location and diffusion of calcium cations in chabazite. The authors found that there was little difference to the energy barrier for crossing a six ring when the aluminium content or aluminium configuration changes. The aluminium atoms are believed to increase the flexibility of the zeolite framework, so one might expect there to be a lower energy barrier as the number of Al atoms increases.

The work described below details a study of the energetic barriers to the migration of sodium cations from a SI' to a SII site in NaY zeolite using the defect energy minimisation method under the Mott-Littleton scheme.

Methodology

The Shell Model, Defect Energy Minimisation and The Mott-Littleton Method

Defects are present in materials due to thermodynamic and entropic reasons or as a result of doping or crystal dislocations and shearing. Using computational methods, both classical and quantum, one can describe their interactions with their surroundings and calculate effects due to their motions. Information regarding defect formation, types of defects and their occurrence is available in most basic texts on solid state chemistry, and so this section will describe the implementation of the computational methods specially designed for the treatment of defects.

A feature of many classical defect calculations is the use of the shell model. If one wishes to treat the fact that the nuclei of atoms are surrounded by deformable electron clouds at the 'interatomic potentials' level of calculation, the shell model is a popular and simple method to do so. This model was developed by Dick and Overhauser⁸, and is implemented in the GULP code. In this model, the nucleus and inner electrons are represented by a core which also represents the mass of the atom. The valence electrons are represented by a massless shell which may be distorted, thus allowing for polarisability of the atom. The interactions between the core and the shell are treated by a harmonic function, as though the core and shell were connected together by a spring, of constant k . This is the only interaction treated between the core and the shell. Figure 5.1 illustrates the model.

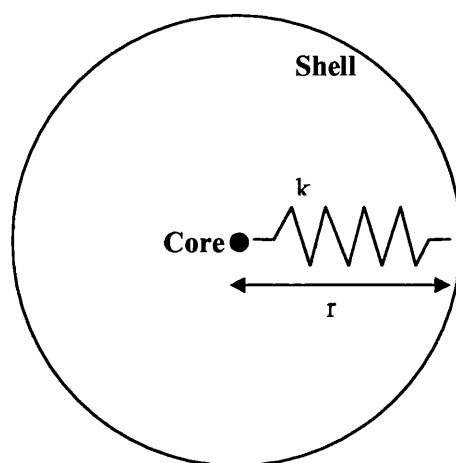


Figure 5.1: An illustration of the shell model

The total charge of the ion is the sum of the charge of the core and the shell, ie.

$$q_{\text{tot}} = q_{\text{core}} + q_{\text{shell}} \quad \text{Eq. 5.1}$$

The interaction energy between the core and the shell is given by a harmonic function

$$\text{(Hooke's Law): } E_{\text{core-shell}} = \frac{1}{2} \cdot k (r - r_0)^2 \quad \text{Eq. 5.2}$$

The polarisability of the ion, α , will depend on the charge of the shell, and the spring constant k . The function governing it reads:

$$\alpha = q_{\text{shell}} / k \quad \text{Eq. 5.3}$$

Treatment of defects, including minimising defect energies, in classical computational chemistry is usually done using the supercell method or the Mott-Littleton method, two commonly used methods available to the computational chemist. Due to the aforementioned successful work using the Mott-Littleton method, the supercell method was not used and is not described here, although a description of it is available elsewhere⁹.

The Mott-Littleton method creates a defect and partitions the material (zeolite in this case) into two regions, denoted as Region 1 and Region 2. The forces on the atoms in Region 1 exerted by a defect are deemed to be strong. Therefore, they are treated using atomistic potentials in order to accurately model the lattice relaxation around the defect. Region 2 is further split into two more regions. Region 2a ions are explicitly treated. They are thought of as being able to respond harmonically to the electrostatic forces due to the defects in Region 1. Region 2b is treated with continuum methods. The forces from the effect of the defect experienced in this region are relatively weak. The behaviour of these atoms is considered to be a dielectric response to the defect's effective charge, and so is treated using methods based on continuum theories.

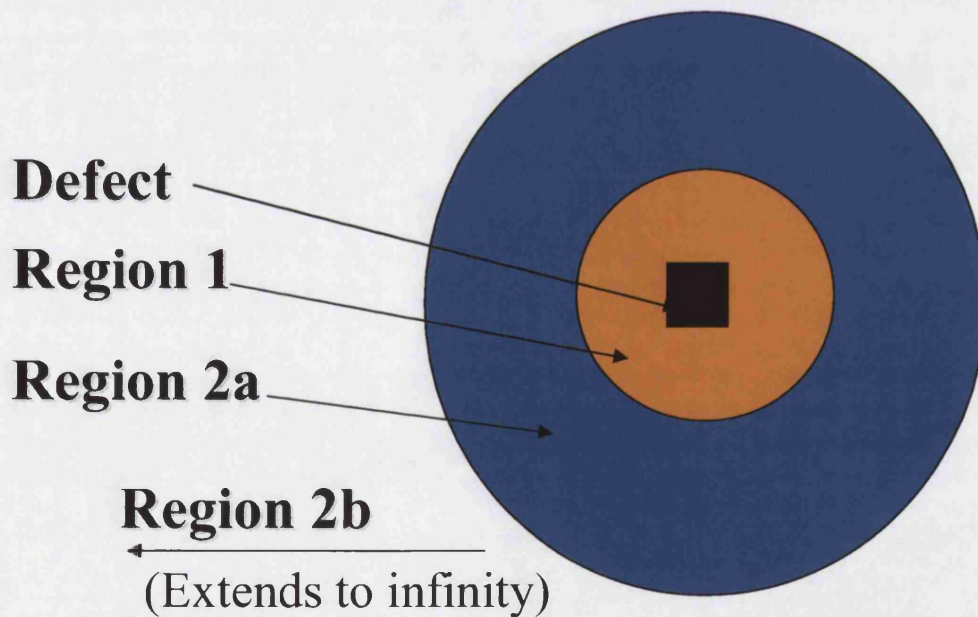


Figure 5.2: The partitions of the Mott-Littleton method.

Creating the Model

The NaY structure refined from powder neutron diffraction data by Fitch *et al.*¹⁰ was used as the ‘perfect lattice’ structure for the calculations presented here. Prior to the defect calculations, the bulk zeolite simulation cell was energy minimised using the GULP code under periodic boundary conditions. The well-known potentials developed initially by Sanders, Leslie and Catlow¹¹⁻¹³ were used as the forcefield, and the parameters are listed in tables 5.1-5.3. The spring constant for the O (core) – O (shell) interaction was 74.92 eV.Å⁻².

The method of calculating the energy barrier is the same as described earlier in this chapter. A cation located in a SI’ site that was observed in the MD simulations to migrate to a SII site upon halocarbon adsorption, as described in chapters 3 and 4, was chosen as the initial site where the defect was to be created. A path along which interstitial sites would be placed was extracted from the trajectory calculated by the molecular dynamics simulations. Extra points were also created along this path, giving a finer grid of points (or “frames”) spaced approximately 0.5 Angstroms apart. In order to explore the area surrounding this migration path, points for interstitial sites were also selected around the migration path, imagining the ‘migration’ interstitial as a centre point (henceforth referred to as CENTRE) on a compass, then surrounding interstitials were placed at the E, W, S, N, SE, SW, NW and NE points on the compass), lying in a plane perpendicular to the direction of migration. Therefore, in effect a migration ‘corridor’ was created within which the CENTRE interstitials were placed. Figure 5.3 shows the centre path and two of the eight surrounding paths.

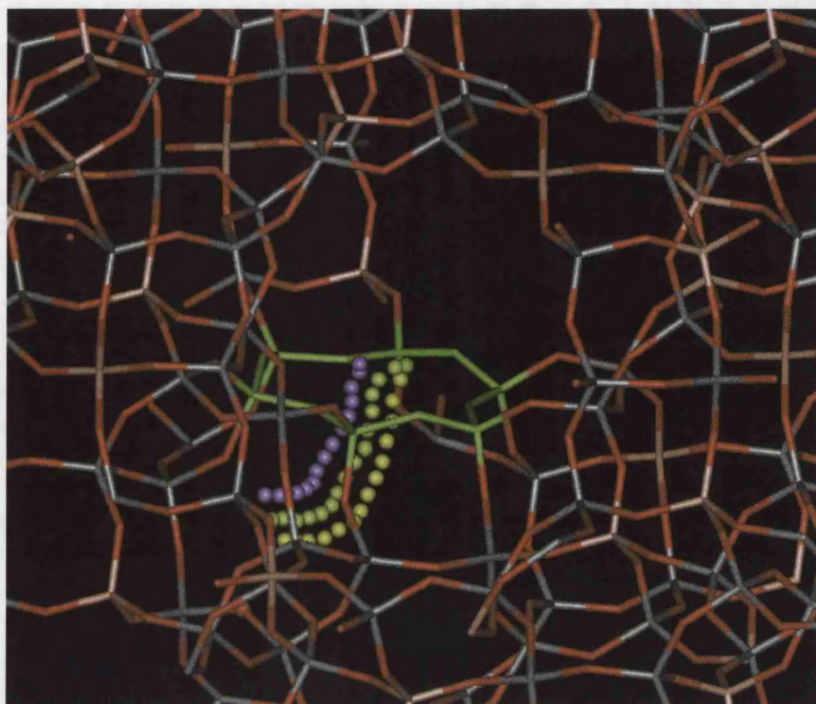


Figure 5.3 Three of the migration paths used as points in the Mott-Littleton calculations.

During the defect optimisation, the interstitial was held fixed in its position. A vacancy was created at the “perfect lattice” SI’ site, the structure already having been energy minimised. The centre of the Region 1 was placed at a point very near the target SII site. Region 1 was made to be 14.5 Angstroms in radius, giving approximately 800 ions. The radius of Region 2a was 27 Angstroms, which equated to approximately 4000 ions.

The calculations were initially performed with three aluminium atoms in the six ring being traversed, as this was the number present in that particular ring. However, the calculations were also performed with one aluminium atom in the six ring in question,

and two sets of calculations were performed with two aluminium atoms in the six ring. These represented the two relative positions possible for the aluminium atoms, the *meta* and the *para* position, assuming only Löwensteinian Al distributions. It is believed that the number of aluminium atoms present in a six ring (or indeed the framework) will affect the extent of flexibility of the framework, and so therefore could determine diffusive properties in that it could control which species may pass through. Furthermore, the presence of the aluminium atoms would have two effects that could facilitate the passage of a cation through the six-ring aperture; the Al-O bonds will be longer than the Si-O bonds, and there would be an increase in negative charge in the neighbourhood of the Al atoms thus lowering the interaction energy with a cation.

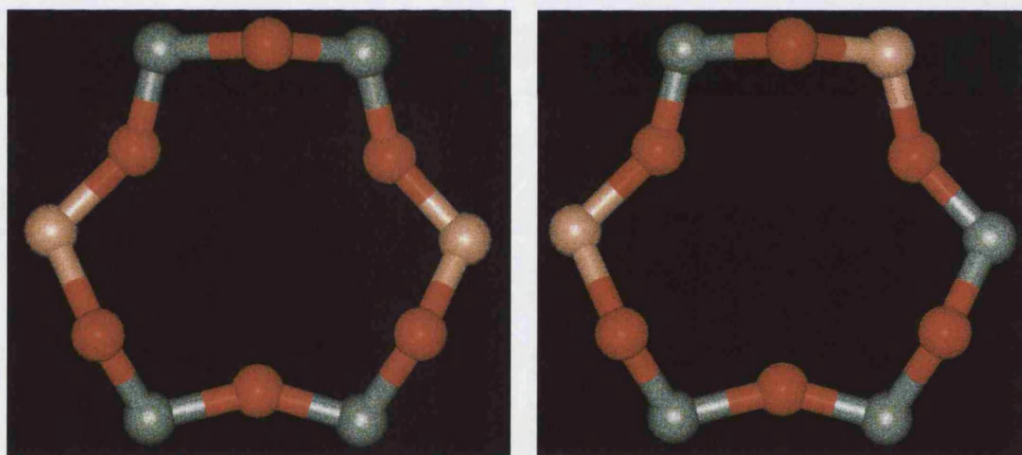


Figure 5.4: The diagram of the six ring through which the migration occurs, showing the Al atoms (represented by the pink spheres) in the *para* positions (left) and the *meta* position (right)

Potential Parameters

Element	Charge
Na (core)	1.00000
Si (core)	4.00000
Al (core)	3.00000
O (core)	0.86902
O (shell)	-2.86902

Table 5.1: The species and their charges used in the Mott-Littleton calculations

Interaction		A (eV)	ρ (Å)	C (eV* Å ⁶)
Na (core)	O (shell)	1226.840	0.30650	0.00000
Na (core)	Na (core)	7895.400	0.17090	0.00000
Si (core)	O (shell)	1283.907	0.32052	10.66158
Al (core)	O (shell)	1460.300	0.29912	0.00000
O (shell)	O (shell)	22764.000	0.14900	27.87900

Table 5.2: The Buckingham potential parameters used in the Mott-Littleton calculations

			K(eV. rad ⁻¹)	Θ (Degrees)
O (shell)	Si (core)	O (shell)	2.09724	109.47
O (shell)	Al (core)	O (shell)	2.09724	109.47

Table 5.3: The three body potential parameters used in the Mott-Littleton calculations

Results and Discussion

The potential parameters used to describe the system in this calculation are well established for calculations involving zeolites and thus are widely acknowledged as being accurately able to reproduce structural properties. Therefore in the optimisation of the bulk crystal structure, the experimental structure was closely reproduced by the potential parameters.

Although a value of 14.5 Angstroms was chosen for the Region 1 radius, a number of other values were tried prior to the calculations. This is because when performing such calculations one must first find a minimum Region 1 size where we can be confident that the results are not dependent on region size. Values of 6.0, 7.0, 8.0, 9.0, 10.0, 11.0, 12.0, 13.0, 14.0 and 15.0 Angstroms were tried as test values for the Region 1 radius. Table 5.4 shows the number of ions corresponding to each value of the radius. Although smaller values than 14.5 are consistent with each other in terms of giving very similar defect energies, the greater the number of ions in Region 1, the better the representation of the structure will be. The results of this test are shown in figure 5.5. Thus there is a trade off that must be decided upon, where a balance is achieved between accuracy of calculation and computational time. A Region 1 radius of 14.5 Angstroms was decided upon.

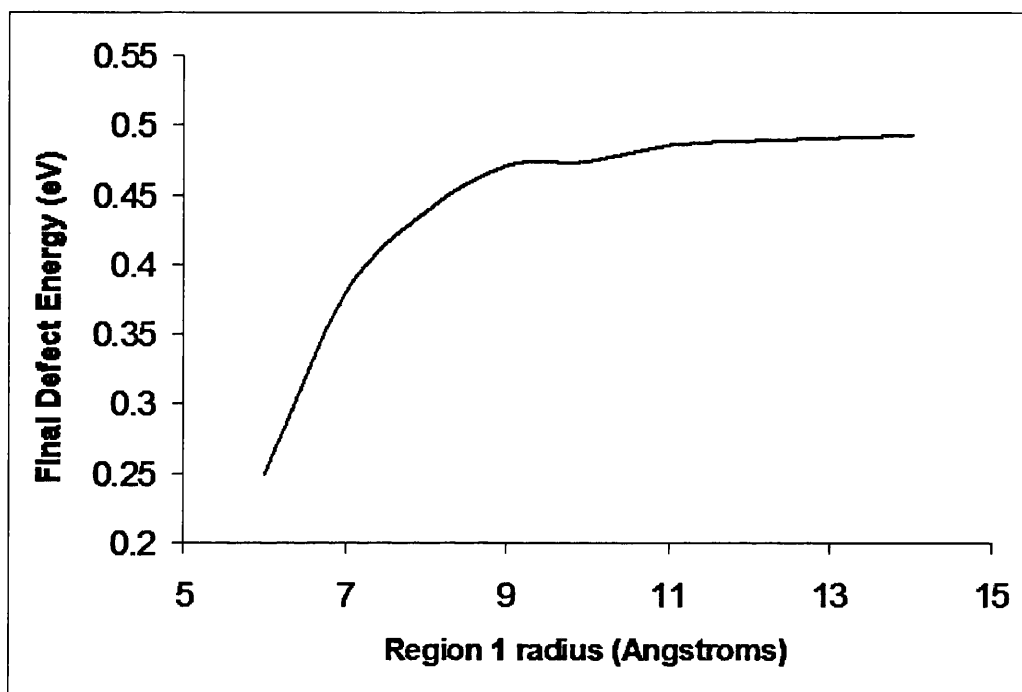


Figure 5.5: A plot of defect energy vs Region 1 radius

Region 1 Radius (Angstroms)	No. of Ions in Region 1
6	72
7	120
8	175
9	245
10	273
11	351
12	462
13	555
14	751
15	950

Table 5.4: Number of ions corresponding to the various Region 1 radii tested

Energetic barriers – general features

The qualitative features of the plot of the defect energy against ‘frame’, shown as figures 5.6 to 5.9, are that there are two barriers to be overcome for the migration of a sodium cation from a SI’ site to a SII site, regardless of the number of aluminium atoms in the six ring being traversed. The first barrier corresponds to the fact that in the middle of the sodalite cage, the cations are not close enough to interact favourably with the zeolite framework oxygen atoms, and such interactions would lower the energy of the cation in that position. The fact that the energy barrier height is different between each case of zeolite six ring content could indicate the effect of varying the local aluminium composition of the zeolite framework on the cation site energies. Varying the number of aluminium atoms in a particular six-ring involved altering the overall aluminium distribution, and hence the long range electrostatics, since the framework composition remained the same. This would be expected to have a subtle effect on the results which we do not attempt to account for quantitatively. It could also be an artefact of the optimisation algorithm, and could just represent a different local minimum (or maximum in this case) on the potential energy surface.

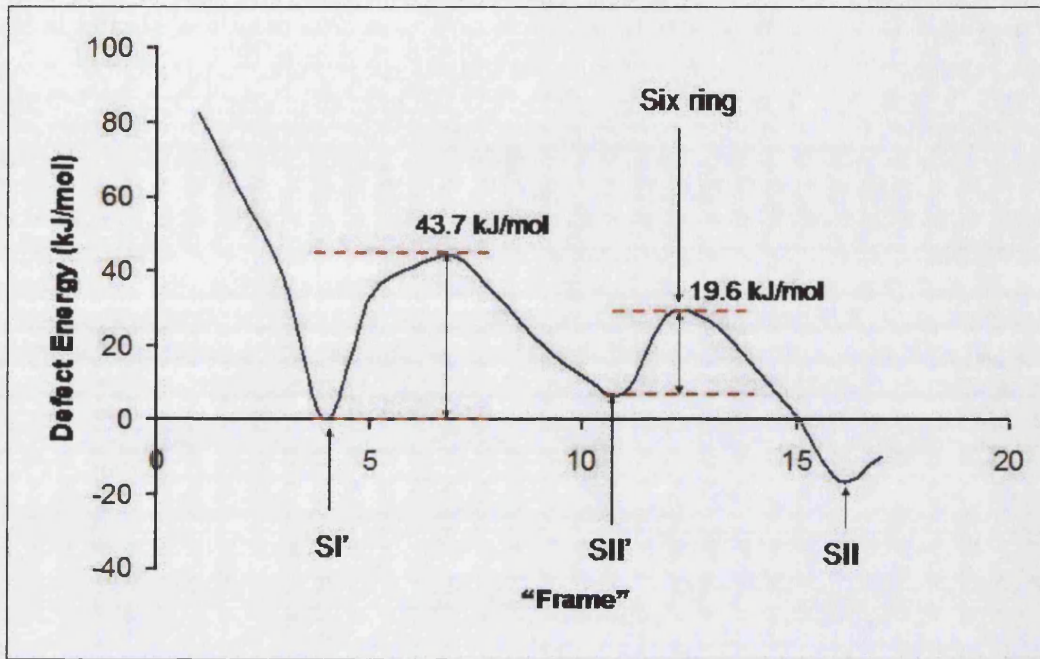


Figure 5.6: energetic barriers for cation motion between SII' and SII sites in NaY for 1 aluminium atom in a six ring.

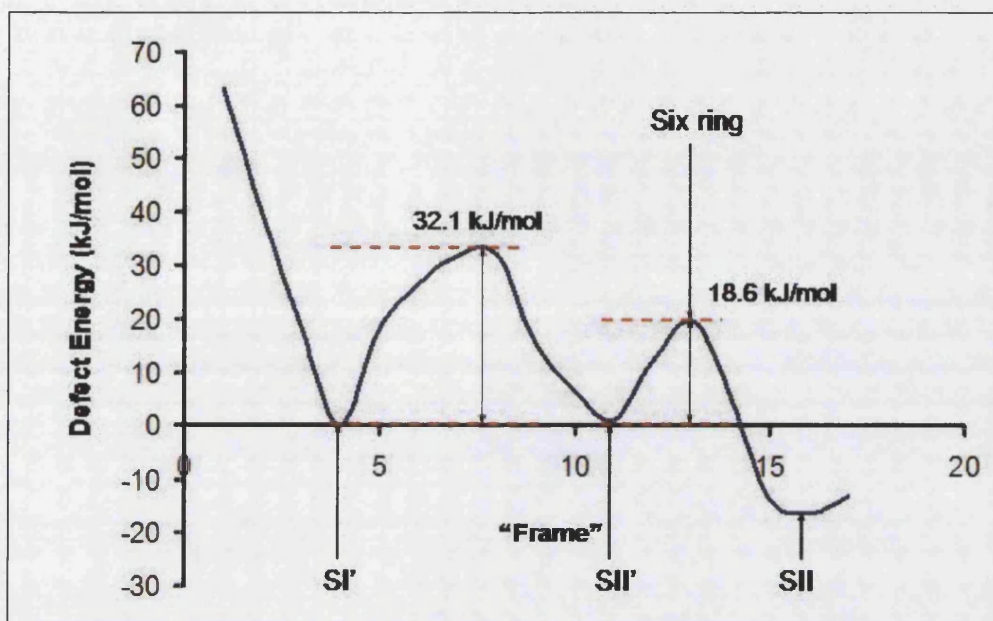


Figure 5.7: energetic barriers for cation motion between SII' and SII sites in NaY for 2 aluminium atoms in a six ring, arranged in a meta position.

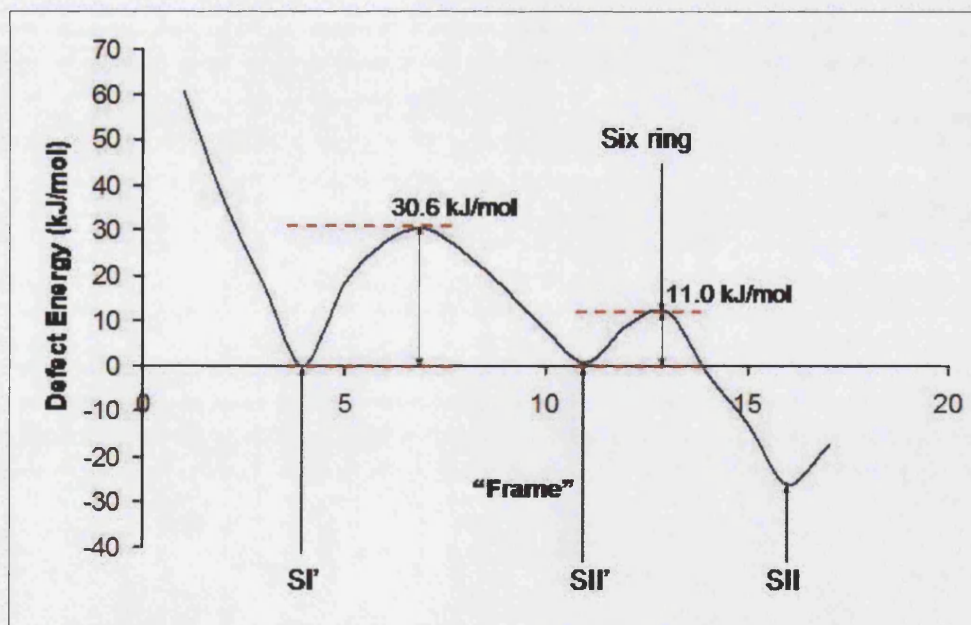


Figure 5.8: energetic barriers for cation motion between SII' and SII sites in NaY for 2 aluminium atoms in a six ring, arranged in a para position.

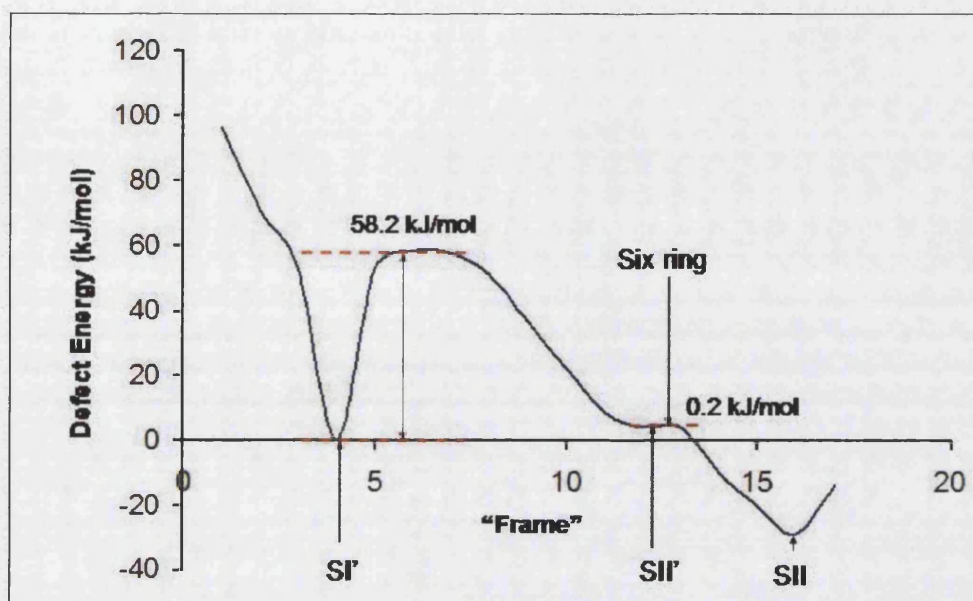


Figure 5.9: energetic barriers for cation motion between SII' and SII sites in NaY for 3 aluminium atoms in a six ring

Another common feature of the energy profiles is that there is a minimum roughly corresponding to the point where a SII' site would lie, although this site is not normally occupied by cations in zeolite NaY. However, the next feature after the SII' minimum is a small energy barrier between the SII' and SII sites, due to steric constraints that may occur as a cation passes through the confined space of the six ring plane. The maximum of this barrier on the graphs occur at the point where the cation is in the plane of the six ring being traversed. In most cases this energy barrier is of the same order as the energy barrier between the SI' site and the SII' site. The fact that after the energy barrier there is a steep downward slope to the SII site shows that the SII site is far more stable than the SII' site. Although Jaramillo, Grey and Auerbach report that the mechanism of cation migration is that the cations move from SI' to SII' to SII and beyond, from our observations of the molecular dynamics simulations performed (described in chapters 3

and 4 of this thesis), it appears that the cations do not spend very much time occupying the SII' site. Energetic evidence from the defect energy minimisation calculations presented in this chapter hints at the fact that this could be because of the relative ease with which the transition from SII' to SII occurs, due to the low energy barrier, especially in the case of a six ring containing 3 aluminium atoms, as will be seen later on. The fact that some cations are seen to migrate from the supercage back through the six ring upon sorbate evacuation is therefore perhaps a little surprising because there is a larger energy barrier for the transition from a SII site to a SII' site than the SII' \rightarrow SII transition. However, other factors may come into play in the molecular dynamics that are not present in the defect calculations, such as the fact that the cations have kinetic energy which is represented in the molecular dynamics simulations.

The reason for the difference in the actual energy of each site between the cases tested may be because of the long range electrostatic contribution. The site extracted from the molecular dynamics contained three aluminium atoms in the six ring, and so the change to two rings would involve moving the aluminium elsewhere in the lattice, which may in turn alter the long range electrostatics. If one compares the two cases where there are two aluminium atoms in the ring, one will see that the minima, ie the actual cation sites SI' and SII, have more or less the same energy. In these cases, the only difference in the lattice is that the aluminiums in the six ring considered have been moved to different relative positions within the ring. Local relaxation, which is believed to also be controlled by the number of aluminiums in the vicinity, could also play a role.

Effect of Differing Aluminium Content in the Six Ring

The number of aluminium atoms present in the zeolite framework will have an effect on the flexibility of the framework. As the number of aluminium atoms increases in a specific ring, one might also expect the flexibility of that particular ring to increase. The reason for this is the fact that one of the bonds in an AlO_4 tetrahedron is weaker than the other three bonds. The weaker Al—O bond is related to some extent in the interatomic potentials used. Another consequence could be that the electrostatic interaction between a cation and the zeolite framework is stronger at a site with more aluminium atoms than another cation site, as the negative charge on the oxygen atoms increases (although in our model, the atom charges do not vary, and so this effect is represented by the fact that the aluminium charge is +3, whereas for silicon it is +4).

From the calculations presented here, a varying number of aluminium atoms in the six ring being traversed is seen to have an effect on the energetic barriers to the cation migration from the SII' to SII site. Figures 5.6 to 5.9 illustrate the energetic barriers to the cation migrations for various numbers of aluminium in the six ring. The increase in flexibility of the framework would mean that the ring diameter would vary during the molecular dynamics simulation and in the defect calculations depending on the location of the aluminiums. The general trend seen from the calculations is that as the number of aluminium atoms in the zeolite framework increases, the energy barrier between the SII' site and the SII site decreases. This would be as expected, given the aforementioned fact that the framework flexibility increases with aluminium content. Therefore, at certain instances, the ring diameter would be larger in rings with a greater number of aluminium atoms. The energy of the SII' site is calculated to be lower than the SI' site in this particular case. This may be because the number of aluminium in the six ring at

which the SI' site is located is one. The aluminium is shared with the six ring of the supercage. In the case of when the six ring contains more than one aluminium atom, this may be explained by the greater interactions possible of a cation with a ring containing multiple aluminium atoms which would increase the negative charge on the surrounding oxygen atoms.

One will also notice from figures 5.7 and 5.8 that the difference between the two cases where there are two aluminium atoms in the six ring is small. The difference is 5.0 kJ/mol. During a study of calcium cations moving through six rings in chabazite, Grey *et al.*⁷ also found that there were quite small differences to the energetic barriers due to the relative position of two aluminium atoms in the same ring (of the order of 16.8 kJ/mol).

As might be expected, the minimum energy migration path differs slightly between the cases tested, although most of the points lie along the original migration path. The difference is because the cation may be drawn towards certain areas of the six ring in question due to the position and number of the aluminium. For example, in the case of one aluminium in the six ring, the cation would be drawn closer to that atom as opposed to the other T atoms present in the ring (silicon atoms). The migration pathway is thus slightly different for each case.

The effect of the cation moving through the six ring is a 'breathing effect', where the diameter of the ring changes, depending on the proximity of the cation. Inspection of the O-O distances across the six ring at stages in the migration shows that the ring of the 1 aluminium case and 2 aluminium cases are slightly elongated, and become even more

elongated as the cation approaches the ring. In the case of there being 3 aluminium atoms in the ring, the elongation is also observed. Regardless of the number of aluminium atoms in the six ring, the greatest elongation seems to be always between O2 and O5 (see labelling scheme below). Looking at the Al – Si distances, these are also seen to vary, but not to the extent of the O – O distances. However, as is mentioned in chapter 3 of this thesis, it is not common practice to explicitly model T atom interactions with the cations as they are considered to be obscured from the cation by the surrounding oxygen atoms due to their position in the centre of the TO₄ tetrahedra.

When comparing the average diameter (calculated from the O-O distances) it can be seen that the average is larger for the 3 aluminium case, despite the elongation of the ring, which would help to contribute to allowing easier passage of a cation through a six ring.

The positioning of the oxygen atoms in the six ring is such that they lie in two different planes, three in one plane, and three in another plane. Inspection of the ring geometries at different points along the energy curve shows that there is no change in the plane each oxygen atom lies in during the migration.

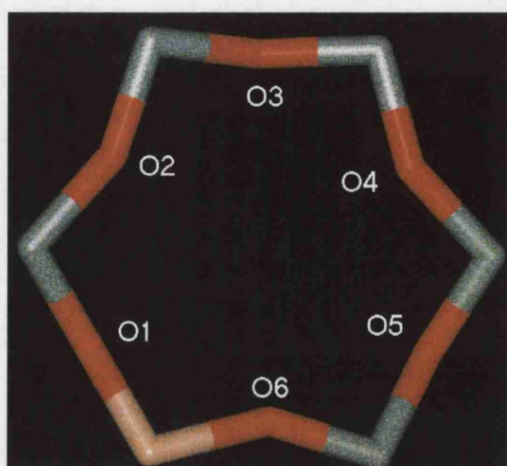


Figure 5.10: Labelling scheme of the oxygen atoms for the O – O distances reported in tables 5.5 to 5.8. For the case of two aluminium atoms in the six ring, the meta case has an Al atom between O2 and O3, and the 2nd Al is located between O3 and O4 in the para case

Frame	O1 - O4	O2 - O5	O3 - O6	Average (Å)
11	4.89	5.13	5.03	5.02
12	4.93	5.16	4.98	5.02
13	4.91	5.23	4.94	5.03
14	4.95	5.15	4.96	5.02
15	4.95	5.12	4.94	5.00

Table 5.5: Oxygen – oxygen distances (in Å) during the traverse of a Na cation from SII' site to SII site for the case where there is 1 aluminium in the six ring

Frame	O1 - O4	O2 - O5	O3 - O6	Average (Å)
11	5.07	5.2	4.97	5.08
12	5.14	5.27	4.84	5.08
13	5.07	5.31	4.91	5.10
14	5.11	5.2	4.94	5.08
15	5.12	5.15	4.93	5.07

Table 5.6: Oxygen – oxygen distances (in Å) during the traverse of a Na cation from SII' site to SII site for the case where there are 2 aluminiums in the six ring (meta position)

Frame	O1 - O4	O2 - O5	O3 - O6	Average (Å)
11	4.85	5.4	5	5.08
12	4.91	5.48	4.86	5.08
13	4.87	5.52	4.9	5.10
14	4.9	5.42	4.94	5.09
15	4.9	5.38	4.94	5.07

Table 5.7: Oxygen – oxygen distances (in Å) during the traverse of a Na cation from SII' site to SII site for the case where there are 2 aluminiums in the six ring (para position)

Frame	O1 - O4	O2 - O5	O3 - O6	Average (Å)
11	5.14	5.11	5.19	5.15
12	5.14	5.15	5.15	5.15
13	5.1	5.26	5.09	5.15
14	5.14	5.16	5.12	5.14
15	5.17	5.11	5.11	5.13

Table 5.8: Oxygen – oxygen distances (in Å) during the traverse of a Na cation from SII' site to SII site for the case where there are 3 aluminiums in the six ring.

However, although the shell model may be used to treat the effect of the polarisation of the oxygen atoms, without performing electronic structure calculations on these scenarios, one could not really study the effect of any distortion of electron clouds around the oxygen atoms which would affect the ease of the traverse through the six ring.

Conclusion

It has been shown in this chapter that the cation migration mechanism from SI' \rightarrow SII, observed in the molecular dynamics simulations by ourselves and others occurs with the cation travelling through a SII' site. The energy barrier to such a migration is dependent upon the number of aluminium atoms present in the six ring being crossed. It should be remembered though that the local environment around the six ring may also have an effect. However, from the results of the calculations, one may draw the conclusion that as the number of aluminium is increases, the energy barrier between the SII' site and the SII site decreases. Part of the reason might be because of the influence of the aluminium atom on the structure of the ring when the cation is passing through, whereby 1 or 2 aluminiums in the six ring elongate the ring, with the greatest O-O distance being between those furthest from the aluminium atoms. In the case where there is 3 Al atoms present in the six ring, the ring is also elongated. However, in this case, the other oxygen atoms are still further away from each other than in the 1 aluminium and two aluminium cases. As the Al content increases in the six ring in question, the local framework becomes more negative in charge, and electrostatic interactions between the ring and the sodium cation increases. This would have the

effect of lowering the interaction energy between the cation and the zeolite framework. Electrostatic contributions might also have a hand in the elongation, as increasing the Al content in a given six ring would increase the negative charge within that ring, thereby increasing the electrostatic repulsion present across said ring.

It has been suggested, however, that in the case of calcium travelling through six rings in chabazite, little difference is made to the energy barriers by the number of aluminium atoms in the ring. Given that there is a small difference between the one aluminium and the two aluminium case in the results presented here, this might be deemed to be partly true for the 1 and 2 aluminium cases. The 3 aluminium case shows a big decrease from both of the 2 aluminium versions, however. The calcium cation is approximately 0.04 Angstroms bigger than the sodium cation. Although this is a small difference, it still may have an effect in that there would be a 'tighter fit' for a calcium cation to pass through a six ring.

It has been suggested however that a much better way to model such phenomena would be to use electronic structure methods, at either the ab initio level or semi empirical level, such as the INDO method. Although such calculations would most likely prove to be expensive computationally, they would give a better idea of the effect of the distortion of the charge clouds around the oxygen atoms during the migration phenomena, which could be the reason for the energy barriers to the migration through zeolite six rings.

Chapter 5 References

- (1) Mott, N. F.; Littleton, M. J. *Trans Faraday Soc.* **1938**, *34*, 485.
- (2) Islam, M. S. *Solid State Ionics* **2002**, *75-85*, 154.
- (3) Islam, M. S. *J. Mater. Chem.* **2000**, *10*, 1027.
- (4) Cherry, M.; Islam, M. S.; Gale, J. D.; Catlow, C. R. A. *J. Phys. Chem.* **1995**, *99*, 14614.
- (5) Cherry, M.; Islam, M. S.; Gale, J. D.; Catlow, C. R. A. *Solid State Ionics* **1995**, *77*, 207.
- (6) Catlow, C. R. A.; Bell, R. G. *Solid State Ionics* **1994**, *70*, 511.
- (7) Grey, T.; Gale, J. D.; Nicholson, D. N.; Peterson, B. K. *Microporous and Mesoporous Materials* **1999**, *31*, 45.
- (8) Dick, B. G.; Overhauser, A. W. *Phys. Rev* **1958**, *112*, 90.
- (9) Deak, P. Choosing Models for Solids. In *Computer Simulation of Materials at Atomic Level*; Pederson, M. R., Ed.; Wiley-VCH, 1999.
- (10) Fitch, A. N.; Jovic, H.; Renouprez, A. *Journal of Physical Chemistry* **1986**, *90*, 1311.
- (11) Sanders, M. J.; Leslie, M. J.; Catlow, C. R. A. *J. Chem. Soc. Chem. Comm.* **1984**, 1271.
- (12) R.A.Jackson, R. A.; C.R.A., C. *Molecular Simulation* **1988**, *1*, 207.
- (13) Schroder, K. P.; Sauer, J.; Leslie, M. J.; Catlow, C. R. A.; Thomas, J. M. *Chem. Phys. Lett.* **1992**, *188*, 320.

**Chapter 6: Cluster and
Periodic DFT Studies of
CHCl₃ Sorption on
Aluminosilicates**

Introduction

The work described in previous chapters in this thesis used techniques based on interatomic potentials. Site to site cation migration mechanisms upon halocarbon adsorption and the energetic barriers to cation migration across aluminosilicate six-rings have been studied. One might now ask questions regarding the electron distribution in the zeolite framework, and its subsequent changes upon adsorption of halocarbon molecules and perturbation of the extraframework cations. Molecular dynamics and the Mott Littleton technique cannot explicitly treat electronic degrees of freedom. Therefore in order to study problems where knowledge of electronic densities are necessary, one must use electronic structure methods such as Hartree Fock or Density Functional Theory (DFT). DFT is a popular method of probing the electronic structure of materials and was developed by Kohn and Sham in the 1960s. The DFT method is described in chapter 2.

The Cluster Model

If one wished to study the basic properties of zeolites, one might “adsorb” an acidic molecule on a zeolite or aluminosilicate surface and use DFT methods to study the electron density distribution changes upon the adsorption. Although large scale quantum calculations are becoming more and more computationally feasible with the increase in computing power seen in recent years, many quantum calculations in materials chemistry are still performed using the cluster approximation. This means that an ‘active’ region of the material is selected and represented as a hydrogen terminated cluster of atoms. It is assumed that all the interesting chemistry that takes

place locally can be sufficiently represented by such a cluster. In these calculations, in order to reproduce the steric effect of the bulk crystal on the cluster, the terminal atoms are usually held fixed in their positions during geometry optimisations.

However, for a zeolite containing charged species, such as sodium cations, and for clusters containing aluminium atoms, one might ask questions regarding the adequacy of the use of a cluster approximation to gain information on the electronic structure of materials. The cluster approximation has been extensively used to extract information about the electronic structure of adsorbed species on the surfaces of a number of materials including various metals, oxides and zeolites using both DFT and Hartree-Fock theory. However these types of systems are extended systems in reality, and so using the cluster approximation would have the shortfall that the long range electrostatic contribution by the lattice to interaction energies would not be adequately represented. Furthermore one must be careful to choose a cluster that is big enough to represent adequately the steric forces exerted by the bulk lattice on the region of interest. Even so, the cluster approximation has enjoyed some success in describing zeolite structures and phenomena related to zeolites at the electronic level.

The technique has been extended to the calculation of NMR shielding tensors, and such calculations by Simperler *et al.*¹ have shown good agreement with experimentally determined values for the case where toluene is adsorbed on alkali cation containing aluminosilicate clusters representing zeolites X and Y. The results of these calculations can then be used to help improve and interpret data yielded from MAS NMR experiments. Cation locations have also been studied in clusters representing zeolites A, X and Y. An example of such work is that of Uzunova and St. Nikolov². Small

zeolite structural fragments were used to study the relative energetics of cation binding in six rings, and also the cation positions in rings with different aluminium content. One might express concern for the use of such clusters as the sites may not be adequately represented. This is especially the case when modelling cation sites that are situated in the zeolite supercage, as the authors used only a single 4 ring to model SIII and SIII' sites, although the clusters did contain 32 atoms. Steric constraints exerted by the bulk structure on the region of interest need to be adequately reproduced, and would be difficult to do with too small a cluster. Furthermore, the aforementioned long range electrostatic interactions are of course neglected in this particular case. However, a qualitative idea of the energetics might be reliably obtained from these calculations. Vayssilov *et al.*³ also performed DFT on zeolite clusters to study the effect of varying aluminium content on cation location in zeolite six-rings, and of CO adsorbed on such clusters. Their clusters were larger than those of Uzunova, and therefore better represented the steric constraints on the region of interest. The authors reported that the values obtained for the CO vibrational frequencies agreed well with experimental data, as did the binding energies of CO to the cluster.

Embedded Cluster Models and Periodic Systems

One can extend the cluster approximation to include a better treatment of the steric constraints placed upon a local area of interest by the rest of the lattice. Simply extending the cluster size and treating everything at the same level of theory would be computationally expensive, although recent increases in computer power are making this more and more feasible. Instead, one could turn to the embedded cluster approximation, where an 'active' cluster, treated at a high level of theory is surrounded by a region treated at a lower level of theory, thus saving on computation time. This

method has been used in a number of recent works on adsorption on silica and zeolite materials. Hartree-Fock theory or DFT have been popular methods to treat the high level, active region in the cluster, and atomistic or semi-empirical methods to treat the lower, peripheral region of the system. This type of methodology is implemented as the ONIOM⁴⁻⁶ method in the Gaussian 98 code⁷. The ONIOM method is described later in this chapter.

The lower region might be made up of point charges, instead of being part of a larger cluster split into two regions. The electrostatic effect of the zeolite lattice can be included in the calculation of adsorption energies, and add a further degree of realism into a model. Greatbanks *et al.*⁸ and Sherwood *et al.*⁹ adopted this approach in their study of acidic sites in zeolites. This was also the approach used by Goursot *et al.*¹⁰ who studied the adsorption of oxygen and nitrogen on Li-, Na- and Ca- LSX zeolites. Conclusions included an assertion that an electric field generated by the zeolite lattice will play an important role in determining adsorption energies, as it will contribute a screening effect from the zeolite to the polarisation of a molecule by a cation. It is also important to represent properly the values of the point charges surrounding the adsorption site. This indicates a possible role for fully periodic calculations. However, work by Ricci *et al.*¹¹ and Erbetta *et al.*¹² indicates that embedded methods (using the ONIOM scheme) can be a reliable alternative to fully periodic quantum calculations. Their study was on the modelling of defects in amorphous silica, and so the electric fields generated by aluminium atoms and extraframework cations were not present. The formation of a charged defect would mean polarisation of the lattice and the authors treated this effect by the use of point charges. The authors conclude that although the method is not the most accurate for treating this sort of problem, it is a method which

can yield useful results, despite the approximations made for treating the long range electrostatic effects. This is also the conclusion reached by Roggero *et al.*¹³, who modelled the physisorption of ammonia on silica using the ONIOM scheme, using DFT and semiempirical methods. The authors believe that the results can be used for semi-quantitative predictions on larger proportions of siliceous materials.

A computationally cheaper alternative to using electronic structure methods in the lower level region in an embedded cluster calculation is the use of interatomic potentials to describe the mechanical flexibility of the zeolite framework, i.e. the so called 'QM/MM' method. Here the site of interest is treated using a high level electronic structure method, and the surrounding environment is modelled with classical interatomic potentials. This methodology is implemented in a number of codes, such as Gaussian 98 and ChemShell. Using the ChemShell code, Sinclair *et al.*¹⁴ demonstrated that when probing the details of guest molecule adsorption and reactivity at specific sites in specific zeolite clusters, incorporation of as much of the surrounding environment is important in order to get a complete picture. de Vries *et al.*¹⁵ also find that the use of the QM/MM method can have advantages over the cluster model, for example, in the QM/MM method the electronic structure is altered by interaction with the surrounding lattice rather than by changes in the terminal T—H or O—H bonds, as is the case in the cluster approximation.

Although the embedded cluster approximation has been shown to have advantages over the cluster approximation, some problems may still arise when using it, such as artificial contributions of the terminal hydrogen atoms when the two regions are treated separately with their respective calculation method. Correction schemes have been

implemented to reduce these errors¹⁴, but such a problem would not be present in a fully periodic calculation.

Another embedding scheme available is that offered by the QM-Pot method¹⁶, where the region treated with interatomic potentials is periodically repeated. This scheme was used by Sierka and Sauer¹⁷ in a study of a range of silica and zeolite catalysts, and the authors found that the scheme is a reliable tool for calculating the structures and properties of silica and protonated zeolite catalysts. Their work was extended to a study of Cu⁺ sites in CuZSM-5 and NH₃ adsorption and deprotonation energies¹⁶. The QM-Pot scheme was successful in predicting the properties of the catalysts and in calculating reaction rates for elementary processes on the surface of solid catalysts.

The case for the use of periodic DFT calculations on silica and zeolite systems has been recently put forward by a number of authors. Such calculations have demonstrated some of the advantages of the periodic model over the cluster model. Rozanska *et al.*¹⁸ state that periodic models offer distinct advantages over the cluster model, such as the accurate inclusion of steric constraints and long range electrostatic effects. Their studies of chemisorption on chabazite and mordenite have shown the importance of proper inclusion of the zeolite framework relaxation on the energetics of isomerisation processes occurring upon sorption of propylene on chabazite and toluene and xylene on mordenite. Hill *et al.*¹⁹ have performed cluster and periodic calculations on bridging hydroxyl groups in faujasite, and concluded that clusters are of limited value for predicting charges and structures of bridging hydroxyl groups, and that the cluster model is useful for describing such a system qualitatively, but not quantitatively.

The major disadvantage of using fully periodic DFT models is of course the great computational expense of performing such calculations. Also, each periodic cell is identical to its neighbours, and this is unrealistic, as proper treatment of defects present in a zeolite and their interactions with the sorbate molecules is not possible.

Adsorption of Halocarbon Molecules in Zeolite Y – Lessons From Classical Simulations

In the field of halocarbon adsorption in zeolites, attempts have been made to depict the contribution of the electrostatic energy to the energy of adsorption of chloroform and other halogen-substituted hydrocarbon molecules by classical methods. Monte Carlo work by Mellot *et al.*²⁰⁻²² has elucidated a binding site in the 12 membered ring of the faujasite structure and the adsorption energy was calculated to be approximately -66 kJ/mol. The authors further state that the contribution of the long range electrostatics is about 24% of the total adsorption energy in NaY, and that there is an important role that the long range electrostatic contributions play in the adsorption of chloroform (and indeed fluoroform).

The authors also performed calorimetric studies of chloroform adsorption and derived an adsorption energy of approximately -55 kJ/mol.

In view of the fact that electrostatics may play an important role in determining binding energies of halocarbons in zeolites, questions arise regarding the adequacy of the cluster approximation in the study of the effects of adsorbed molecules with a high dipole

moment, and their effects on the zeolite. Therefore, alternative models, such as embedded clusters or periodic models might be better for modelling these adsorbates in zeolites.

Methodology

The ONIOM Method

The ONIOM⁴⁻⁶ method subdivides the system into a HIGH (high theory level) layer and LOW (low theory level) layer. The main cluster, or “model” system, is treated at the high level of theory, and the surroundings are treated at the lower level. The entire model is called the “real” system.

The energy is thus defined as:

$$\mathbf{E (HIGH:LOW) = E (HIGH, model) + E (LOW: real) - E(LOW, model)} \quad \text{Eq 6.1}$$

There is no direct charge transfer or polarisation between the two layers of the system. However, the effects of one system on the other are included via the use of the equilibration of energy gradients between the model and real systems, to make them consistent with each other. A more detailed explanation of the ONIOM method is available in references 4-6.

Building and Testing the Clusters

The initial strategy in investigating the problem at hand was to use a cluster approximation at the interatomic potentials level of theory in order to find suitable candidate clusters for treatment using electronic structure methods. This was done by energy optimisation using the GULP code and the Sanders-Catlow (1992) potentials within the shell model. The parameters are given in Chapter 5.

The initial cluster tested was an entire sodalite cage, plus the double six ring prisms surrounding the cage, extracted from a periodic zeolite model of faujasite, as shown in figures 6.1 and 6.2. These clusters were terminated using the oxygen atoms at the end of the cluster. The silicon atoms connected to the oxygen atoms at the terminus of the cluster were substituted for hydrogen atoms to form terminal O-H links. The bond length of the new O-H link was reduced to 0.98 Å, but still along the same 'direction vector' from the oxygen atom. The bond length chosen is a standard bond length of an O-H link. The reason the cluster was designed in this fashion, rather than just randomly adding terminating H atoms was because that by using the position of the silicon atoms in the bulk zeolite, the directionality of the force exerted on the model cluster by the bulk of the zeolite would be more properly represented.

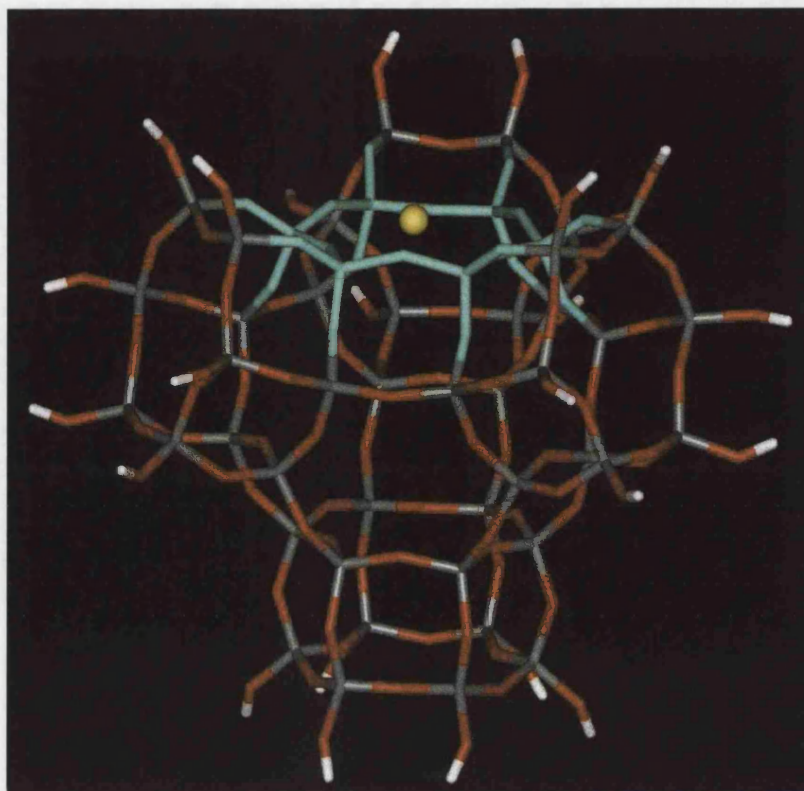


Figure 6.1: Sodalite cage cluster showing the site II cation. The atoms coloured in light blue were treated at the B3LYP level, as was the cation (yellow sphere)

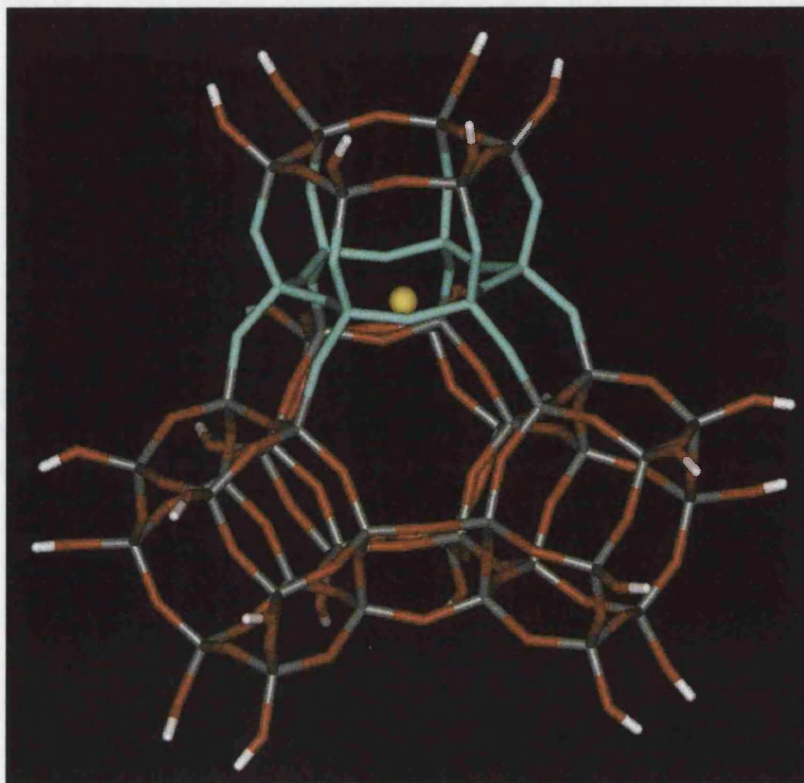


Figure 6.2: Sodalite cage cluster showing the site I' cation site. The atoms coloured in light blue were treated at the B3LYP level, as was the cation (yellow sphere).

Calculations were also performed using an extended version of the above cluster, shown in figure 6.3. This new cluster (denoted as the 'extended SII cluster' included more of the framework surrounding the SII site, thus better representing the SII site.

The sodium cations were placed on the established crystallographic sites in the zeolite, and the corresponding numbers of aluminium atoms needed to give a neutral cluster were substituted for Si atoms, subject to Löwenstein's Rule. Initially, only one cation was tested in a number of site positions. The number of cations was increased to two cations and three cations, and the energies were calculated for different aluminium configurations. However, time restrictions due to the computational expense of

performing high level DFT calculations on large clusters meant that only the one cation cases were used in the DFT calculations.

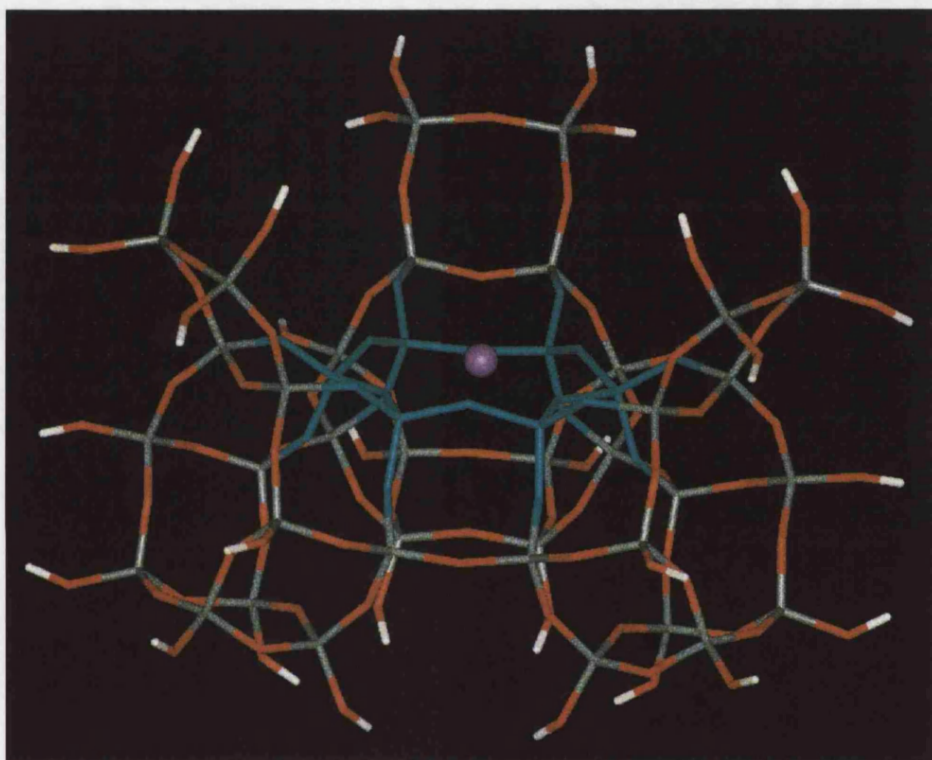


Figure 6.3: 'Extended SII cluster' showing the site II cation site. The atoms coloured in light blue were treated at the B3LYP level, as was the cation (purple sphere)

Embedded Cluster Calculations

The embedded cluster (ONIOM) calculations were performed on clusters with the lowest energy as determined by the atomistic models. These models were split into two regions, as described above. The LOW region was described using semi-empirical quantum methods, MNDO in this case. Although AM1 and PM3 methods are thought of as being better parameterised and more reliable than MNDO, it has been found that MNDO can produce reliable geometries for the silica structure¹³. In the model used, the actual geometry optimisation part of the ONIOM calculation at the LOW level is purely siliceous. The HIGH level part consisted of the cation and the six ring that contained the cation site under study, along with surrounding oxygen atoms, as indicated by the light blue coloured regions in figures 6.1 to 6.3. The ONIOM code automatically terminates this with hydrogen atoms with the O—H distance set at 0.98 Å. The H atoms are placed along the direction of the O—Si bond, with the Si atom being the atom replaced by the H terminal atom. Likewise, for the MNDO part, the cluster is terminated by the silicon atoms, with H atoms set approximately 1.54 Å away. The HIGH level region of the calculation was treated using the DFT method, with the B3LYP functional (in this functional, a combination of Hartree-Fock and the Becke 88 functional is used for exchange, and correlation is treated using the functional of Lee, Yang and Parr)^{23,24} and the 6-31G** basis set. Although it has been found that the 6-31G* basis set is sufficient for modelling aluminosilicate clusters²⁵, the 6-31G** basis set was used in this work as there was a need to include polarisation functions for correctly modelling the CHCl₃ molecule.

The calculations were also performed using the DMol code²⁶⁻²⁸, with the entire sodalite cage 'cluster' illustrated in figures 6.1 and 6.2 being treated at the DFT level. The GGA

approximation was used, with the BLYP functional (Becke 88 exchange combined with Lee, Yang and Parr's correlation functional)^{24,29} and the dnp (double numeric with polarisation functions) basis set.

Periodic DFT Calculations

Fully periodic DFT calculations were performed on an unloaded zeolite Y primitive cell consisting of 155 atoms and on a primitive cell loaded with one molecule of chloroform to test the effect of the contribution of the Coulomb summation on the interaction energy of the sorbate with the zeolite. The zeolite structure and composition in this case was taken from the data published by Fitch *et al*³⁰, with an Si:Al ratio of 2.4. In the sorbate-loaded case, the molecule was docked using a canonical Monte Carlo algorithm implemented in Accelrys Cerius² software. Both models were energy minimised using the GULP code, with the potentials described in Chapter 3 being used for the entire system prior to the DFT calculations. The DFT calculations were performed using the DMOL code, using the GGA approximation (Perdew-Wang 1991 functional) and also the BLYP functional. The dnp basis set was used.

Results and Discussion

ONIOM and DMol Cluster Calculations – Adsorption Geometries

Candidate cluster geometries for treatment using electronic structure methods were selected on the basis of the results of the GULP forcefield calculations. The lowest energy configuration for a cation in site SII was selected and subjected to geometry optimisation under the ONIOM method. A case where a sorbate molecule was docked onto the cluster was also tested, with the geometry copied from a low energy configuration found from a Monte Carlo docking run (see figure 6.4), where the hydrogen atom on the sorbate molecule is close to a framework oxygen atom located on a four ring and one of the chlorine atoms on the molecule is able to interact with the sodium cation.

Although the initial geometry was copied from the Monte Carlo generated minimum configuration, the optimised geometry was drastically different in that the molecule had moved to a large extent, to a new binding site on the six-ring itself. This is shown in figure 6.5.

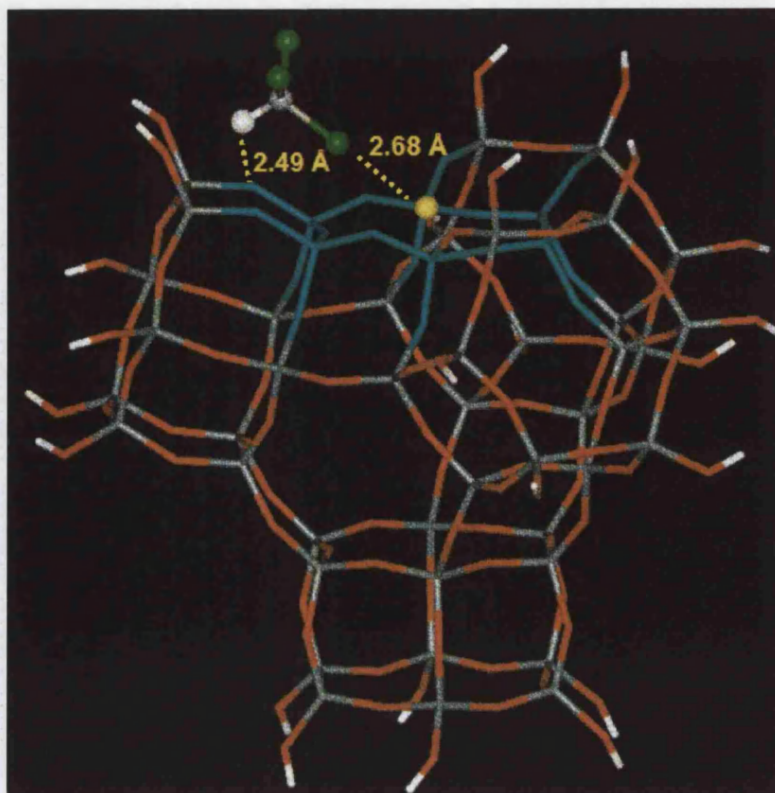


Figure 6.4: Sodalite cage cluster showing the binding site copied from the Monte Carlo docking. The atoms coloured in light blue illustrate the zeolite SII six-ring, and the yellow sphere indicates the sodium cation.

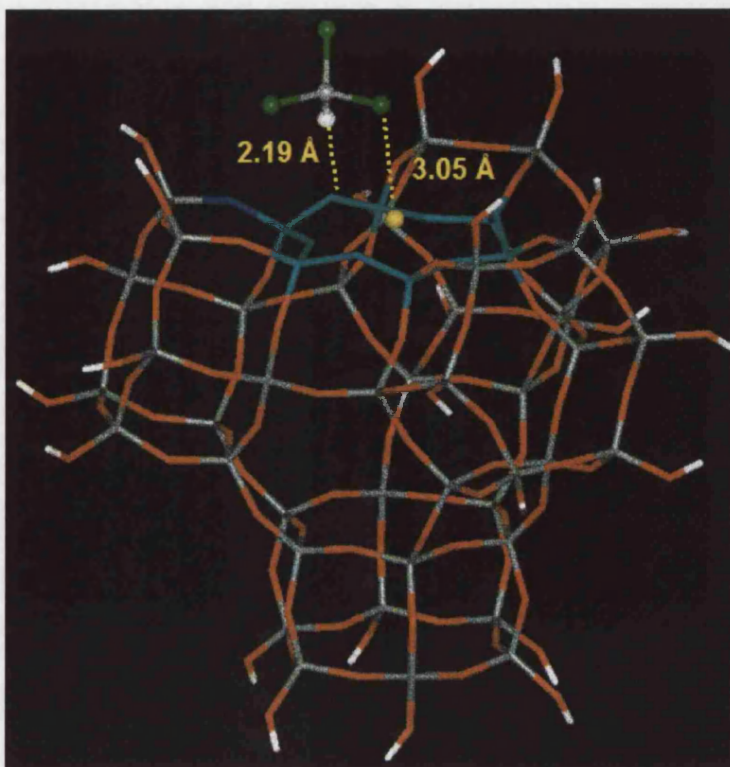


Figure 6.5: Sodalite cage cluster showing the new binding site. The atoms coloured in light blue illustrate the zeolite SII six-ring. The dark blue atom indicates the oxygen atom with which the hydrogen was originally interacting, prior to geometry optimisation (compare with fig 6.4).

The dual interaction mentioned in the molecular dynamics chapters of this thesis for chloroform and fluoroform was still evident, with the hydrogen atom close to an oxygen atom on the six ring, and the chlorine interacting with a sodium cation. In the case of the 'extended SII cluster', the ONIOM calculated geometry is somewhat unusual. The framework oxygen atom with which the chlorine atom is seen to interact, forms part of a terminal hydroxyl group of the inner (DFT) region. Although Mellot *et al.*²² state that attractive Cl--O interactions are present when halocarbons containing chlorine are adsorbed on NaY, one would not expect a distance of 2.87 Å between two highly electronegative atoms, and one might expect that electrostatic repulsion would be the dominant contribution to such a Cl—O interaction. Thus, a pitfall of the ONIOM method might be highlighted by this particular case, as the two regions effectively cannot 'see' each other, and there is no charge transfer between the regions. In order to model such a system effectively, one would either have to include a bigger DFT region, although this would increase the computational expense. An alternative would be to model the system using a code such as the ChemShell software, where the embedding scheme is implemented in a way such that polarisation of each region is taken into account³¹. Repeating the calculation starting from the DMol optimised geometry (see below) also resulted in a Cl atom moving closer to the framework oxygen.

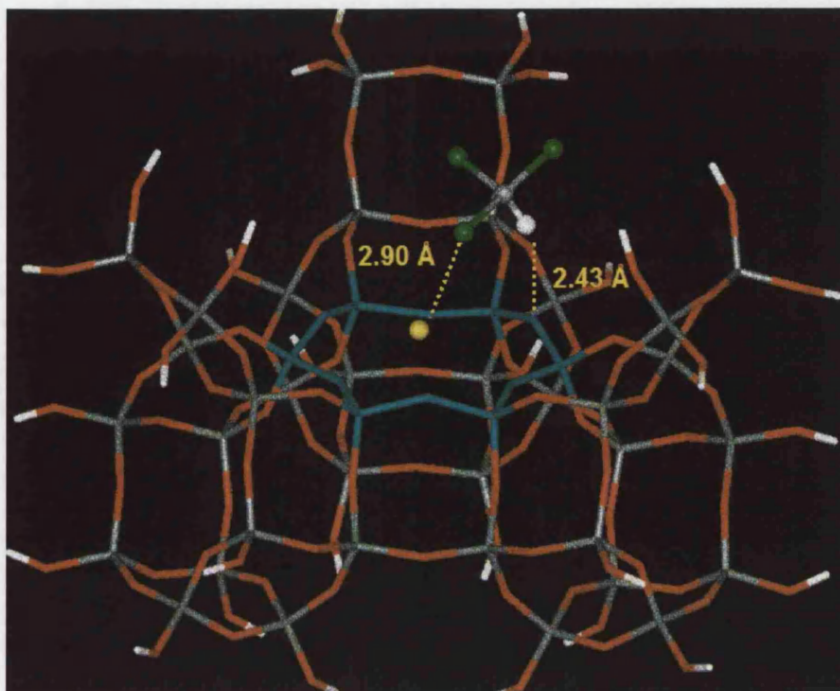


Figure 6.6: DMol Optimised 'Extended SII cluster' showing the site II cation site and the sorbate molecule in the newly found docking site. Some atoms are coloured in light blue to show the position of the zeolite six-ring. The Cl–Na and H–O interaction distances are also shown. As can be seen, the H–O interaction occurs with an O atom situated on the six-ring, and not on one of the surrounding four-rings.

The geometries were also optimised using the DMol code, whereby the entire cluster was treated using DFT. Both the Monte Carlo generated geometry and the ONIOM calculated geometry were optimised in this way (see figures 6.6 and 6.7). In the case where the extended SII cluster was employed, both of the molecule geometries were found to be stable, unlike the cluster incorporating a smaller region of the supercage (denoted 'small SII cluster'). In this particular cluster, the effect of a molecule being too close to the terminal hydrogen atoms, or interacting with a framework oxygen atom bonded to a terminal hydrogen atom can again be seen. Although the molecule was

docked in a favourable position, as found by Monte Carlo and in the extended SII cluster, the final geometry was found to be very similar to the configuration predicted by the DFT calculations under the ONIOM scheme.

Adsorption Energies: DMol and ONIOM

From the cluster calculations, it was possible to calculate an adsorption energy from:

$$E_{\text{ads}} = E_{\text{cluster_molecule}} - (E_{\text{cluster}} + E_{\text{molecule}}) \quad \text{Eq 6.2}$$

Looking at the calculated adsorption energies in table 6.5, it can be seen that the cluster approximation for a zeolite is not adequate to model and reproduce adsorption energies of chloroform on aluminosilicates. The experimentally determined adsorption energy is approximately -60 kJ/mol. Therefore, our clusters only represent approximately 50% of the adsorption energy. However, it should be noted that the experimental adsorption energy would also depend on the zeolite's composition, the presence of defects within the zeolite and other effects such as chemisorption. Monte Carlo studies discussed earlier in this thesis and by Mellot *et al.*²² have shown that the average adsorption energies can be reproduced to a good degree using interatomic potentials. Mellot *et al.*²² further estimate that the contribution of the long range electrostatic interactions is approximately 25% of the adsorption energy. Therefore, if this assertion held true, then the cluster models used in this thesis should reproduce 75% of the total binding energy, as this contribution is the only aspect that is missing from the cluster model. However, as shown above, this is not the case. It is further shown that an increase in the cluster size has little effect on the adsorption geometry, and consequently the binding energy,

although the case where the ONIOM calculated energies are different could be an anomaly due to the model and the size of the region treated at the DFT level.

	DMol Cluster (kJ/mol)	ONIOM Cluster (kJ/mol)
Extended SII Cluster	-30	-33
Small SII Cluster	-29	-23

Table 6.5: The calculated adsorption energies for chloroform adsorbing on a silica cluster substituted with one aluminium atom and containing one cation. Both cluster sizes studied are shown. It should be noted that the above energies are not corrected to take into account any basis set superposition errors. However, it is estimated that the energies would only vary by 1 or 2 kJ/mol should they be corrected³².

Cluster Calculation of Original Monte Carlo Generated Geometry

One further calculation was performed using only the extended SII cluster in DMol. The molecule was docked in a position similar to that found by the Monte Carlo simulations, ie, the hydrogen atom interacts with an oxygen atom on a four-ring, and not on the SII site six-ring. The final geometry is shown in figure 6.7. The adsorption energy was calculated using the formula shown as Eq 6.2, and the calculated adsorption energy is -33 KJ/mol. Although this is lower than the binding site on the six-ring (when compared to the extended SII site DMol calculation for that binding site), the difference is small.

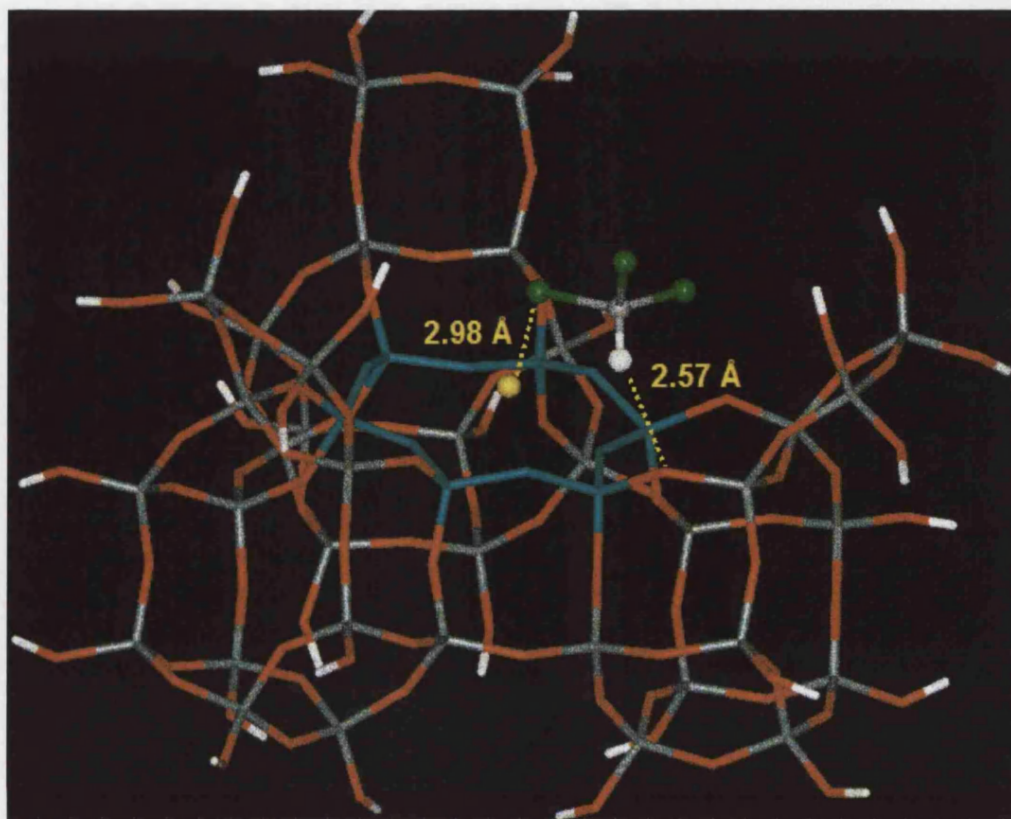


Figure 6.7: Optimised 'Extended SII cluster' showing the site II cation site and the sorbate molecule docked in the original Monte Carlo generated configuration. The atoms coloured in light blue were treated at the B3LYP level, as was the cation (yellow sphere)

Differences Between DMol and ONIOM

One should note two important differences between the ONIOM and DMol calculations. The first is that different functionals were used between the two different programs to describe the electron exchange and correlation. The ONIOM method used the B3LYP hybrid functional. This had been acknowledged by a number of authors to give good results when treating molecular adsorption. The calculations performed

using the DMol code employed the BLYP functional. Therefore care must be taken when comparing calculations between the two functionals. When comparing these two functionals for molecular sorption on zeolite clusters, Zygmunt *et al.*³³ found that both functionals gave very similar results when compared to second-order Møller-Plesset perturbation theory (MP2) based calculations on water adsorption on zeolite clusters.

However, in the case of the cluster calculations described in this thesis, two different basis sets were used, due to the availability of different types of basis sets between the two programs. Although both basis sets used included capabilities to treat the polarisation of the molecule, they were both different. The basis sets in the Gaussian 98 program are analytical basis sets based on Gaussian or Slater type functions. The basis sets in the DMol program are built of numerical values corresponding to points on a atomic-centred spherical polar mesh. The use of these spherical atomic orbitals has a number of advantages, including the fact that the basis set superposition errors can be minimised.

The basis sets between the two programs are sufficiently different that a direct comparison of the results is not possible, although one could still compare the results to experimental results.

Relaxation of the Cation Position

In each case, the final adsorption geometry resembles that of species III, proposed by Bosch *et al.*³⁴ (see figure 1.6 in chapter 1, page 34). In this configuration, the double interaction between a chlorine atom and a sodium cation, and between the hydrogen

atom and a framework oxygen atom are possible. The cation moves towards one oxygen atom connected to the aluminium atom. Therefore, although cations were observed to move away from their extraframework sites in the molecular dynamics simulations, in the case of a molecule that has already been adsorbed on the framework, the electrostatic influence of the aluminium atom appears to work in tandem with the cation—molecule interaction to help determine the adsorption geometry and final cation position. This was the case in both the ONIOM and the DMOL treated clusters. Figure 6.8 shows the movement of the cation.

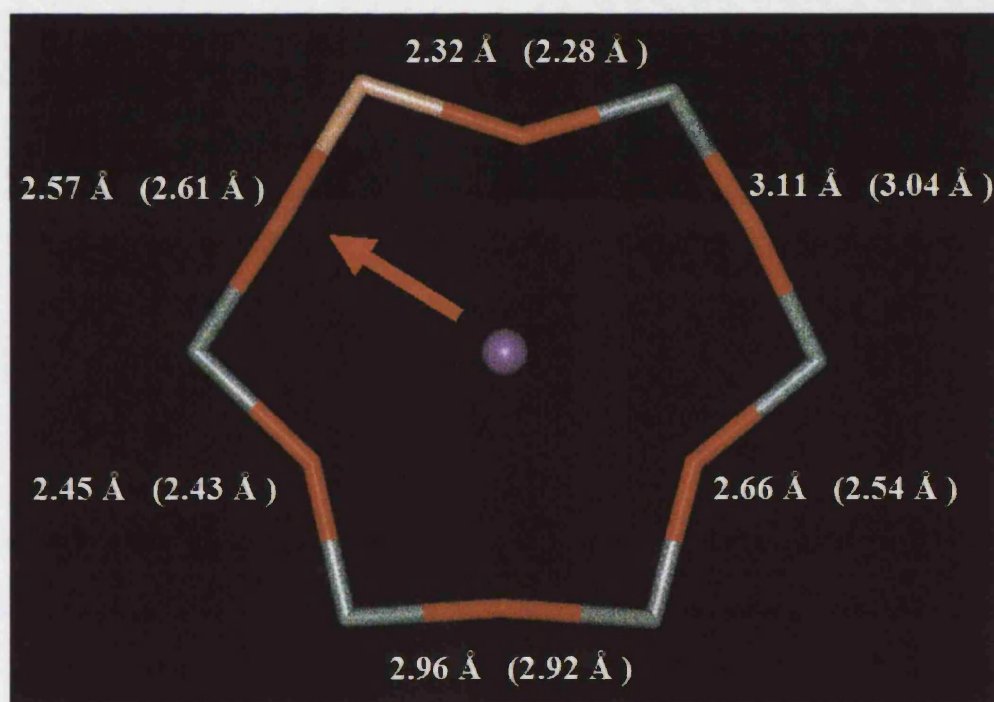


Figure 6.8: The cation—oxygen distances are shown in this figure, with the values in parentheses representing the distances before CHCl_3 adsorption, and those outside parentheses showing the values after adsorption. This is for the DMol extended cluster, although the same trends were observed for the other cluster calculations.

Periodic DFT Calculations – Adsorption Energies and Geometries

Periodic DFT calculations were performed on a docking configuration generated by the aforementioned Monte Carlo docking algorithm. The original docking configuration was the same as the one used as the starting configuration for the cluster calculations, i.e. with the molecule interacting with an oxygen atom in the four-ring, and the chlorine atom interacting with the cation located in an SII site. Energy optimisation under the DFT scheme indicated that this configuration was stable, as the docking configuration found by the DFT optimisation matched that of the DMol DFT cluster and the Monte Carlo calculation.

The calculations were undertaken using a periodic zeolite model on the assumption that this would enable a more accurate reproduction of the experimentally derived adsorption energies. This certainly seems to be the case when using the PW91 exchange-correlation functional during the DFT calculation. Although the energies cannot be compared to the cluster calculations, one can compare to the experimental value, and in this case the periodic model gave an adsorption energy value of -65 kJ/mol, which can be deemed to be a reproduction of the experimentally derived value of the adsorption energy of a chloroform molecule adsorbed in an aluminosilicate material.

$$E_{\text{ads}} = E_{\text{cell_molecule}} - (E_{\text{cell}} + E_{\text{molecule}}) \quad \text{Eq 6.3}$$

In order to make all the calculations comparable with the cluster DMol and ONIOM calculations, the periodic calculations were also performed using the BLYP functional

available in the DMol code to treat the exchange and correlation of the electrons. The results of this geometry optimisation are surprising in that the adsorption energies yielded are very high (negative), leading to the suspicion that the calculation had not properly converged on a minimum point. It was not a trivial matter to simply repeat the geometry optimisation largely due to the huge computational expense of the periodic DFT calculations on cells of that size.

Periodic Single Point Calculation of ONIOM Derived Adsorption Site

In order to test the transferability between the ONIOM method and periodic DFT, an attempt was made to derive an estimate of the adsorption energy that included the long range electrostatic effects on the ONIOM calculated chloroform adsorption site, where the H—O interaction is via a 6-ring oxygen atom. However, the method used would only have yielded an approximate energy. In this calculation the optimised geometry of the chloroform from the DMol extended SII cluster was superimposed onto a similar site in the periodic cell. The resulting structure was then subjected to a DFT single point energy calculation. When employing the BLYP functional the calculation yielded a large value of the adsorption energy -385 kJ/mol. A further single point energy calculation using the same configuration and employing the PW91 functional gave a positive energy of approximately +25 kJ/mol. Although a reasonable value for the adsorption energy might be yielded from a full geometry optimisation in each case, one cannot say whether such calculations would reproduce the experimentally derived energy. It should be noted however that the PW91 functional gave a reasonable adsorption energy value for the optimised periodic calculation starting from the periodic

Monte Carlo derived geometry. The large energy differences for each single point calculation are probably artefacts due to the fact that the ONIOM-based geometry has not been refined to include effects such as the long-range electrostatic contribution, and also the adsorption geometry is one generated from a structure containing only one aluminium atom. Local framework relaxation, which is affected by the number of aluminium atoms present in the framework, would also have an effect, subtle or otherwise, on the final geometry. These effects would help to determine the final calculated value of the adsorption energy in a truly periodic environment but are neglected in our ONIOM-based configuration. The results of these calculations are indicative of technical problems encountered when attempting to use a cluster geometry in a periodic calculation further, demonstrating the lack of transferability between the two methods when long-range effects are significant.

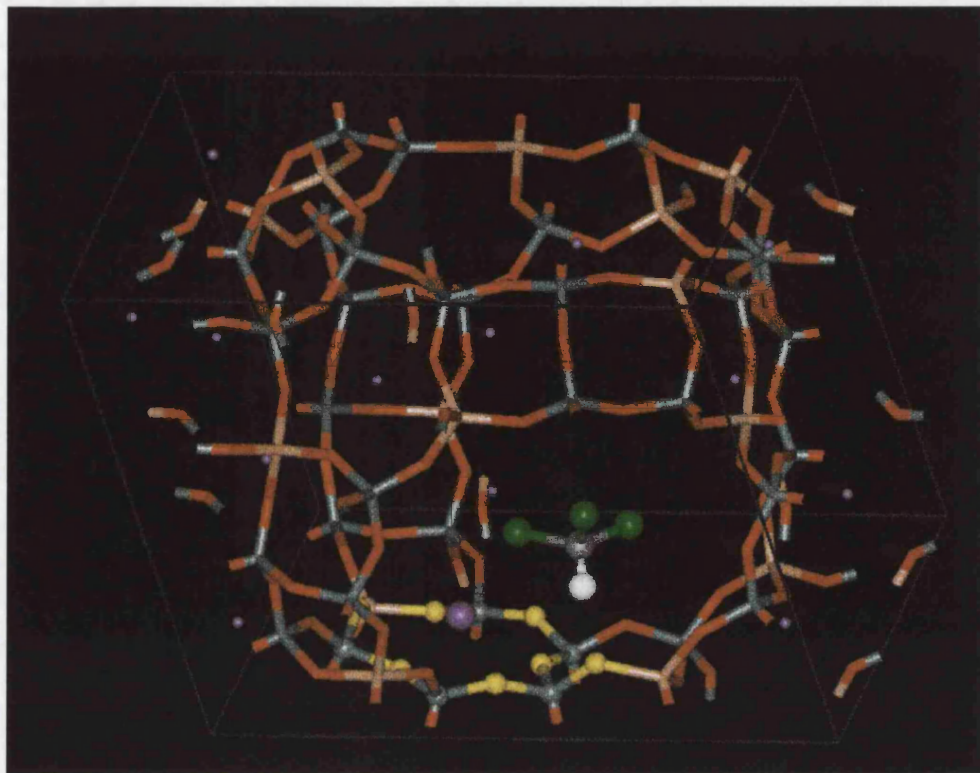


Figure 6.9: The geometry optimised primitive periodic cell of NaY with a chloroform molecule adsorbed. The optimisation was carried out using DFT with the PW91 functional.

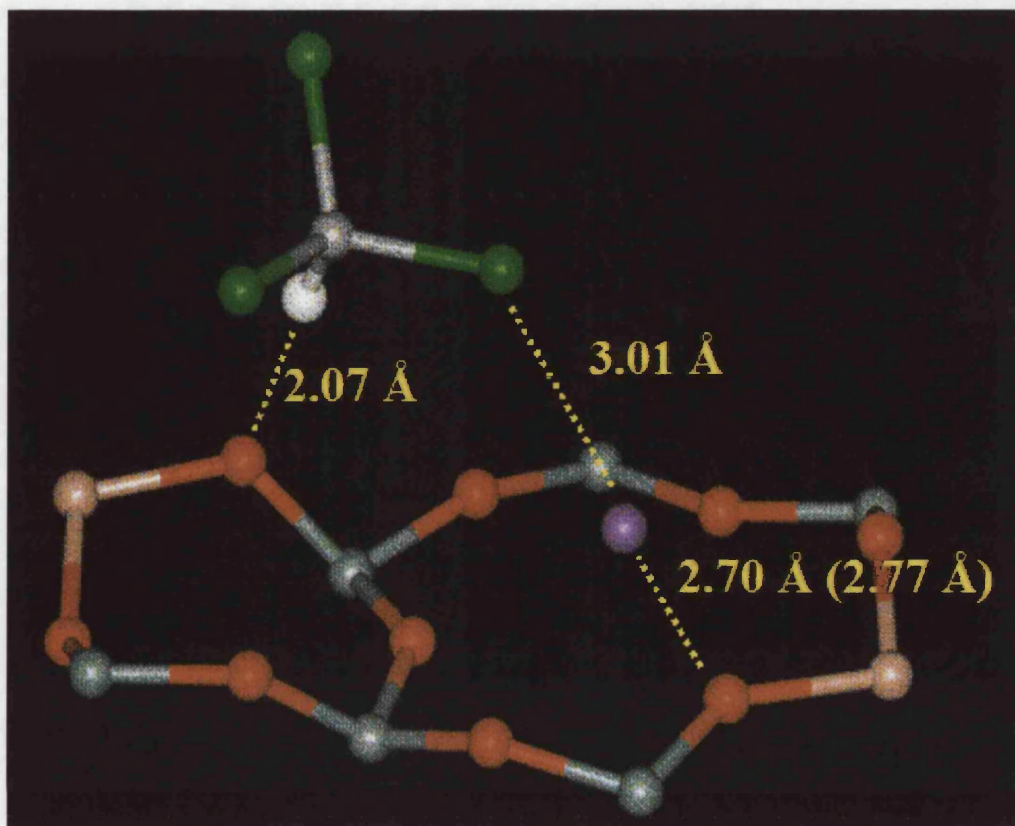


Figure 6.10: Adsorption geometry of the periodic DFT calculation using the PW91 functional.

Effect of the Sodium Relaxation on Six Ring Electronic Charge

Kyrlidis *et al.*³⁵ reports that although the long range electrostatic contribution to the adsorption energy has a significant effect when studying molecular adsorption in zeolites, the electronic properties are not affected. Therefore, this supports the use of cluster models to study the local electronic effects of molecular adsorption in zeolites, and aluminosilicate clusters.

As mentioned above, the cation was seen to relax towards an oxygen atom adjacent to the aluminium atom, due to the greater negative charge present in that particular area.

Considering the DMol cluster calculations, one can easily see that this is the case.

From the relative electronegativities of the constituent atoms of chloroform, one would expect an increase in negative charge on the chlorine atom upon coming into close proximity to a positive charge, i.e. a stronger dipole would be induced. This is what is observed. The diagrams below (figures 6.11 to 6.14) illustrate. In terms of charges on the six ring, the adsorption of chloroform has some very subtle effects on the charge distribution on the oxygen atoms. This is the case whether the embedded cluster, the full DFT cluster or the periodic system is considered. The cation moves towards an oxygen atom adjacent to the aluminium atom (due to the electrostatic influence of the aluminium), and this particular oxygen atom becomes more positive in charge. The oxygen on the other side of the aluminium atom, i.e. the oxygen atom deemed to be interacting with the chloroform molecule's hydrogen atom, becomes more negative in charge. The positively charged hydrogen atom is also involved in the adsorption interactions as it is able to interact with basic oxygen atoms on the zeolite framework. Given the geometries observed and the H—O distances for the docking configurations where the hydrogen atom is involved, this particular interaction might be considered as a weak hydrogen bond.

However, when studying the values presented, it should be noted that the Mulliken Population Analysis scheme does not take into account electronegativities of the atoms involved, and so therefore the actual values of the partial charges would be different if such considerations were taken into account (a brief description of the Mulliken

Population scheme is given in chapter 2 of this thesis). As mentioned in the said chapter, this scheme is acceptable for studying trends in charge changes.

The changes in bond lengths of the six ring in question are also very small when a chloroform molecule is placed on the cluster. The bond lengths of the oxygen atom interacting with the hydrogen atom with the two T atoms that it is bonded to both increase, this being consistent with the statement by Barthomeuf³⁶ that an increase in T—O bond length leads to an increase in negative charge on the framework oxygen atom. However, the arguments for this are based on utilising the electronegativities of the atoms, thus it is difficult to say whether the two phenomena are related in this way in this case. However, for the two oxygen atoms where one could predict the trend in charge change, it is encouraging that the corresponding change in bond length follows the statement by Barthomeuf³⁶. Figure 6.15 illustrates. Although there are differences in the trend for certain bond lengths between the different clusters, a common feature is that the T—O bond length increases around the oxygen atom where the H_{chloroform}—O_{zeolite} interaction takes place. At least one of the T—O bond lengths increases for other oxygen atoms that become more negative in charge following the molecular adsorption.

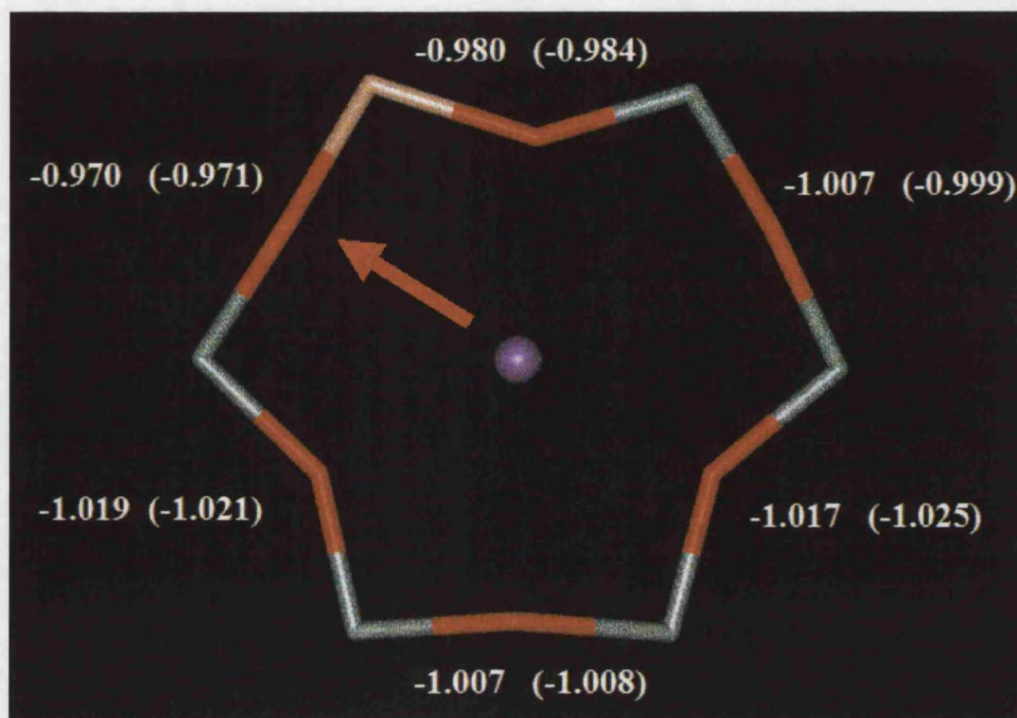


Figure 6.11: Partial charges on the six ring as calculated by the Mulliken scheme for the DMol calculations on the extended cluster. The values in parentheses are the partial charges before adsorption on the cluster, and the others are the values after adsorption. The oxygen atom where the sorbate interacts is the one with a partial charge of -1.007.

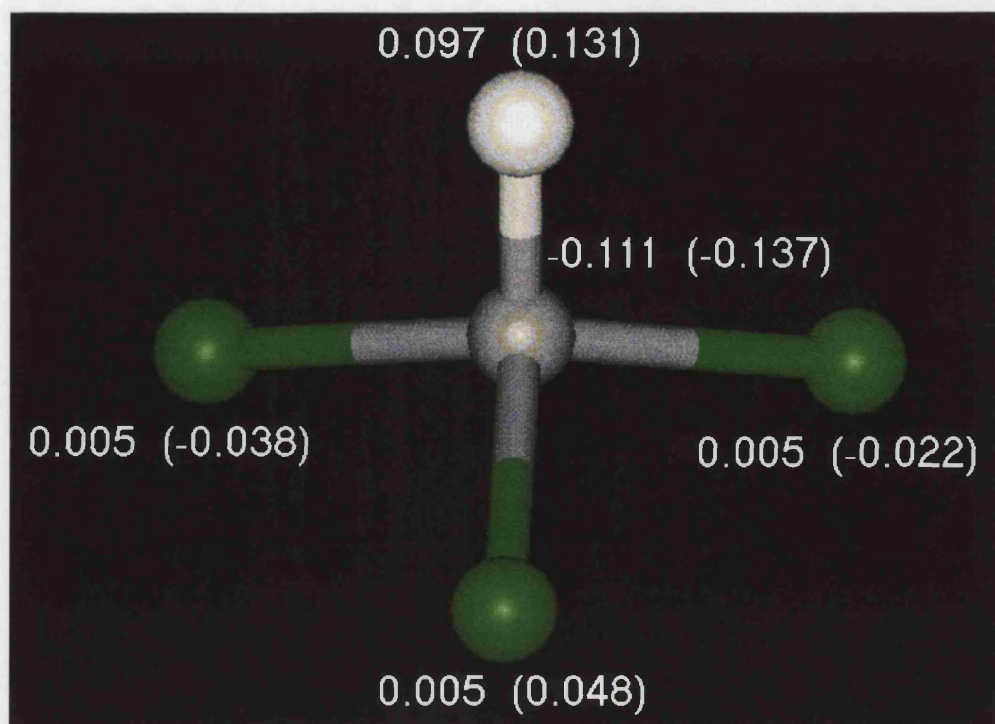


Figure 6.12: Partial charges on the chloroform molecule as calculated by the Mulliken scheme for the DMol calculations on the extended cluster. The values in parentheses are the partial charges after adsorption on the cluster, and the others are the values before adsorption.

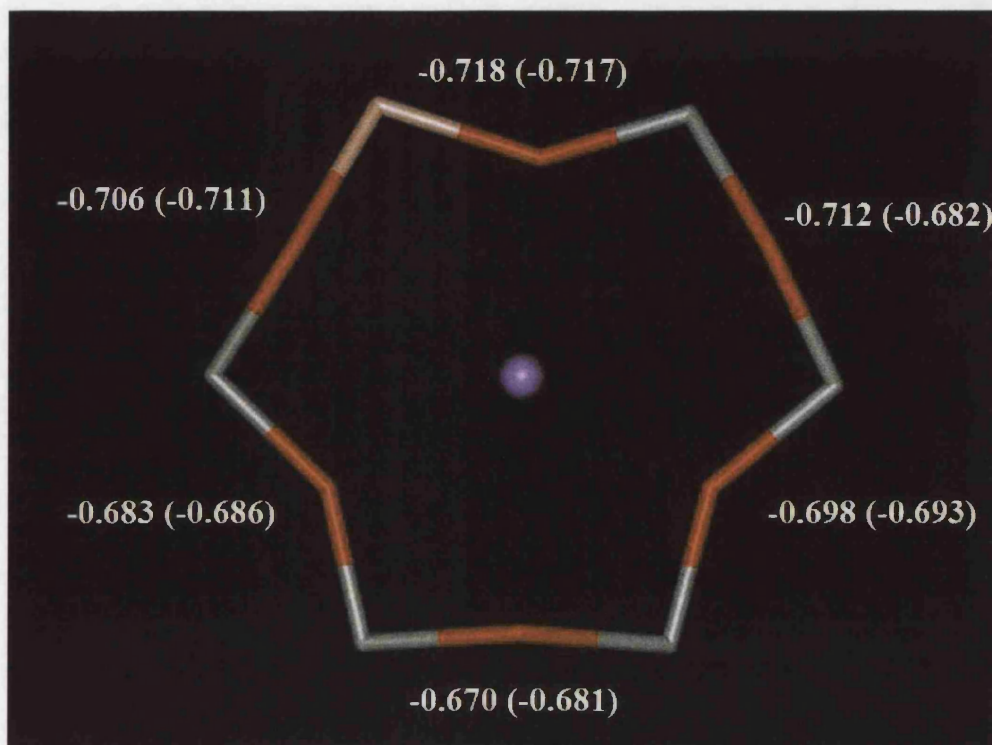


Figure 6.13: Partial charges on the zeolite SII six-ring as calculated by the Mulliken scheme for the ONIOM calculations on the extended cluster. The values in parentheses are the partial charges before adsorption on the cluster, and the others are the values after adsorption. The oxygen atom where the sorbate interacts is the one with a partial charge of -0.712..

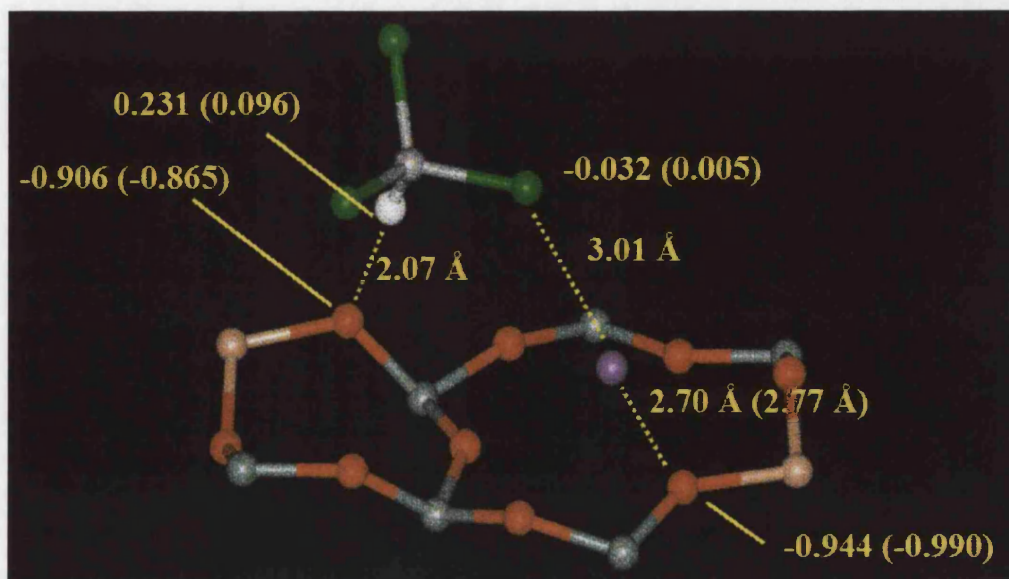


Figure 6.14: The close-up docking configuration from the periodic DMol calculation (PW91 with the DNP basis set) showing the charges on various atoms, as well as interaction distances. The values added, indicated by solid lines, are the Mulliken charges, with the values in parentheses being the charges before adsorption, and those outside of the parentheses being the values after adsorption.

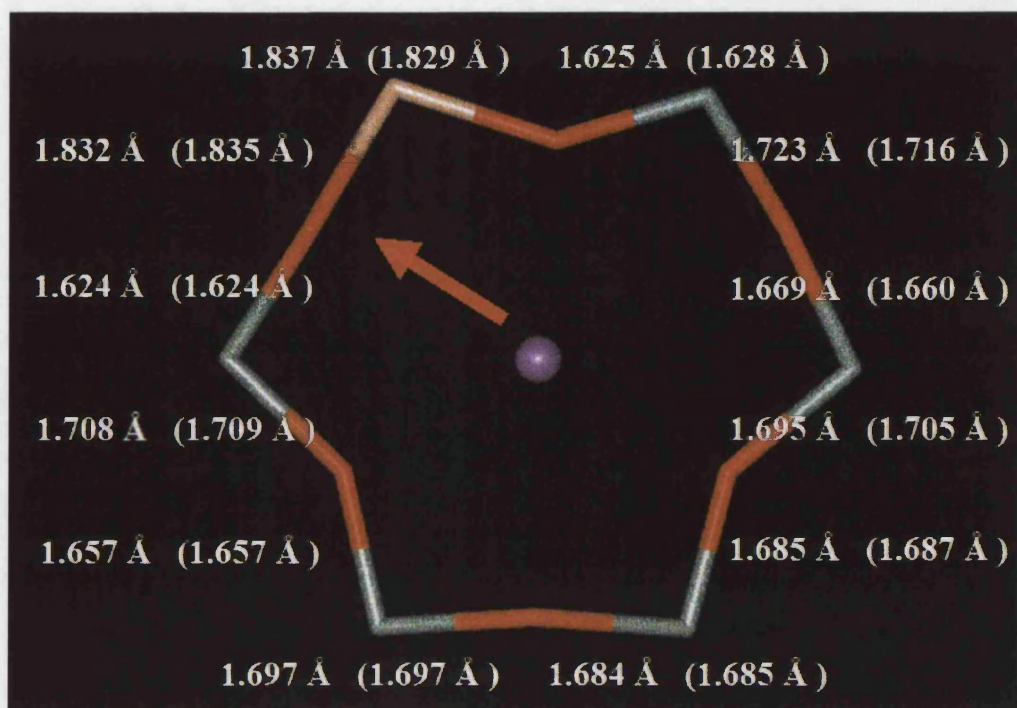


Figure 6.15: The T—O bond lengths before and after adsorption for the extended cluster optimised with the DMol program. In this representation, the middle of the bond is the point where the colours change, indicating a change of atom. The values in parentheses are the bond lengths before adsorption, and those outside of the parentheses are the values after adsorption.

Contribution of the Hydrogen—Oxygen Interaction to the Adsorption Energy

One question that might be raised is ‘what is the relative strength of the hydrogen bond compared to that of the halogen – cation interaction?’ In the light of the results of the molecular dynamics simulations described in chapters 3 and 4, one can see that in the case of the model used, the simulation seemingly favoured configurations where the

docking interactions were via the halogen – cation interaction as opposed to a hydrogen – oxygen_{zeolite} interaction.

An attempt was made to try and isolate a configuration whereby the interaction was via a hydrogen – oxygen interaction in order to calculate the energy due to this kind of interaction. This calculation was performed in DMol only, and so therefore, the entire cluster was treated at the DFT level.

The molecule was orientated in such a way that only the hydrogen could interact with the cluster framework, a configuration akin to species 1, proposed by Bosch *et al.*³⁴, and shown in figure 1.6 on page 34 of this thesis. The dihedral angle between the carbon, hydrogen, a framework oxygen atom and a neighbouring silicon atom was held fixed during the geometry optimisation in order to maintain the starting configuration, as shown in figure 6.16. Thus in effect, the hydrogen – oxygen distance was optimised during the calculation, and any halogen – cation interactions were excluded as much as possible.

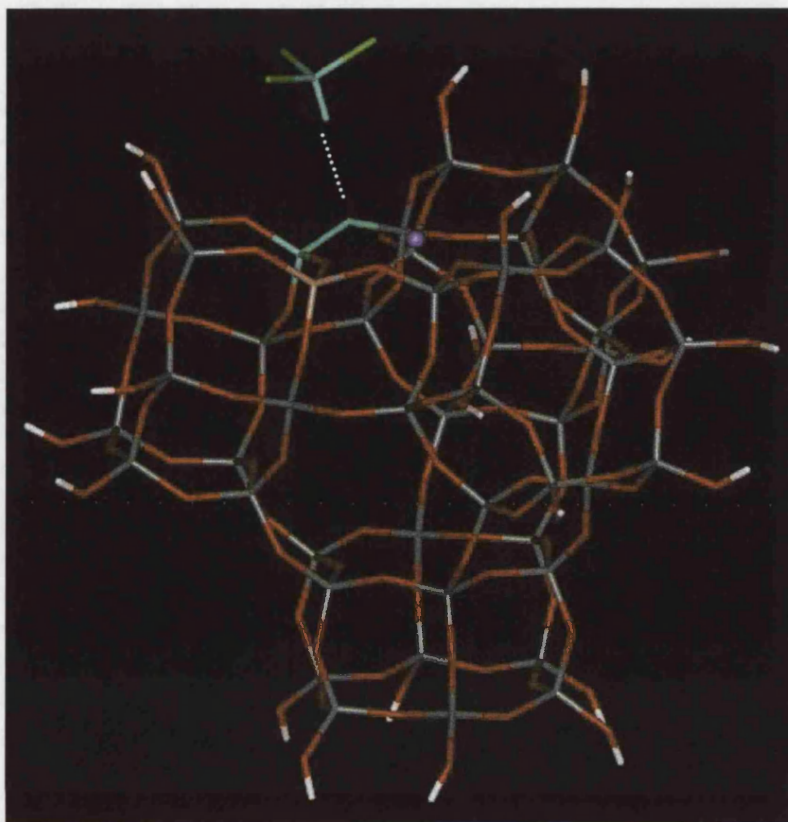


Figure 6.16: The cluster used to calculate the energy due to the $H-O_{\text{zeolite}}$ interaction. The atoms coloured in light blue are those defined for the purposes of fixing a dihedral angle, so as to maintain the above configuration.

The final geometry obtained for the cluster had the hydrogen at a distance of 2.67 Å from the oxygen atom. This distance is greater than the distance predicted by the clusters where both the hydrogen and chlorine are interacting with the zeolite and cation respectively. The closest Cl—Na distance throughout the optimisation is 5.57 Å, which is sufficiently large that the interaction can be considered as negligible compared to the $H-O_{\text{zeolite}}$ interaction. The final, optimised geometry is shown in figure 6.17. The calculated adsorption energy is 4 kJmol⁻¹. The value obtained might be a consequence of the constraints placed upon the model, and of the final geometry, as previous

calculations using the Monte Carlo method (see chapter 3) predict the H—O distance to be smaller than the distance attained in this case. However, given that the distances are greater than 2.3 Å, it can be said that the H—O interaction can be considered as a weak hydrogen bond. All in all, the calculations could provide further evidence of the improvements made on using a periodic model and including the long range electrostatic effects on the geometry. In order to obtain a more accurate energy, one must include these effects, although one can obtain a feeling for the relative energetics of the Na—Cl and the H—O interaction.

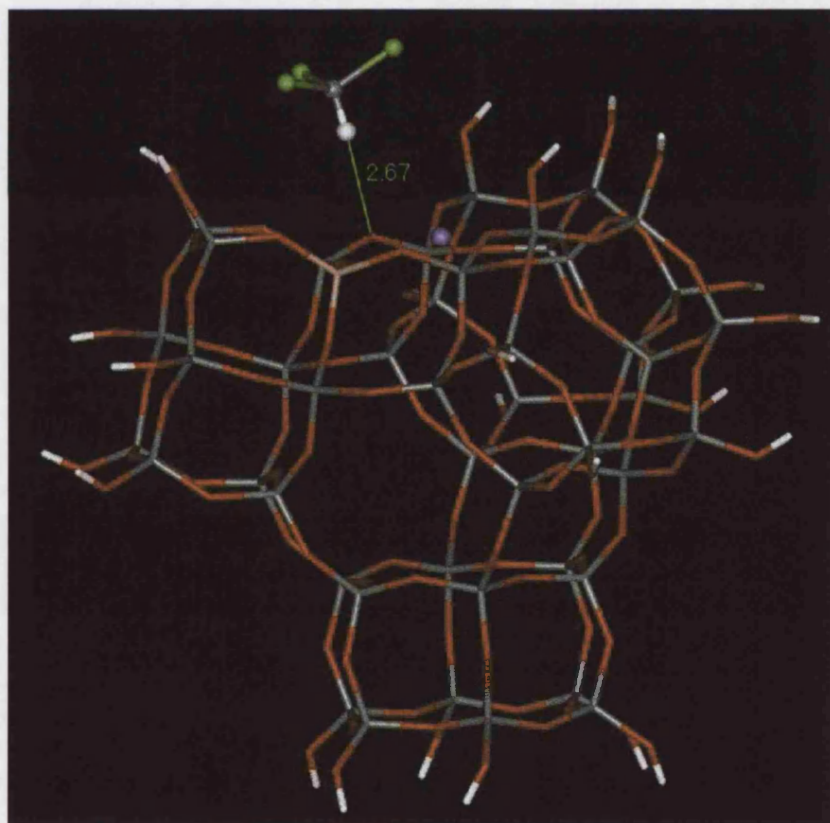


Figure 6.17: The optimised geometry of the calculation to determine the strength of the hydrogen—oxygen interaction when chloroform is adsorbed on an aluminosilicate cluster.

Conclusions

This chapter has described electronic structure calculations on sodium substituted aluminosilicate clusters with a chloroform molecule adsorbed onto them. The calculations were also carried out with a periodic model of NaY zeolite with an Si:Al ratio of 2.4.

The importance of including long range electrostatic effects when calculating adsorption energies of halocarbon molecules adsorbed on aluminosilicates has been shown by the results of this study. Comparisons of cluster DFT calculations with experimentally determined values of CHCl_3 adsorption on NaY zeolite shows that the cluster calculations reproduce approximately 50% of the adsorption energy. This is the case when using the BLYP and B3LYP functionals, and whether using the embedded cluster method or treating the entire cluster at the DFT level of theory. Periodic DFT calculations using the BLYP functional have yielded adsorption energies that are much more negative than the true adsorption energy. However, when using the PW91 functional in the periodic calculations, the adsorption energy as determined by calorimetry is reproduced to a good degree. Either way, it is evident that the long range electrostatic contributions do play an important part in the determination of adsorption energies of chloroform adsorbing on NaY zeolite.

The effects on the charge distribution on the six-ring oxygen atoms after molecular adsorption were found to be very subtle, with any changes being very small. This may be due to the Mulliken Population Analysis method used to calculate the partial charges. In particular, the fact that the electronegativities of the atoms in question are not taken

into account. However, whether considering the cluster or periodic calculations, the trends are as expected. The cation moves towards an oxygen adjacent to an aluminium atoms, and this particular oxygen becomes more positive in charge. The final cation position is determined by two effects working in tandem; that of the Na—Cl interaction, and that of the Na—O interaction. The hydrogen atom on the chloroform molecule becomes more positive in charge and interacts with a basic oxygen atom on the zeolite, which becomes more negative. This effect is coupled with the lengthening of T—O bond lengths where the oxygen charges become more negative, and a shortening of bond lengths where they become more positive.

Chapter 6 References

- (1) Simperler, A.; Bell, R. G.; Philippou, A.; Anderson, M. W. *J. Phys. Chem. B* **2002**, *106*, 10944.
- (2) Uzunova, E. L.; St. Nikolov, G. *J. Phys. Chem. A* **2000**, *104*, 5302.
- (3) Vayssilov, G. N.; Notker, R. *Phys. Chem. Chem. Phys.* **2002**, *4*, 146.
- (4) Humbel, S.; Sieber, S. N.; Morokuma, K. *J. Chem. Phys.* **1996**, *105*, 1959.
- (5) Dapprich, S.; Komaromi, I.; Byun, K. S.; Morokuma, K.; Frisch, M. J. *J. Mol. Struct (THEOCHEM)* **1999**, *1*, 461.
- (6) Svensson, M.; Humbel, S.; Froese, T.; Matsubara, T.; Sieber, S. N.; Morokuma, K. *J. Phys. Chem* **1996**, *100*, 19357.
- (7) Frisch, M. J. *Gaussian 98* **1998**, Revision A.7, Gaussian Inc, Pittsburg, PA.
- (8) Greatbanks, S. P.; Sherwood, P.; Hillier, I. H.; Hall, R. J.; Burton, N. A.; Gould, I. R. *Chem. Phys. Letts.* **1995**, *234*, 367.
- (9) Sherwood, P.; de Vries, A. H.; Collins, S. J.; Greatbanks, S. P.; Burton, N. A.; Vincent, M. A.; Hillier, I. H. *Faraday Discussions* **1997**, *106*.
- (10) Goursot, A.; Arbuznikov, A.; Vasilyev, V. In *Density Functional Theory: A Bridge Between Chemistry and Physics*; Geerlings, P., De Proft, F., Langenaeker, W., Eds.; VUB University Press: Brussels, 1999; pp 155.

- (11) Ricci, D.; Pacchioni, G.; Szymanski, M. A.; Shluger, A. L.; Stoneham, A. M. *Phys. Rev. B* **2001**, *64*, 224104.
- (12) Erbetta, D.; Ricci, D.; Pacchioni, G. *J. Chem. Phys.* **2000**, *113*, 10744.
- (13) Roggero, I.; Civalleri, B.; Ugliengo, P. *Chem. Phys. Letts.* **2001**, *341*, 625.
- (14) Sinclair, P. E.; de Vries, A.; Sherwood, P.; Catlow, C. R. A.; van Santen, R. A. *J. Chem. Soc., Faraday Trans.* **1998**, *94*, 3401.
- (15) de Vries, A.; Sherwood, P.; Collins, S. J.; Rigby, A. M.; Rigutto, M.; Kramer, G. *J. J. Phys. Chem* **1999**, *103*, 6133.
- (16) Sauer, J.; Sierka, M. *J. Comp. Chem.* **2000**, *21*, 1470.
- (17) Sierka, M.; Sauer, J. *Faraday Discussions* **1997**, *106*, 41.
- (18) Rozanska, X.; van Santen, R. A.; Hutschka, F. *J. Catal.* **2001**, *200*, 79.
- (19) Hill, J. R.; Freeman, C. M.; Delley, B. *J. Phys. Chem. A* **1999**, *103*, 3772.
- (20) Mellot, C. F.; Cheetham, A. K.; Harms, S.; Savitz, S.; Gorte, R. J.; Myers, A. L. *Journal of the American Chemical Society* **1998**, *120*, 5788.
- (21) Mellot, C. F.; Davidson, A. M.; Eckert, J.; Cheetham, A. K. *Journal of Physical Chemistry B* **1998**, *102*, 2530.
- (22) Mellot, C. F.; Cheetham, A. K. *Journal of Physical Chemistry B* **1999**, *103*, 3864.
- (23) Becke, A. D. *J. Chem. Phys.* **1993**, *98*, 5648.
- (24) Lee, C.; Yang, W.; Parr, R. G. *Phys. Rev. B.* **1988**, *37*, 785.
- (25) Nedelec, J. M.; Hench, L. L. *J. Non-Cryst. Solids* **2000**, *277*, 106.
- (26) Delley, B. *J. Chem. Phys.* **1990**, *91*, 508.
- (27) MSI. DISCOVER Theory and Methodology. In *Biosym Manuals*, 1993; Vol. 1.
- (28) Molecular Simulations Inc. *Program DMol3* **1997**, version 3.5.
- (29) Becke, A. D. *Phys. Rev. A.* **1988**, *38*, 3098.
- (30) Fitch, A. N.; Jobic, H.; Renouprez, A. *Journal of Physical Chemistry* **1986**, *90*, 1311.
- (31) Bromley, S. T., Private Communication.
- (32) Gale, J. D. *Topics in Catalysis* **1996**, *3*, 169.
- (33) Zygmunt, S. A.; Mueller, R. M.; Curtiss, L. A.; Iton, L. E. *J. Mol. Struct (THEOCHEM)* **1998**, *430*, 9.
- (34) Bosch, E.; Huber, S.; Weitkamp, J.; Knozinger, H. *Physical Chemistry Chemical Physics* **1999**, *1*, 579.

- (35) Krylidis, A.; Cook, S. J.; Chakraborti, A. K.; Bell, A. T.; Theodorou, D. N. *J. Phys. Chem.* **1995**, *99*, 1505.
- (36) Barthomeuf, D. *Catalysis Reviews-Science and Engineering* **1996**, *38*, 521.